Universität Linz
Netzwerk für Forschung, Lehre und Praxis

*To Increase the Photon Harvesting
in the Photoactive Layer of
Bulk Heterojunction Organic Solar Cells*

Dissertation zur Erlangung des akademischen Grades

Doctor Technicae

im *Doktoratsstudium der technischen Wissenschaften*

Angefertigt am Linzer Institut für Organische Solarzellen

Eingereicht von:
Dipl. Ing. Christoph Winder

Betreuung:
*o. Univ. Prof. Dr. Serdar Niyazi Sariciftci
Dr. Helmut Neugebauer*

Beurteilung:
o. Univ. Prof. Dr. Serdar Niyazi Sariciftci
o. Univ. Prof. Dr. Wolfgang Buchberger

Linz, Oktober 2004

Eidesstattliche Erklärung:

Ich erkläre an Eides statt, dass ich die vorliegende Dissertation selbstständig und ohne fremde Hilfe verfasst, andere als die angegebenen Quellen und Hilfsmittel nicht benutzt bzw. die wörtlich oder sinngemäß entnommenen Stellen als solche kenntlich gemacht habe.

Linz, September 2004   Winder Christoph

Die vorliegende Diplomarbeit entstand zwischen November 2001 und September 2004 am Linzer Institut für Organische Solarzellen der Technisch-Naturwissenschaftlichen Fakultät der Universität Linz unter Betreuung von Prof. Dr. N. S. Sariciftci und Dr. Helmut Neugebauer.

Abstract

Thin film solar cells based on conjugated polymer-fullerene interpenetrating networks gained increased scientific and industrial interest in the last decade. Today, such devices have power conversion efficiencies of 3.8 % under AM 1.5 illumination, high internal photon to current conversion efficiencies and show excellent diode behaviour. The main advantages of organic materials are the possible cheap synthesis and the easy fabrication technology.

One limitation towards higher power conversion efficiencies is the limited absorption of the today's used photoactive materials. The absorption range of most of the conjugated polymers is too small and located between 400 and 600 nm. Fullerenes absorb mainly in the UV, their absorption in the VIS is symmetry forbidden and therefore weak. However, the maximum of the solar emission spectrum is located between 600 and 800 nm.

In this thesis, several approaches to increase the photon harvesting in polymer based solar cells are presented. New conjugated polymers with a lower band gap, electron acceptor polymers as possible alternatives to fullerenes, donor-acceptor dyad molecules with a highly absorbing dye molecule and multi component blends are investigated. New materials and material combinations are investigated by means of absorption, photoluminescence and photoinduced absorption spectroscopy. Photovoltaic devices are built from the new materials and characterised by current-voltage and photocurrent spectra measurements.

Zusammenfassung

Dünnschichtsolarzellen, basierend auf Mischungen von konjugierten Polymeren und Fullerenen, haben im letzten Jahrzehnt an akademischem und industriellem Interesse gewonnen. Solarzellen mit Energieumwandlungseffizienzen von 3.8 % unter AM 1.5 Bedingungen, hohen internen Photonen-zu-Strom Umwandlungseffizienzen und ausgezeichnetem Diodenverhalten wurden demonstriert. Die wichtigsten Voreile von organischen Materialien liegt in der Möglichkeit einer billigen Synthese und der einfache Verarbeitung.

Ein Limit zu höheren Umwandlungseffizienzen liegt in der Absorption der heutzutage benützten photoaktiven Materialien. Die Absorptionsbreite der meisten konjugierten Materialien ist schmal und liegt zwischen 400 und 600 nm. Fullerene absorbieren hauptsächlich im UV, ihre Absorption im sichtbaren Bereich ist symmetrieverboten und daher schwach. Das Maximum des Sonnenspektrums liegt jedoch zwischen 600 und 800 nm.

In dieser Doktorarbeit werden Möglichkeiten zur Erhöhung der optischen Absorption in polymer-basierenden Solarzellen untersucht. Es werden neue Polymere mit kleineren Bandlücken, Elektronenakzeptorpolymere als mögliche Alternative zu Fullerenen, Donor-Akzeptor-Diaden mit einem hochabsorbierenden Farbstoffmolekül und Mehrkomponentensysteme untersucht.

Die neuen Materialien und Materialkombinationen werden mittels optischer Absorption, Photolumineszenz und photoinduzierter Absorptionsspektroskopie untersucht. Solarzellen werden aus den neuen Materialien hergestellt und mittels Strom-Spannungskurven und Photostromspektren charakterisiert.

Table of Content

0. Motivation

Organic molecular and polymeric materials with an extended π-conjugated system gain interest as alternative semiconductors materials in the last decade. Several applications were demonstrated for these materials. Devices like light emitting diodes, field effect transistors and also photovoltaic devices have got industrial interest.

Organic materials show several advantages for the application in solar cells. Their synthesis can be much cheaper as compared to conventional inorganic materials. Processing from solution is possible and offers an easy way the for device fabrication. Spin coating, printing techniques and roll to roll processing are possible and realized. Further, the properties organic materials can be tuned for the desired application. A wide range of possible materials is accessible.

Recently, polymer photovoltaic devices were demonstrated with power conversion efficiencies $\eta_e = 3.8$ % under solar simulated light. These devices show internal quantum efficiencies near unity and excellent diode behaviour.

Solar cells from polymeric materials show several advantages. The devices can be made flexible and semi-transparent. Plastic solar cells can be easily integrated into other devices. Materials are light weight and different colour can be selected.

For the application in solar cells, material properties like good environmental stability, broad and intense absorption spectra and high charge carrier mobility are needed.

In this work, the problem of the material absorption is approached. The number of absorbed photons is directly related with the device efficiency and the main limitation towards higher efficiencies. Different approaches are demonstrated using new materials and device concepts.

1. Conjugated Polymers, Fullerenes, the Excited State

1.1. Conjugated Polymers

1.1.1. *Electronic Properties*

Polymers with an extended π-electron system show the property of conducting electrical charges.[1] This effect was discovered in 1976 for polyacetylene by Hideki Shirakawa, Alan MacDiarmid and Alan Heeger.[2,3] The science and application of conjugated polymers CP´s has made rapid progress since that time and this discovery was honoured by awarding the Nobel Price in 2000 to the three discoverers.

In the intrinsic state, such conjugated polymers are semiconductors. The conductivity can be tuned by doping, from nearly insulating for undoped to metal like conductivity for highly doped CP´s. Doping in CP´s are either oxidation or reduction reactions.

The valence band (VB) and conduction band (CB) are formed by the extended π-orbital system (p_z-electrons, the wavefunctions are perpendicular to the polymer backbone). Between the filled VB and the empty CB is the band gap E_g. The band gap is a result of the bond length alternation. This was predicted by Rudolf Peierls in 1956, long before the first synthesis of a CP.[4] The π-electron band is split in a filled, bonding π-band (VB) and an empty, antibonding π^* band (CB). The charge carriers are empty states (holes, p-doping) in the VB or filled states (electrons, n-doping) in the CB. The charge carrier mobility is predominantly along the chain. The bottleneck is the hopping between the chains. Doping in conjugated polymers is equivalent to oxidation (p-doping) and reduction (n-doping) and is generally reversible[5]. Doping in CP´s can be induced by a variety of techniques:

- Chemical doping is done by either oxidation (p-doping) or reduction (n-doping). Simultaneously, a counterion has to move into the lattice.
- Electrochemical doping, where the CP is doped by an electrochemical redox reaction. The electrochemical potential is shifted either in the VB or CB.
- Acid–base chemistry in the case of polyaniline
- Interfacial doping at a CP/ metal interface
- Photodoping, where a photoexcited electron-hole pair (exciton) is split at an interface or defect. This process will be discussed in more detail in chapter 1.3.

The electronic structure of CP´s was first calculated by Su, Schrieffer and Heeger (SSH), who formulated the SSH Hamiltonian.[6, 7] According to the SSH theory, conjugated polymers are divided into two classes of electronic structures:

CP´s with a degenerate groundstate (*trans*-polyacetylene) and with a non-degenerate groundstate (*cis*-polyacetylene and all the others). Figure 1.1 shows the potential energy as a function of the bond length alternation ΔE_r for trans-acetylene (degenerate groundstate) and poly-*para*-phenylene PPP (non-degenerate groundstate). For both cases, the potential energy shows two minima and a maximum. At the maximum, the bond length alternation is vanished and the π-electrons are not paired.

In degenerate groundstate CP´s, the change in the bond length alternation leads to equivalent structures (phase A, phase B) with the same energy. In non-degenerate groundstate CP´s, the bond length alternation leads to two different structures (aromatic and quinoid). The two structures have different energies.
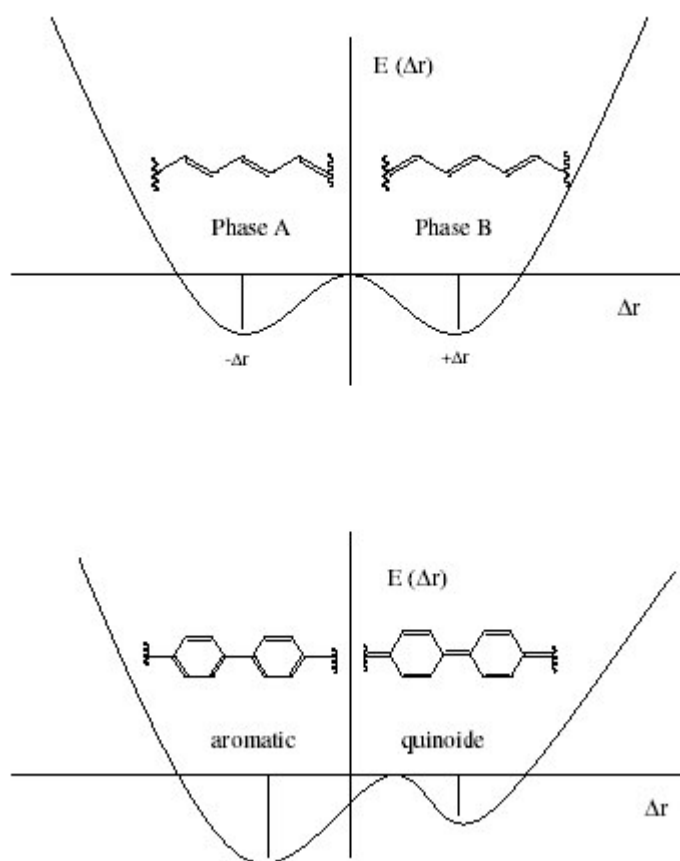
Figure 1. 1: Potential energy as a function of bond length alternation is shown for the two classes of conjugated polymers. The upper picture for a conjugated polymer with degenerate groundstate, trans-polyacetylene. The lower picture show the potential energy for a conjugated with non-degenerate groundstate, in the given example poly-para-phenylene PPP.

Following from electronic structure, different non-linear excitations are derived for degenerate and non-degenerate groundstate polymers.

Degenerate groundstate CP´s form solitons. These are quasi particle with one new electronic state in the middle of the band gap, see Figure 1.2. This state can be singly occupied (neutral soliton), double occupied (negative solitons) or empty (positive soliton). It is interesting to note that the spin charge symmetry is inversed in solitons.
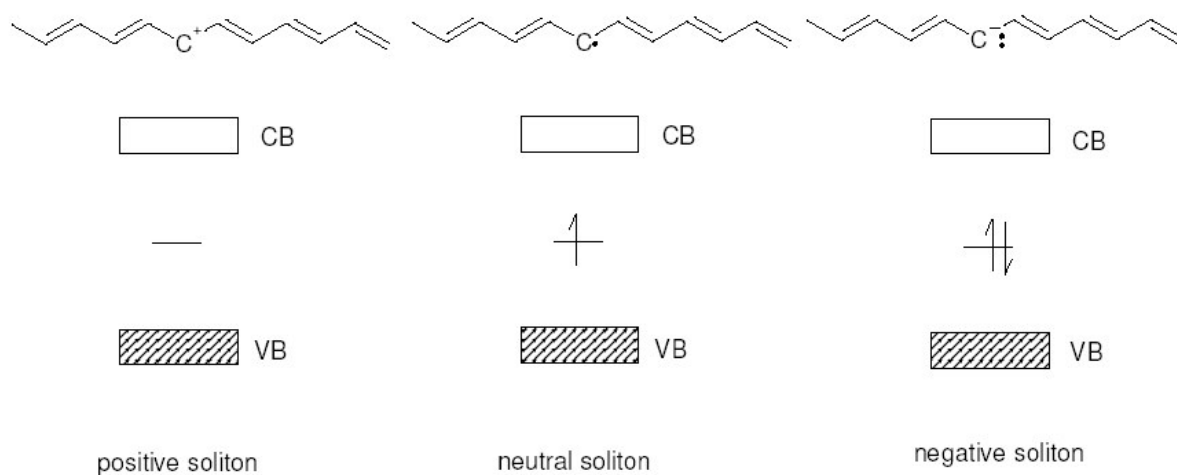
Figure 1. 2: Schematic representations and energy diagram is shown for solitons in CP´s. One new energy state is induced in the gap. This can be either empty (positive soliton), half (neutral soliton) or double filled (negative soliton).

In non-degenerate groundstate polymers, the structural relaxation of the backbone leads to two new states within the band gap. The quasi particles are excitons (neutral), polarons (one charge) and bipolarons (double charged). Schematic structures and energy diagrams are shown in Figure 1.3.

Polarons show two new electronic transitions (high energy HE and low energy LE peak, others are symmetry forbidden) and are radicals. Therefore, they show an electron spin resonance (ESR) signal.

Bipolarons show only one symmetry allowed transition and have no unpaired electron. They are ESR silent. The spectroscopic features of polarons and bipolarons will be further discussed in section 1.3 and chapter 3.
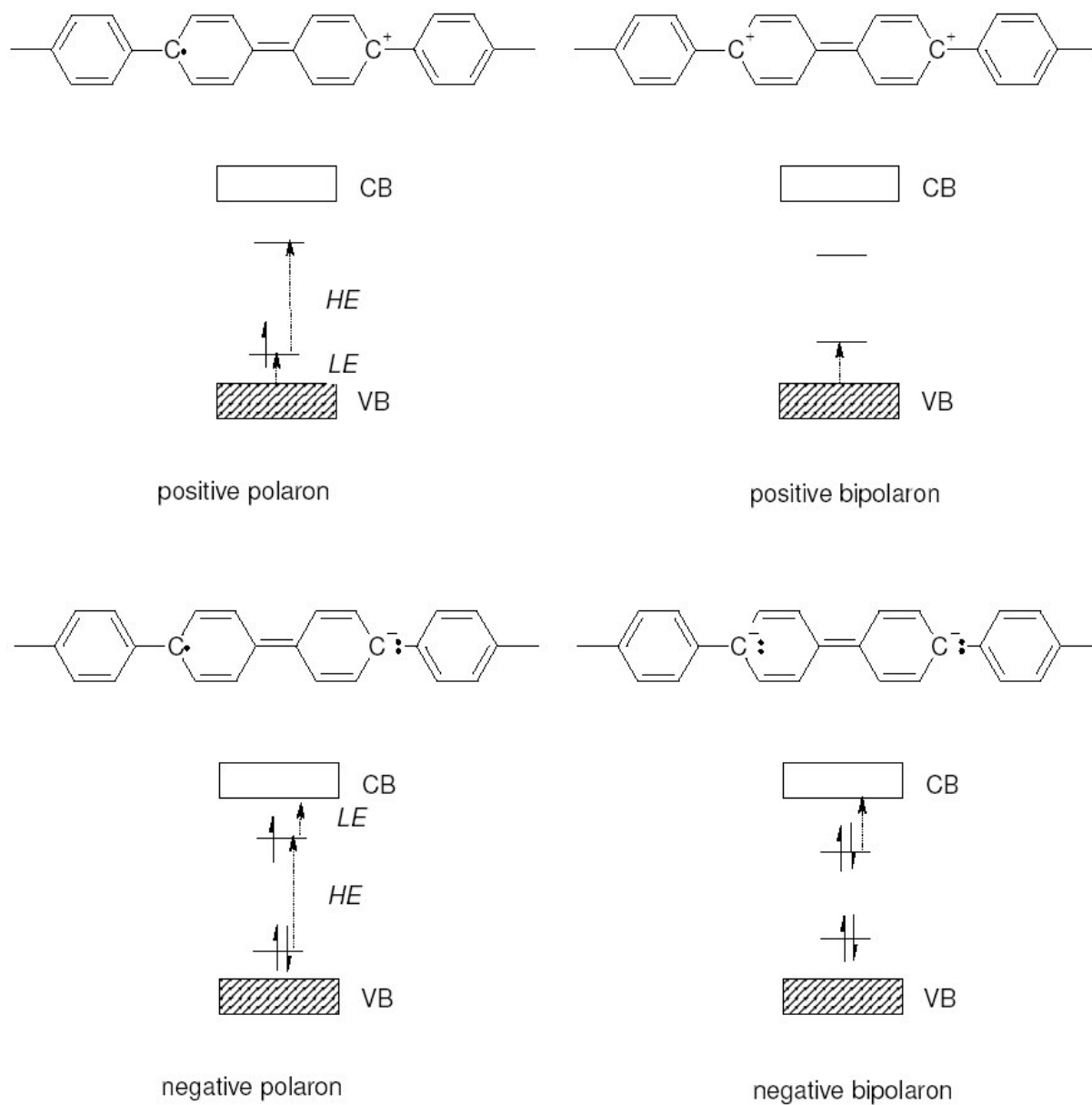
Figure 1. 3: Schematic representation and band diagrams for nonlinear excitation in non-degenerate groundstate CP´s. Allowed optical transitions are shown as dashed arrow.

1.1.2 Materials

Figure 1.4 shows the two of the mostly used and best known CP´s for photovoltaic application, poly-[2-methoxy-5-(3´,7´-dimethyloctyloxy)]-*para*-phenylene vinylene (MDMO-PPV[8]) and regio-regular poly-3-hexylthiophene (rr-P3HT).[9,10]
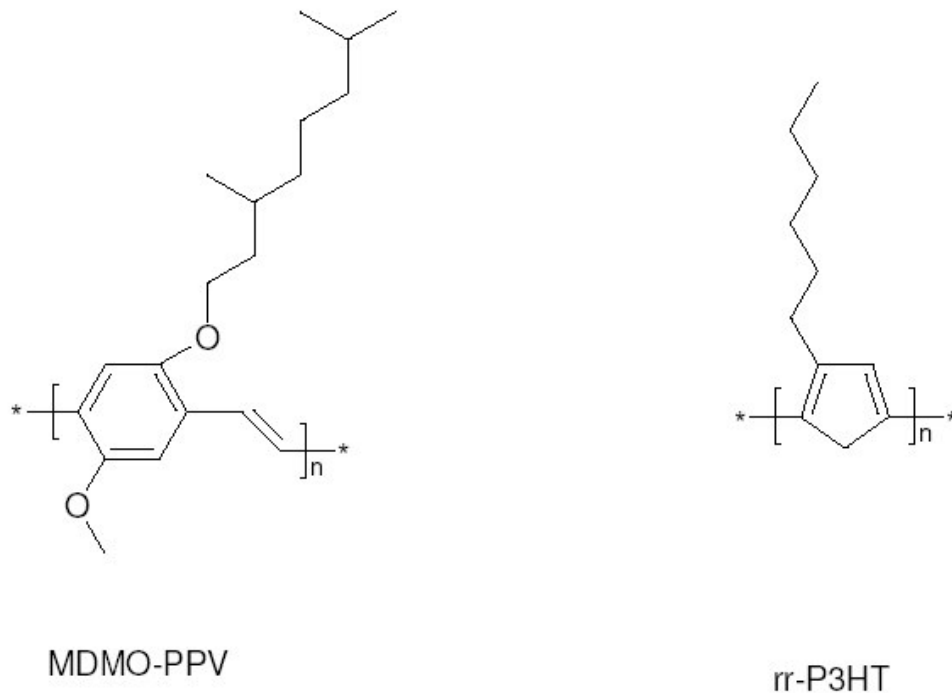
MDMO-PPV

rr-P3HT

Figure 1. 4: Structure of poly-[2-methoxy-5-(3´,7´-dimethyloctyloxy)]-*para*-phenylene vinylene MDMO-PPV and regio-regular poly-3-hexylthiophene (rr-P3HT).

The band gap and the band energy levels are two important parameters of a material. Such knowledge is necessary for engineering solar cell devices. The optical band gap E_g^{Opt} can be determined by the absorption or luminescence onset. This is shown for the two materials in Figure 1.5. The onset is around 580 nm, equivalent to 2.1 eV, for MDMO-PPV and around 650 nm (1.9 eV) for P3HT, respectively.

The band energy levels are determined by electrochemistry[11,12] or photoemission spectroscopy.[13,14] In electrochemical measurements, the valence band edge is estimated by the oxidation onset and the conduction band edge is estimated by the reduction potential. For the conversion from the electrochemical energy scheme into the vacuum level, a value of 4.75 eV is assumed for the normal hydrogen electrode (NHE).[15,16]

Further, electrochemical measurements can be used as an alternative method to determine the band gap. The electrochemical band gap E_g^{EC} is defined as the difference of the oxidation and

reduction potential. Table 1.1 shows the energy values for MDMO-PPV, P3HT and the fullerene derivative PCBM, for details see next chapter.

Table 1. 1 : Energy levels of MDMO-PPV, P3HT and PCBM, calculated from electrochemical measurements. For PCBM, no oxidation is observed. [11]

	HOMO / eV	LUMO / eV	E_g^{EC} / eV	E_g^{Opt} / eV
MDMO-PPV	5.3	3.0	2.3	2.1
P3HT	5.1	2.9	2.2	1.9
PCBM	--	4.3	--	1.8
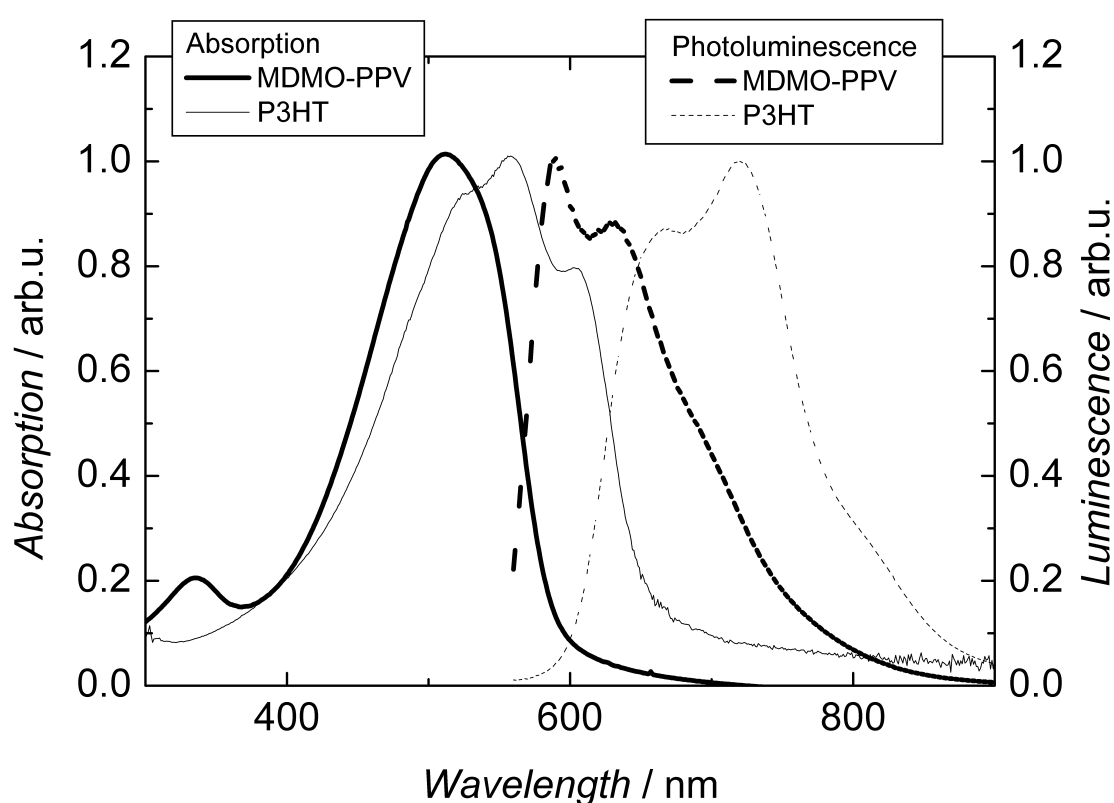
Figure 1. 5: Absorption and Photoluminescence at room temperature of MDMO-PPV and rr-P3HT is shown, all spectra normalized to their maximum.

1.2. Fullerenes

Fullerenes were discovered by Robert Curl, Harold Kroto and Richard Smalley in 1985 as the third allotropic form of Carbon.[17] For this discovery, they were awarded the 1996 Nobel Prize in Chemistry. C_{60} is the most abundant form of the class of fullerenes, other forms are C_{70}, C_{78}, C_{84}, etc. At the end of this series are the nanotubes.

The 60 carbon atoms are arranged as 12 pentagons and 20 hexagons. The shape is the same as that of a soccer ball: The black pieces of leather are the pentagons, the hexagons are white. C_{60} was named after the architect Buckminster Fuller, who used this geometry in his buildings. Fullerenes show a lot of interesting electronic properties. The HOMO is five times degenerate and has h_u symmetry, the LUMO is triply degenerate and has t_{1u} symmetry, the LUMO+1 is triply degenerate as well and has t_{1g}.[18] The HOMO-LUMO energy gap is around 1.8 eV, but the HOMO-LUMO optical transition is symmetry forbidden. The band gap absorption is weak. The electrochemistry of C_{60} shows six reversible one-electron reductions, reflecting the good electron acceptor property.[19]

1.2.1 Soluble Fullerene Derivative PCBM

C_{60} itself is rather insoluble. Side groups are attached to increase its solubility for the application in solution-cast processes. The most widely used C_{60} derivative in solar cell devices is 1-(3-methoxycarbonyl)propyl-1-phenyl-[6,6]methanofullerene PCBM.[20] The structure of PCBM is shown in Figure 1.6. It shows increased solubility in organic solvents, for example up to 40 mg/mL in chlorobenzene and 10 mg/ mL in toluene. The electrochemical reduction of PCBM is shifted 100 mV to cathodic, what is equivalent to less acceptor strength. This is caused by the loss of one double bond in the cage. Nevertheless, PCBM is an excellent electron acceptor.
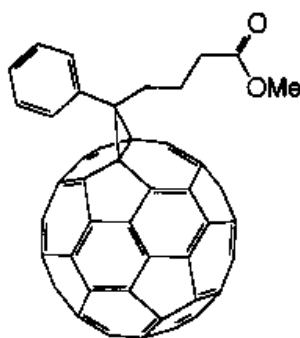
Figure 1. 6: Structure of 1-(3-methoxycarbonyl)propyl-1-phenyl-[6,6]methanofullerene PCBM.

The electron mobility in PCBM was investigated recently by several techniques and show values in the range of $2*10^{-3}$ -$4.5*10^{-3}$ cm^2 V^{-1} s^{-1}.[21,22,23]

Figure 1.7 shows the optical absorption and photoluminescence of a PCBM film. According to the symmetry of the energy levels, the HOMO-LUMO transition is forbidden and the absorption is therefore weak around 700 nm. The photoluminescence spectrum at room temperature shows a maximum at 740 nm and a shoulder 810 nm.
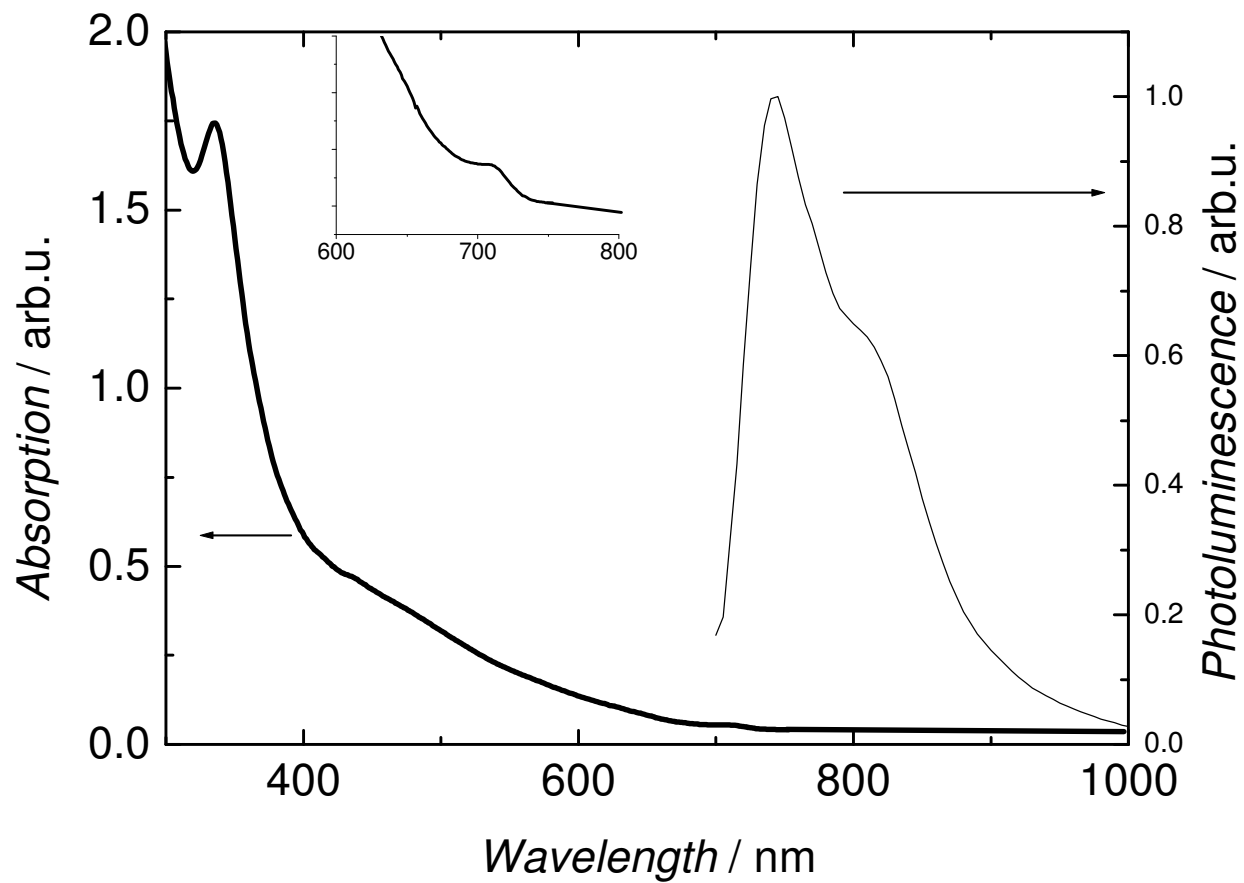
Figure 1. 7: Absorption and luminescence of a PCBM thin film are shown. The inset shows the absorption of PCBM around the onset.

1.3. The Excited State

Photoexcitation across the band gap leads in CP´s generally to the first excited singlet state S_1. Various de-excitation processes can start from this state. Typical processes are photoluminescence, radiationless decay, intersystem crossing into the triplet state or interactions with other molecules, energy and charge transfer. Figure 1.8 gives an overview of the processes involved.
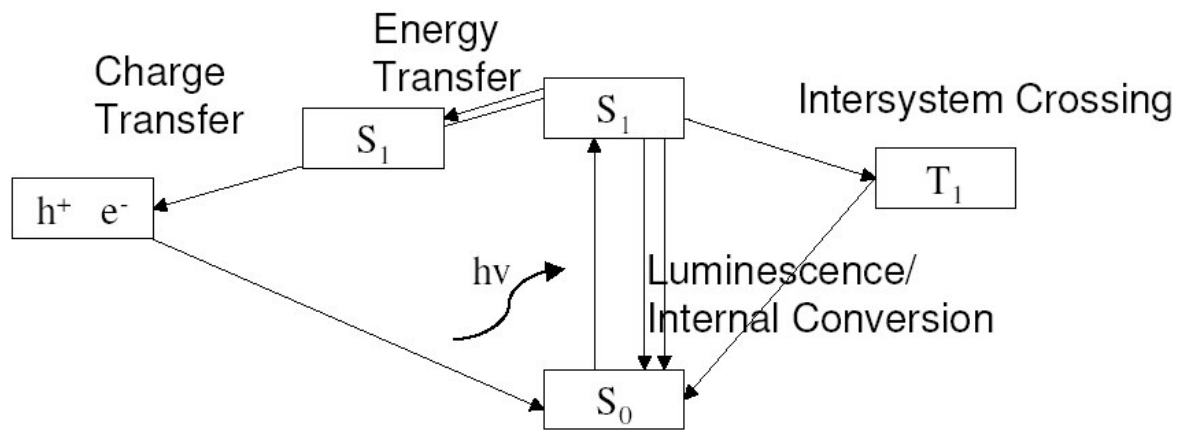
Figure 1. 8: Energy diagram for possible relaxation pathways of a photoexcitation. S_0 is the groundstate, S_1 is the first singlet excited state, T_1 is the first triplet excited state.

1.3.1. Energy transfer

Energy transfer is an interaction between two molecules in which the excited state energy from one molecule (donor) is transferred to the other (acceptor). Such processes are often described by the Foerster mechanism. The rate constant k_{FET} for the Foerster transfer, shown in equation 1.4, depends on the inverse distance r of the molecules involved to the power of six.

$$k_{FET} = \tau_d^{-1} (R_0 / r)^6 \qquad\qquad 1.4$$

τ_d is the lifetime of the excited state without acceptor and R_0 the characteristic transfer radius. R_0 is given by equation 1.5.

$$R_0 = \alpha \int_0^\infty F_h(v)\, \varepsilon_g(v)\, (v)^{-4}\, dv \qquad\qquad 1.5$$

F_h and ε_g describe the donor emission and acceptor absorption spectra, respectively. α is a proportionality constant. At the distance R_0, transfer probability of 50 %.

Spatial closeness and overlap of donor emission and acceptor absorption are the crucial parameters for efficient energy transfer. Foerster energy transfer is a radiationless process *i.e.* without emission and re-absorption of photons.

Alternatively, energy transfer can also be described by an electron exchange mechanism, so called Dexter transfer. The transfer rate k_{DET} is described by equation 1.6

$$k_{DET} = K * J * \exp(-2R_{DA}/L) \qquad 1.6$$

whereas K is a prefactor related to the specific donor-acceptor orbital interaction, J is the spectral overlap integral, R_{DA} is the donor-acceptor separation relative to L, and L are the van der Waals radii. Dexter transfer mechanism is important for the interaction of triplet states.

1.3.2. Photoinduced Charge Transfer

Photoinduced charge transfer is an interaction between an excited state and a ground state. The excited state energy is used to separate an electron-hole pair. Figure 1.9 shows an energetic scheme for such a process.[24,25] Either the donor or acceptor molecule is excited by light $h\nu > E_G$ and is transferred into an excited state. Then, an electron is transferred from the donor LUMO into the acceptor LUMO or vice versa (hole transfer from acceptor HOMO into donor HOMO). The energetic requirement is given by the equation 1.7 (electron transfer).

$$I_D^* - A_A - I_C \leq 0 \qquad\qquad 1.7$$

Where I_D^* is the ionization energy of the photoexcited donor, A_A the electron affinity of the acceptor and I_C is including all coulombic interactions.

Unlike in inorganic materials, primary photoexcitations in organic materials do not directly lead to free charge carriers in general, but to coulombically bound electron-hole pairs (excitons). The nature of these excitons in conjugated polymers was heavily discussed in the scientific community over the last years.[26] Especially, the magnitude of the exciton binding energy (i.e. weakly bound Wannier type excitons versus strongly bound Frenkel excitons) plays an important role in understanding the nature of the primary photoexcitations.
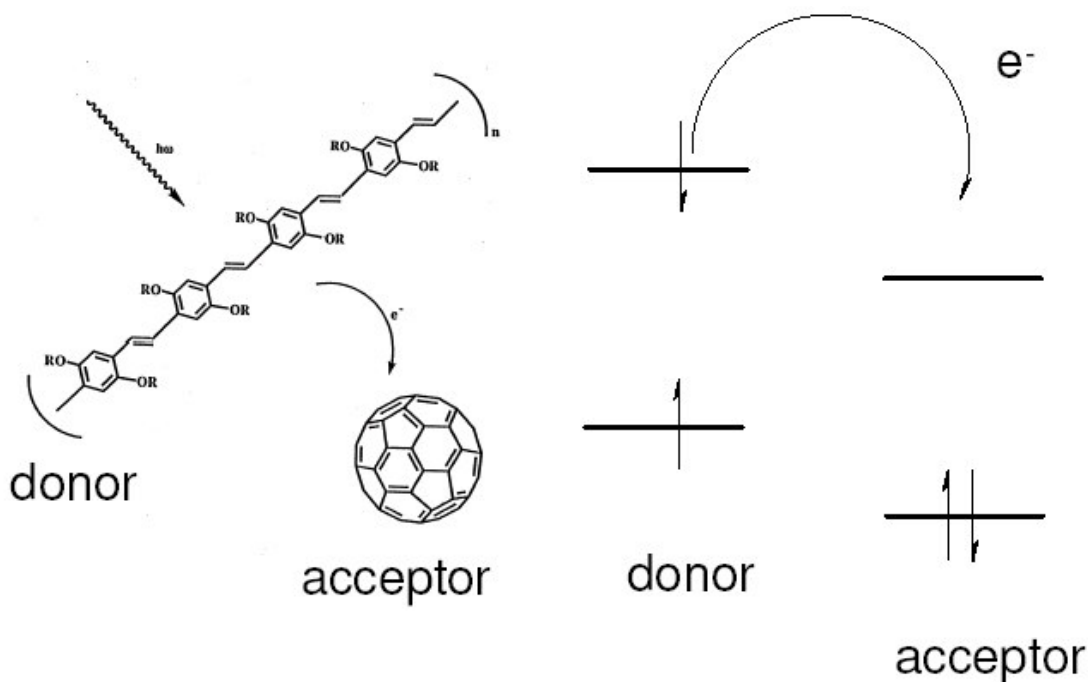
Figure 1.9: Schematic presentation for electron transfer between a PPV and a C_{60} molecule (to the left); energy diagram for an electron transfer (to the right); LUMO of the donor is above the LUMO of the acceptor.

In conjugated polymers, it has been estimated that approx. 10% of the photoexcitations lead to free charge carriers at room temperature.[27] All the other excitons decay via radiative or non-radiative recombination pathways and their energy is lost for the power conversion. One possibility to break these excitons in CP´s into charge carriers is the combination with an electron acceptor. Prominent examples for such acceptors are fullerenes.[28] Charge separation by photoexcitation with high quantum efficiency was demonstrated for many combinations of various conjugated polymers with fullerenes. The photoinduced charge transfer in such blends happens in a timescale much faster (up to 45 fs) than any competing relaxation process[29]. The efficiency can therefore be close to unity.

The separated charges are in return metastable at low temperatures and their lifetime at room temperature is sufficiently long (up to milliseconds) to be transported to the electrodes in a thin film photovoltaic device.

Whereas the absorption spectrum of these donor/acceptor blends is in the first approximation the linear combination of the single component's absorption spectra, the photoinduced charge transfer leads to drastic changes in the absorption/emission behaviour as observed via excited state spectroscopic techniques:[30]

(i)   The photoluminescence of the CP´s is heavily quenched: conjugated polymers show a strong photoluminescence as well as electroluminescence. In a blend with fullerenes, the depopulation of the photo-excited state of the conjugated polymer by the charge transfer to the fullerenes is much faster than the radiative decay ($\tau \sim 500\text{-}800$ ps). The addition of 10 % w/w fullerene to the polymer is sufficient to quench the luminescence of the conjugated polymer by a factor >100.

(ii)   Two strong light induced electron spin resonance (LESR)[31] signals are observed due to the radical nature of the photoinduced charge carriers. The signal with the g-value $g = 2.0026$ is assigned to a positive polaron on the conjugated polymer. The signal with the g value $g = 1.9997$ is assigned to the negative fullerene anion.[32,33] The g-value of the C_{60}^- is unusually low as compared to other carbon based organic radical ions.

(iii)   Two photoinduced absorption bands within the optical bandgap are observed by pump-probe techniques. These two bands are assigned to the high- (HE) and low energy (LE) absorption of the polaronic state of the conjugated polymer. The formation of the polaronic bands occurs in a time scale of 45 fs. The stimulated emission, as probe for the excited state, is quenched at a similar timescale.[20] The signal of the polaronic peaks is observable up to the µs and even ms time regime, showing the long lifetime of the photoinduced charges.[34] In the mid infrared regime (MIR), photoinduced infrared active vibrations (IRAVs) are observed as a signature of polaronic relaxation of the lattice. Due to the formation of charged polarons, symmetry forbidden A_g vibrations of the polymer are activated in the IR and thus observed in the photoinduced IR absorption spectra.[35,36,37]

(iv)   Time resolved transient photocurrent spectroscopy shows strong sensitization of the photoconductivity of the conjugated polymer upon addition of small percentage of fullerenes.[38] Both, the magnitude and the lifetime of the photocurrent are increased significantly.

These experimental results show undoubtedly the formation of separated and long living charge carriers in poly-*para*-phenylene vinylenes (PPV) or poly- thiophene (PT) -fullerene blends. The quantum efficiency of this process is close to 100 % at the donor-acceptor interface. The presented techniques are useful probes for photoinduced charge transfer in polymer-acceptor blends and are used routinely for the investigation of new materials and materials combinations.[39]

1.4. References

[1] A. J. Heeger, *Journal of Physical Chemistry B* 2001, **105**, 8475

[2] H. Shirakawa, E. J. Louis, A. G. MacDiarmid, C. K. Chiang, A. J. Heeger, *Journal of The Chemical Society: Chemical Communication* 1977, 578

[3] C. K. Chiang, C. R. Jr. Fincher, Y. W. Park, A. J. Heeger, H. Shirakawa, E. J. Louis, S.C. Gau, A. G. MacDiarmid *Physical Review Letters* 1977, **39**, 1098

[4] R. E. Peierls, "Quantum Theory of Solids", Oxford, Clarendon Press, London 1956

[5] C. K. Chiang, S. C. Gau, C. R. Jr. Fincher, Y. W. Park, A. G. MacDiarmid, *Applied Physics Letters* 1978, **33**,18

[6] W. P. Su, J. R. Schrieffer, A. J. Heeger, *Physical Review Letters* 1979, **42**, 1698

[7] W. P. Su, J. R. Schrieffer, A. J. Heeger, *Journal of Physical Review B* 1980, **22**, 2099

[8] H. Spreitzer, H. Becker, E. Kluge, W. Kreuder, H. Schenk, R. Demandt, H, Schoo, *Advanced Materials* 1998, **10**, 1340

[9] R. D. McCullough, R. D. Lowe, M. Jayaraman, D. L. J. Anderson, *Journal of Organic Chemistry* 1993, **58**, 904

[10] T.A. Chen, X. Wu, R. D. Rieke, *Journal of The American Chemical Society* 1995, **117**, 233

[11] D. Muehlbacher, Diploma thesis, University of Linz 2002

[12] J. H. Kaufman, J. W. Kaufer, A. J. Heeger, R. Kaner, A. G. MacDiarmid, *Physical Review B* 1982, **26**, 2327

[13] M. Loegdlund and W. R. Salaneck, **"**Electronic Structure of Surfaces and Interfaces in Conjugated Polymers," in *Semiconducting Polymers*, edited by G. Hadziioannou and P. F. van Hutten (VCH, Weinheim, 1999), pp. 115 - 148.

[14] H. Ishii, K. Sugiyama, E. Ito, K. Seki, *Advanced Materials* 1999, **11**, 605

[15] R. J. Gomer, G. Tryson, *Journal of Chemical Physics* 1977, **66**, 4413

[16] R. Koetz, H. Neff, K. Mueller, *Journal of Electroanalytical Chemistry* 1986, **215**, 331

[17] H. Kroto, J. Heath, S. O'Brien, R. Curl, R. Smalley, *Nature* 1985, **318**, 167

[18] R. C. Haddon, L. E. Brus, H. Raghavachari, *Chemical Physics Letters* 1986, 125,459

[19] Q. Xie, E. Pérez-Cordero, L. Echegoyen, *Journal of the American Chemical Society* 1992, **114**, 3978

[20] J. C. Hummelen, B. W. Knight, F. LePeq, F. Wudl, J. Yao, C. L. Wilkins, *Journal of Organic Chemistry* 1995, **60**, 532

[21] V. D. Mihailetchi, J. K. J. van Duren, P. W. M. Blom, J. C. Hummelen, R. A. J. Janssen, J. M. Kroon, M. T. Rispens, W. J. H. Verhees, M. M. Weink, *Advanced Functional Materials* 2003, **13**, 43

[22] C. Waldauf, P. Schilinsky, M. Perisutti, J. Hauch, C. J. Brabec, *Advanced Materials* 2003, **15**, 2081

[23] R. Pacios, J. Nelson, D. D. C. Bradley, C. J. Brabec, *Applied Physics Letters* 2003, **83**, 4764

[24] J. J. M. Halls, J. Cornil, D. A. dos Santos, R. Silbey, D. H. Hwang, A. B. Holmes, J. L. Brédas, R. H. Friend, *Physical Review B* 1999, **60**, 5721

[25] M. J. Rice and Yu N. Garstein, *Physical Review B* 1996, **53**, 10764

[26] "Primary Photoexcitations in Conjugated Polymers: Molecular Exciton versus Semiconductor Band Model" edited by N. S. Sariciftci, World Scientific Publ., Singapore (1997)

[27] P.B. Miranda, D. Moses, A. J. Heeger, *Physical Review B* 2001, **64**, 081201

[28] N. S. Sariciftci, L. Smilowitz, A. J. Heeger, F. Wudl, *Science* 1992, **258**, 1474

[29] C. J. Brabec, G. Zerza, G. Cerullo, S. De-Silvestri, S. Luzzati, J. C. Hummelen, S. Sariciftci, *Chemical Physics Letters* 2001, **340**, 232

[30] N. S. Sariciftci, A. J. Heeger, in *Handbook of Organic Conductive Molecules and Polymers*, Vol 1 (Ed. H. S. Nalwa.), Wiley, New York 1996, 414-450

[31] X. Wei, Z. V. Vardeny, N. S. Sariciftci, A. J. Heeger, *Physical Review B* 1996, **53**, 2187

[32] P. M. Allemand, G. Srdanov, A. Koch, K. Khemani, F. Wudl, Y. Rubin, F. N. Diedrich, M. M. Alvarez, S. J. Anz, R. L. Whetten, *Journal of The American Chemical Society* 1991, **113**, 2780

[33] M. C. Scharber, N. A. Schultz, N. S. Sariciftci, C. J. Brabec *Physical Review B* 2003, **67**, 085202

[34]A. F. Nogueira, I. Montanari , J. Nelson, J. Durrant, C. Winder, N. S. Sariciftci, C. J. Brabec, *Journal of Physical Chemistry B* 2003, **107**,1567

[35] E. Ehrenfreund, Z. V. Vardeny, O. Brafman, B. Horovitz, *Physical Review B* 1987, **36**, 1535

[36] K. Lee, R. A. J. Janssen, N. S. Sariciftci, A. J. Heeger, *Physical Review B* 1994, **49**, 5781

[37] Y. Furukawa, *The Journal of Physical Chemistry* 1996, **100**, 15644

[38] C. H. Lee, G. Yu, D. Moses, K. Pakbaz, C. Zhang, N. S. Sariciftci, A. J. Heeger, F. Wudl, *Physical Review B* 1993, **48**, 15425

2. Organic and Polymeric Solar Cell Devices

Organic materials gained broader interest for implementing in photovoltaic solar cells in the last decade.[1,2,3,4] Since the report of the first organic thin film solar cell by Tang,[1] several concepts have been presented using small molecules,[1,2] conjugated polymers,[5] conjugated polymer blends,[4,6,7] polymer-small molecule bilayers[8,9] and blends[3,10,11] or combinations of organic-inorganic materials.[12,13] Organic materials have several advantages like low cost synthesis and comparably easy manufacturing of thin film devices by vacuum evaporation or solution cast technologies.

Furthermore, organic thin films may show optical absorption coefficients[14] exceeding 10^5 cm^{-1}, what makes them good chromophores for optoelectronic applications.

Among these materials, conjugated polymers are of special interest due to several reasons:

(i)   The possibility of an all polymer device (plastic solar cell).

(ii)   Possibility of using solution cast processes like spin coating or doctor blade[15] or screen-printing[16] or roll to roll processes for thin film fabrication.

(iii) Solution cast processes offer an easy way for forming blends of materials, i.e. bulk heterojunction devices by processing from common solutions.

2.1 Photovoltaic Device Architectures

Bilayer devices, consisting of a p- and n-type (donor and acceptor, respectively) organic semiconductor materials, were realized for many combinations.[1,2,8,9,17,18] The conversion efficiency of such devices is limited by the charge generation at the donor/ acceptor interface. In the case of PPV type materials, the interfacial photoactive layer thickness is in the range of 5-10 nm [18,19,20,21] i.e. only excitons created within this distance to the interface can reach the heterojunction interface. This leads to the loss of photons absorbed further away from the interface and consequential to low quantum efficiencies. Antibatic behaviour of the photocurrent action spectra as compared to the optical absorption spectrum of the active material is observed due to optical filter effects. Most of the light is absorbed to far from the interface.[22]

Further, the film thickness has to be optimised for interference effects[23,24] and charge transport. With the invention of the bulk heterojunction,[3,6] blending the donor and acceptor material, the exciton diffusion bottleneck could be overcome and efficient charge generation in the whole volume of the active layer is ensured. For soluble materials, such blends can be easily realized by casting the composite film from a common solution of the donor and acceptor.

The driving force for the transport of the photoinduced charges to the opposite electrodes in such bulk heterojunction solar cells is still unclear. Several concepts have been proposed, attributing the charge transport either to electric field induced drift of charge carriers or concentration gradient induced diffusion of them, respectively.[25]

The metal-insulator-metal picture (MIM),[26] was introduced by Parker to describe current-voltage curves of polymeric light emitting diodes. The charge transport is attributed to an electric field induced drift. The work function difference of the contacts induces the electric field.

The diffusion-limited concept sees the diffusion of charge carriers induced by concentration gradients as driving force for transport. The directionality of the diffusion is attributed to selective electrodes.[27] Common for both concepts is that the charge transport is directed by the asymmetry of the electrodes properties.

Recently, Gregg and Hanna[28] proposed a new model of an excitonic solar cell, describing all types of organic solar cells. The driving force for the charge transport is assigned to the chemical potential gradient, formed by the charge generation at the interface. The charges are moving away from this interface to the opposite electrodes. In contrast to the classical inorganic solar cells, the built in field is not limiting the open circuit potential, but the photoinduced quasi fermi level difference for positive and negative charges.
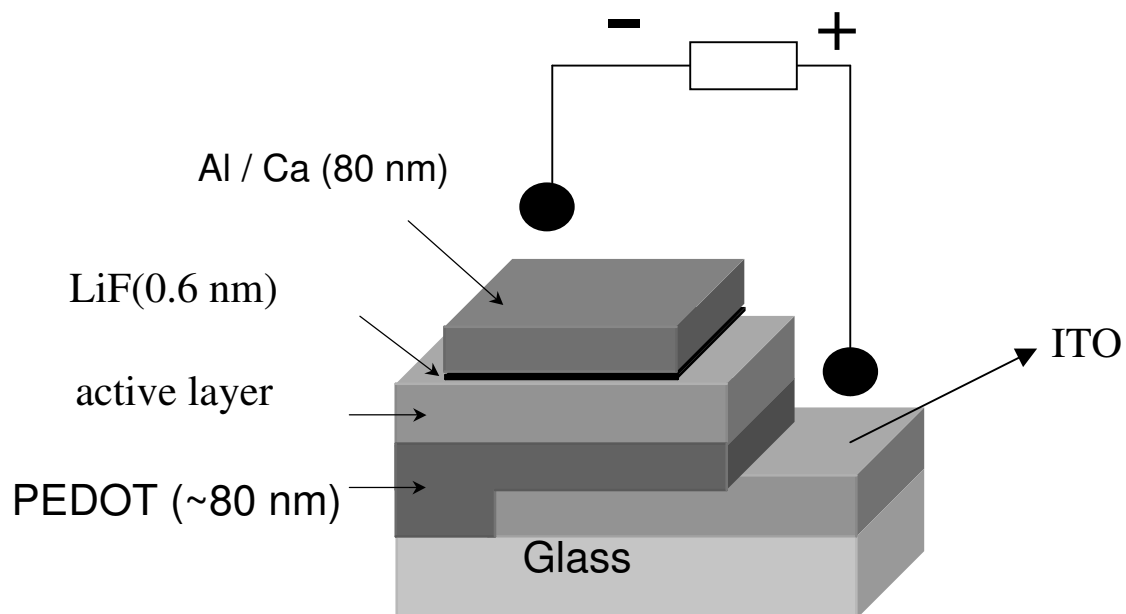
Figure 2. 1: Device architecture for a thin film bulk heterojunction photovoltaic device.

Figure 2.1 shows the device structure, which is typically used today for bulk heterojunction devices. As positive electrode, indium-tin-oxide ITO coated glass or plastic is used. ITO belongs to the class of transparent and conductive oxides (TCO) and is widely used as electrode in photovoltaic and LED application.

The ITO is further coated with a layer of poly-(3,4-ethylene-dioxy)-thiophene: polystyrene-sulfonic acid (PEDOT:PSS) blend, see Figure 2.2. PEDOT is, highly p-doped, a water-soluble conjugated polymer. In solid state, PEDOT:PSS can be considered as a metal and therefore as a quasi electrode. The PEDOT: PSS influences and increases the work function of the positive electrode. The workfunction of PEDOT: PSS is at ~ 5eV vs. vacuum,[29] whereas the workfunction of ITO is rather undefined and reported to be between 4.7 and 4.9 eV dependent on the treatment.[30,31] Both materials, the ITO and the PEDOT:PSS are highly transparent in the region between 350 and 900 nm.
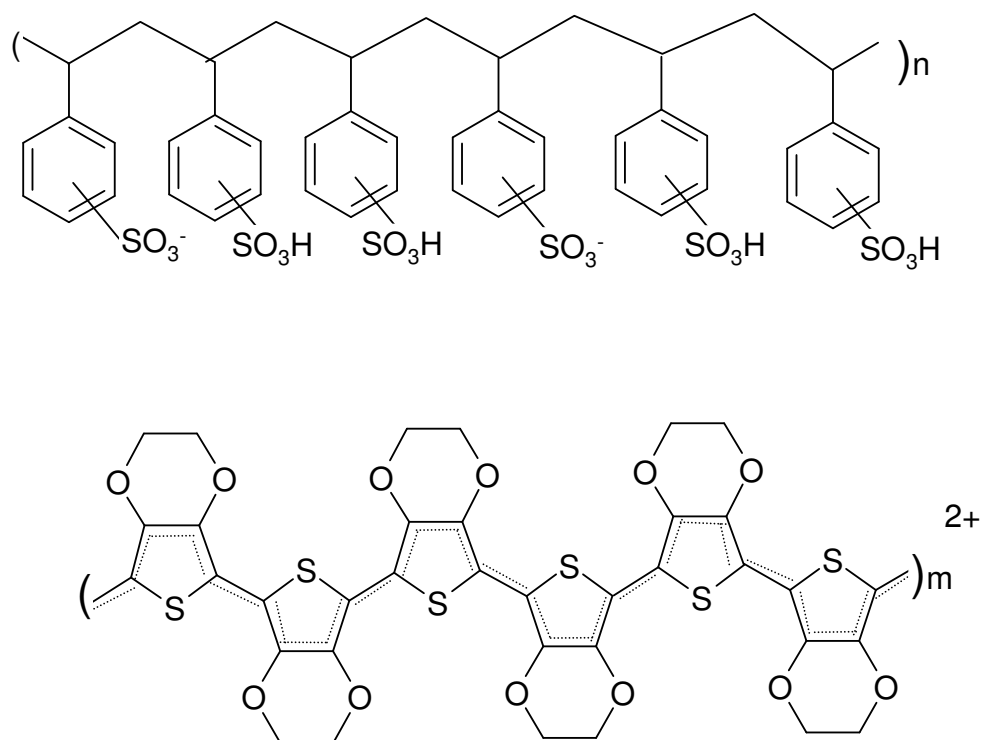
Figure 2. 2: Chemical structure of pEDOT-PSS (poly-(3,4- ethylendioxy)-thiophene:polystyrene-sulfonic-acid).

On top of the bottom electrode, the active layer, consisting of the conjugated polymer-fullerene mixture, is coated. An excess of fullerene is favourable for the percolated transport of the negative charges. So, an optimised polymer to fullerene ratio of 1:4 w/w has been reported for MDMO-PPV and PCBM and 1:2 for P3HT: PCBM, respectively. These two systems show power conversion efficiencies of 2.5 % for MDMO-PPV [10,32] and over 3 % for P3HT.[33,34]

As top (negative) electrode, a metal layer, like Al, Ca or Au, is evaporated.[35] An interfacial layer of thermally evaporated LiF was demonstrated to be favourable between the organic and the metal layer in combination with Al and Au.[36] LiF is known to form better electron injecting/collecting contacts with organic thin films in LED devices. [37,38]

2.2 Improving the Solar Cell Device Efficiency

The photovoltaic power conversion efficiency η_e is defined by equation (2.1).

$$(2.1) \qquad \eta_e = \frac{V_{OC} * I_{SC} * FF}{P_{in}}$$

$$(2.2) \qquad FF = \frac{I_{mpp} * V_{mpp}}{V_{OC} * I_{SC}}$$

V_{OC} is the open circuit voltage, I_{SC} is the short circuit current, and FF is the fill factor, defined after equation 2.2 and P_{in} the incident light power. The incident light power is standardized for solar cell testing as AM 1.5 (air mass 1.5) spectrum. This is the solar irradiation (diffuse and direct) on sea level on a 37° tilted, sun facing surface and attenuated by the earth atmosphere.[39] In incident power is 1000 W m^{-2}. I_{mpp} and V_{mpp} are the current and voltage at the maximum power point in the fourth quadrant of the current-voltage characteristics. For the testing in the laboratory, solar simulators are used to imitate the AM1.5 solar irradiation.

The critical cell parameters will now discussed in detail:

- *Open Circuit Voltage*: The thermodynamic limit for the V_{OC} is given by the bandgap of the active materials. The band gap is limiting the splitting of the quasi fermi level of electron and hole, induced by the light absorption.[40] For heterojunction devices, the energetic distance between the HOMO of the donor and the LUMO of the acceptor has to be considered as the limitation for the V_{OC}.

  For bulk heterojunction devices containing fullerene acceptor, it was shown that the open circuit potential is directly dependent on the LUMO level of the fullerene derivative. The dependence of the V_{OC} on the top electrode metal workfunction is shown to be neglible.[35] The metals electrodes Ca, Al, Ag and Au were used with a workfunction range from 5.1 to 2.9 eV vs. vacuum. The experimental findings were attributed to Fermi level pinning of the metal to the C_{60} anion.

  Mihailetchi, Blom et al[41] studied the same system, using LiF/Al, Ag, Au and Pd as electrode materials. They concluded a strong dependence of the V_{oc} on the metal

workfunction for non ohmic contact, but no dependence in the case of an ohmic contact. For the non ohmic contact, a MIM like picture is favoured. For the ohmic contact case, Fermi level pinning is assumed.

Ramsdale[42] et al observed a linear relation of the negative electrode workfunction and the observed open circuit voltage for donor-acceptor polyfluorene bilayer devices. An additional contribution of 1 V to the workfunction difference of the electrodes was observed. This contribution was attributed to the photoinduced dipole formed at the interface due to the charge transfer.

ITO coated with PEDOT: PSS is regularly used as positive contact. The workfunction of the PEDOT can be manipulated by adjusting the doping level. A strong dependence of the open circuit voltage on the work function of the PEDOT:PSS[43] was demonstrated. In contrast to this, Kwanghee Lee et al[44] and Ole Inganäs et al[45] observed a linear dependence of the open circuit voltage on the HOMO level of the polymeric donor used in the bulk-heterojunction device.

- *Short Circuit Current*: The I_{SC} is determined by the amount of absorbed light and the internal conversion efficiency. Experimentally accessible is the external quantum efficiency or incident photon to current efficiency, IPCE [%]. It is defined and calculated after equation 2.3.

$$\text{IPCE } [\%] = \frac{\#_{El}}{\#_{Ph}} = \frac{1240 * I_{SC} \, [\mu A \, cm^{-2}]}{\lambda \, [nm] * P_{In} \, [W \, m^{-2}]} \qquad 2.3$$

λ [nm] is the incident photon wavelength, I_{SC} [$\mu A \, cm^{-2}$] is the photocurrent of the device and P_{In} [W m^{-2}] is the incident power. IPCE values up to 76 % at the absorption maximum are reported for bulk heterojunction solar cells. [33,34] The internal quantum efficiency is estimated to be close to 100 % for conjugated polymer-fullerene blends.[32] For an increase in the photocurrent, the light absorption has to be increased.

The absorption profile of the active layer shows a strong mismatch to the solar photon flux, as compared in Figure 2.3. Materials absorbing in the maximum of the solar photon flux, between 600 and 800 nm, are needed to increase the short circuit current. New concepts to overcome this problem are the major part of this thesis.
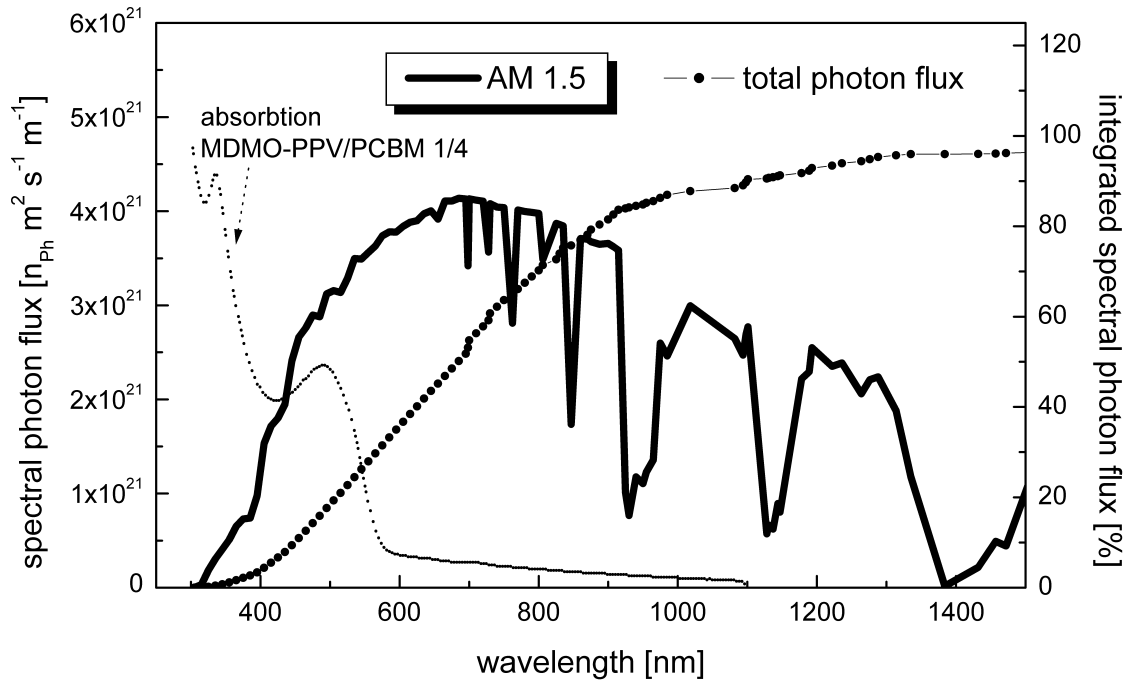
Figure 2. 3: The terrestrial AM1.5 sun spectrum (———) and the integrated spectral photon flux (starting from 0 nm) (-•-) in comparison with the absorption (---) of an MDMO-PPV:PCBM 1:4 blend.

- *Fill factor* FF: The FF is defined by equation 2.2 and describes the quality of the diode in the 4th quadrant. The fill factor is mainly influenced by the series and shunt resistances, see the simplified equivalent circuit for a photovoltaic device in Figure 2.4. The equivalent circuit is described by equation 2.4

$$I = I_0 (\exp(\frac{q}{nkT}(U - IR_S)) - 1) + \frac{U - IR_S}{R_{SH}} - I_{PH} \qquad 2.4$$

The current *I* consist of following three parts:

i) *Diode current*: The diode is described by the exponential Shockley equation. I_0 is the saturation current of the diode, q the elementary charge, n the diode ideality factor, k the Boltzmann constant and T the temperature. The applied voltage U is reduced by the series resistance R_S of the diode. R_S should ideally be low.

ii) *The shunt current* through the shunt resistance R_{SH}. The applied voltage is again reduced by the series resistance. R_{SH} should be ideally high.

iii) *The photo generated current* I_{PH}, representing the current generation of the solar cell under illumination.
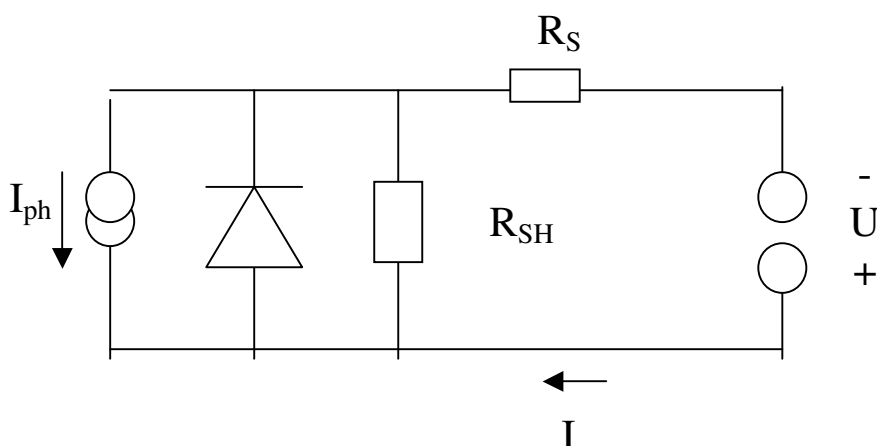
Figure 2. 4: Equivalent circuit for a single junction solar cell. The photogenerated current I_{ph} shows in the inverse direction of the diode. Shunt resistance R_{SH} and series resistance R_S are important for the fill factor. Ideally, series resistance should be low and shunt resistance high.

The nanomorphology of donor/acceptor composite is known to have an important influence for the device efficiency.[46] The conditions for the film preparation, i.e. the choice of solvent, are crucible for the domain size in the interpenetrating network. On the one hand, a large interface between the donor/acceptor phases is desired for efficient charge separation. The domain size should be not larger the exciton diffusion length (approx. 10 nm for most CP´s) On the other hand, interpenetrating paths of the individual phases are required for the charge transport to the electrodes. It is also expected that a larger interface increase recombination of charge carriers. The blend morphology is investigated by several techniques like atomic force microscope[47], transmission electron microscope,[48,49] scanning electron microscopy,[47] photoluminescence[47] and near field optical microscope. It is generally found that smaller domain sizes lead to higher efficient devices in the case of solution cast processes.

Several approaches were suggested in the literature to control or manipulate the morphology:

- "*Double cables*" are materials, which are consisting of a conjugated polymer backbone with acceptor molecules covalently attached. They can be seen as a molecular heterojunction.[50] The field of double cables has been recently reviewed be Cravino et al.[51]

- *Block copolymers* are materials which consist of alternating conjugated donor and fullerene bearing blocks.[52] It was shown that these materials are able to form supramolecular self-assemblies.[53]

- The composite nanomorphology can be influenced by changing the *conditions during film formation.* [10,54,55] Shaheen et al observed for the system MDMO-PPV: PCBM power conversion efficiencies of 1 % devices cast from toluene and 2.5 % for devices cast from chlorobenzene.

- *Diffusion bilayers* were demonstrated, formed by either lamination of a donor-rich and an acceptor-rich layer[4] or by temperature induced diffusion of an acceptor molecule into the donor polymer matrix.[56],[57]

- Jenekhe et al demonstrated the formation of encapsulated *fullerene nanoparticles*.[58]

- Kietzke et al showed the formation of *nanospheres* by a miniemulsion process to control phase separation and demonstrated the application for photovoltaic devices.[59]

2.3 Production of Bulk Heterojunction Devices

2.3.1 Experimental

Organic thin film photovoltaic devices are fabricated in a sandwich structure, as shown in Figure 2.1. As substrates, glass sheets of 1.5x1.5 cm^2 covered with indium tin oxide ITO, from Merck KGaA Darmstadt, with an ITO thickness of d = 125 nm and a sheet resistance <15 Ωcm^{-2} are used.

The ITO is structured by etching with an acidic mixture of HCl$_{konz}$:HNO$_{3\ konz}$:H$_2$O 4.6:0.4:5 for ~ 15 minutes. Half of the substrate is coated with a commercial varnish to protect the active ITO area against the etching acid. The varnish is removed afterwards by acetone in an ultrasonic bath. Then, the ITO is cleaned in an ultrasonic bath again with acetone and finally in isopropanole as cleaning solvents.

On the ITO substrate, a layer of PEDOT:PSS, Baytron PH, purchased from H.C. Starck, is spin cast twice. PEDOT:PSS, for the structure see Figure 2.2 is an aqueous dispersion with a mean particle size of 80 nm. (0.5 w%, PEDOT: PSS 2:3).

The active layers are also spin cast. Solutions were stirred and heated up to ~ 50° for at least twelve hours. For the spin casting, the substrate is mount in the spincoater, Spincoater Model P 6700 Series from SCS Inc. For all spin casting processes a two-step program is used, if not otherwise referred. First spinning speed is 1500 rpm for 40 sec, followed by 2000 rpm for 30 sec. The spin cast process is done in ambient conditions unless otherwise referred. The following evaporations and the characterisation of the devices are done in an argon glovebox, MB 200 from Mbraun.

The top electrode is a two-layer deposition of LiF/Al. The deposition is done by thermal evaporation at a pressure $\leq 10^{-5}$ mbar. Tungsten boats are used as source. The average thickness of the LiF and Al layer is 0.6 nm and 60-100 nm, respectively. The deposition rate of the materials is monitored by a quartz balance, Intellemetrics IC 600. The evaporation is done through a shadow mask in order to define the device area.

2.3.2 Device characterization

Thin layers are characterized by an atomic force microscope (AFM), Dimension 3100" instrument from Digital Instruments, Santa Barbara, CA, in the tapping mode. The AFM is also used to determine the film thickness, by measuring the height difference at a scratch.

I-V characteristics of the devices are measured in the dark and under illumination from a Steuernagel solar simulator (with a metal halogen lamp as light source with an AM 1.5 filter) under an illumination density of 80 or 100 mW cm^{-2}, respectively. The I-V curves are measured with a Keithley 2400. ITO is connected to the positive electrode, Al to the negative. The curves are recorded by continuously sweeping from –2V to +2V and recording data points in 10 mV steps.

The spectral photocurrent is detected by a Lock-in amplifier. The sample is illuminated with monochromatic light with ~ 200 μW cm^{-2} and a FWHM of ~ 4 nm from a 80 W Xenon lamp. The spectrum of the light source is measured each time with a calibrated monocrystalline silicon diode.

2.3.3. PPV: fullerene bulk heterojunction devices

The material combination of poly-para-phenylene vinylene and fullerene is probably the most and best investigated organic heterojunction solar cell. Bulk heterojunction of MDMO-PPV and PCBM were investigated by several groups in the recent years and the power conversion efficiency could be pushed up to 2.5 %.[10,25,32,35,60,61,62,63,64]

The short-circuit current shows nearly linear dependence on the illumination dependence P_{in}; $I_{sc} = P_{in}{}^{\alpha}$, with $\alpha = 0.92$.[65,66] This power law dependence with α close to one shows that bimolecular recombination is negligible.

The open circuit voltage V_{OC} shows a logarithmic behaviour on the illumination dependence,[25] as predicted for classical pn junction by Equation 2.5.

$$V_{OC} = \frac{k_b T}{q} * \ln(\frac{I_{SC}}{I_0}) \qquad (2.5)$$

where k_b is the Boltzmann constant, T the temperature, q the elementary charge and I_0 the saturation current density. The saturation current shows an exponential dependence on the temperature, see Equation 2.6.

$$I_0 \propto e(-\frac{E_g}{k_b T}) \qquad (2.6)$$

The incident photon to current efficiency (IPCE) is 50 % at the absorption maximum of 500 nm. The internal quantum efficiency IQE is estimated for thin devices to be close to 1.[32] Further improvements of the photocurrent are only possible by increasing the amount of absorbed light. For thin film devices with a reflecting back electrode, the absorption is not a logarithmic function of the absorber thickness, but highly influenced by interference effects. Hoppe et al[67] calculated the absorption profile vs. absorber thickness for the combination MDMO-PPV: PCBM 1:4 and found a nearly steplike function. A conversion efficiency of 1, independent of the thickness, was assumed for this calculation.

For thicker devices, parasitic recombination is expected. Only charge carriers, which are created within their mean free path to the electrode are contribution to the photocurrent. In other words, only charge carriers, which can reach the electrode in their lifetime.

The influence of the active layer thickness on the photocurrent and photovoltaic efficiency is discussed in the following. The composition of the blend is kept constant.

Figure 2.5 compares the light and dark curves of MDMO-PPV: PCBM 1:4 solar cells for device thicknesses from 34.5 to 127.5 nm. The photovoltaic efficiency and device parameter are summarized in Table 2.1.
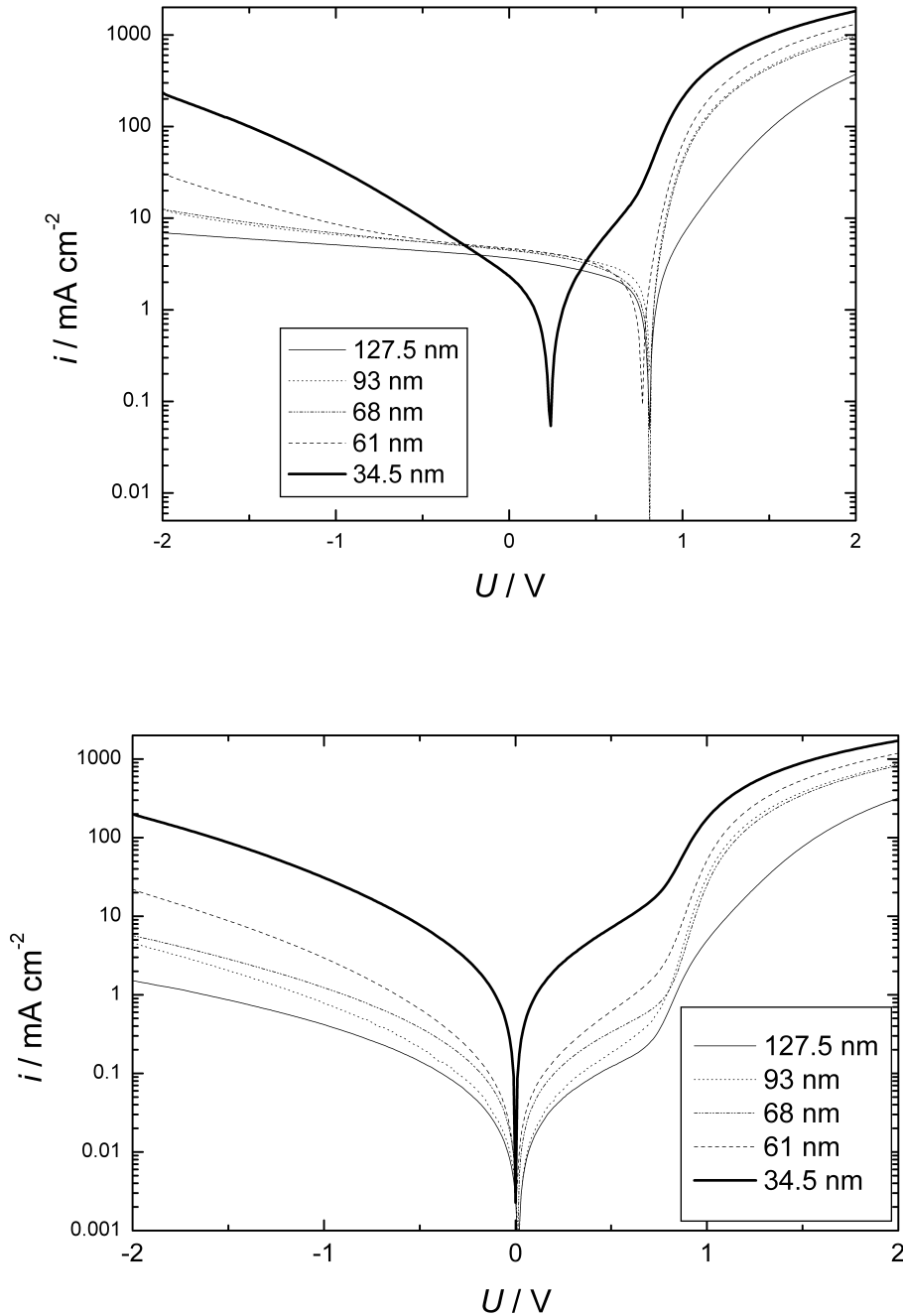
Figure 2. 5: Thickness dependence of the I-V curves under illumination with 80 mW cm^{-2} (upper graph) and in the dark (lower graph) for MDMO-PPV: PCBM 1:4 w/w devices.

The rectification at +/- 2V is found to increase with the device thickness. Such behaviour can be assigned to a decreased saturation current I_0 and to an increased shunt resistance.

The maximal power conversion efficiency is found for a thickness of 93 nm, similar as found by Shaheen et al. The I_{SC} and FF show a maximum for the thickness of 93 nm. The Isc and FF are decreasing for the thicker device. This is assigned to bimolecular recombination and an increased

series resistance. The V_{OC} is constant with the thickness, only decreasing for the thinnest device due to shorts.

Table 2. 1: Diode and photovoltaic parameters are shown as a function of the active layer thickness for a MDMO-PPV: PCBM 1:4, spin cast from chlorobenzene, illumination density is 80 mW cm^{-2}

d / nm	V_{OC} / V	I_{SC} / mA cm^{-2}	FF	Efficiency / %	R (+/- 2)
127.5	0.81	3.67	0.44	1.6	210
93	0.81	4.57	0.50	2.3	190
68	0.81	4.46	0.42	1.9	146
61	0.77	4.51	0.44	1.9	53
34.5	0.24	2.23	0.27	0.2	8
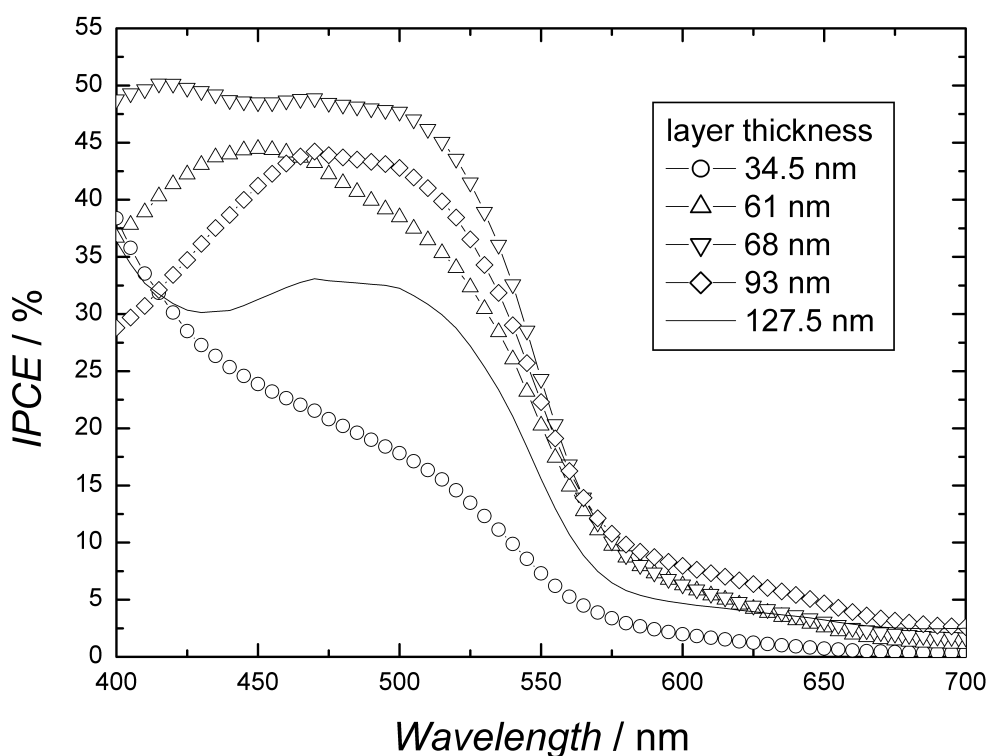
Figure 2. 6: Photocurrent spectra (IPCE) for MDMO-PPV: PCBM 1:4 devices as a function of layer thickness.

Figure 2.6 shows the photocurrent spectra for the MDMO-PPV: PCBM devices for different thicknesses. As predicted from optical simulation, the shape of the photocurrent spectrum is changing with the thickness. In bulk heterojunction devices, the photogeneration rate of charge

carriers should be constant throughout the thickness. Optical filter effects can be ruled out.[22] It is concluded that the difference of shape are originating from interference effects.

2.3.4 P3HT: fullerene bulk heterojunction devices

Polythiophenes are among the best and most investigated conjugated polymers.[68] The possibility of synthesis of polymers with regioregular-ordered side chains leads to high mobility polymers. These polymers show high charge carrier mobilities.[69,70]

Until recently, polythiophenes could not be successfully implemented in bulk heterojunction photovoltaic cells. In the year 2002, Brabec et al and Padinger et al reported independently power conversions efficiency of 3.5 % from P3HT: PCBM solar cells.[33,34] P3HT shows a broader and red shifted absorption compared to MDMO-PPV, resulting in a doubling of the photocurrent under AM 1.5 conditions.

Further, the higher mobility of P3HT allows thicker absorbing layer without recombination losses due to limited transport. IPCE of 76 % at the absorption maximum are reported.

Of special interest is the so-called post production treatement reported by Padinger et al. The device is annealed at a temperature of 80° and simultaneously a voltage of 2.7 V is applied for 4 min. This leads to an improvement in the power conversion efficiency from around 0.5 % to 3.5 %. The detailed photovoltaic data are given in Table 2.2.

Table 2. 2: Photovoltaic parameter for P3HT: PCBM 1:2 devices from chlorobenzene, illumination with 80 mW cm^{-2}.

	V_{oc} / V	I_{sc} / mA cm^{-2}	FF	Efficiency / %
Without treatment	0.3-0.7	2.5	0.3	0.3-0.7
Thermal treatement	0.49	8.3	0.55	2.8
Post production treatment	0.56	9.0	0.6	3.7

Within this thesis, the effect of the post production treatment is investigated. Part of this work was carried out at the *Interuniversity Microelectronic Center* IMEC in Leuven, Belgium. The absorbance (in reflection geometry) and photocurrent spectra were measured with an integrating sphere. Devices with an active are of ~1 cm-2 were prepared for these measurements. The devices are sealed with a glass plate.

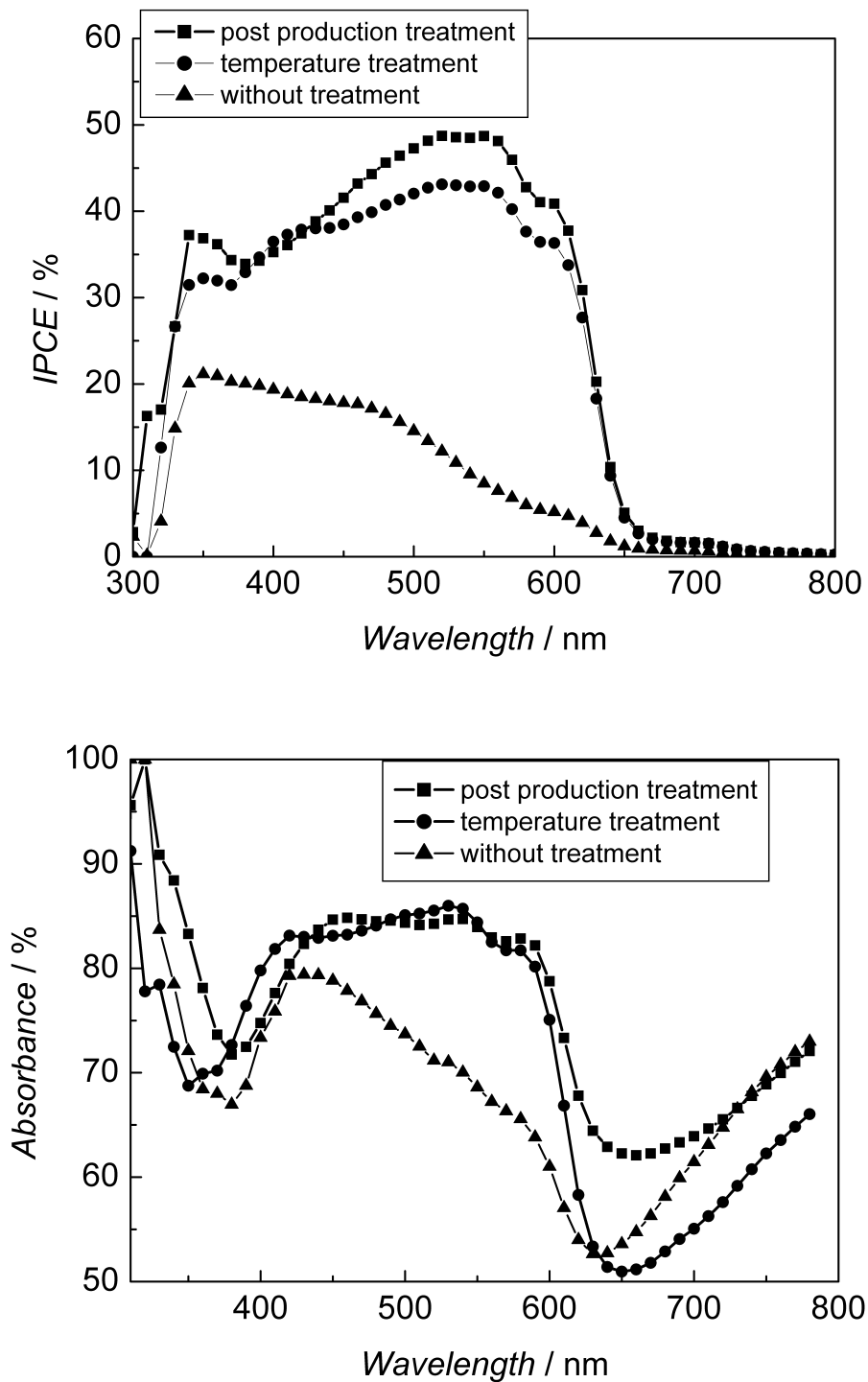**Figure 2. 7:** Photocurrent spectrum (left) and absorbance spectrum in reflection geometry (right) of P3HT: PCBM 1: 2 devices, spin cast from chlorobenzene.

Figure 2.7 shows the photocurrent and absorbance spectra of P3HT: PCBM blend devices with and without post production treatment. The maximum of the photocurrent spectrum is shifted after the thermal annealing from 350 to 550 nm, an additional shoulder is rising at 600 nm. The

same effect is observed in the absorbance for this device. The additional electrical treatment is not changing the photocurrent spectrum nor the absorbance as compared with the thermal treatment. The latter is increased in its strength.

The increased and structured absorption in the range from 450 to 650 nm is assigned to an interchain -ordered phase in polythiophene.[71]

Blend of P3HT and PCBM with a high fullerene content (> 50 %) show as spin cast only weak absorptions in the red. The absorption is less than the simple sum of the individual components absorption. This absorption can be regained by thermal annealing. One might conclude, that the thermal treatment provides the activation energy for the formation of the interchain ordered phase.

The electrical treatment does not change the absorption properties of the material. Generally, the diode behaviour of the device is improved by the post production treatment.

The thickness dependence of the photovoltaic parameters for P3HT: PCBM devices is shown in Table 2.3. Untreated and thermally annealed devices are compared in a range from 52 to 240 nm.

Table 2. 3: Photovoltaic and diode parameter of P3HT: PCBM devices as a function of active layer thickness, thermally treated devices are annealed at 120° C for 5´.

	Untreated					Thermally annealed				
d / nm	U /V	i / mA cm^{-2}	FF	$Eff.$ / %	R (+/-2 V)	U /V	i / mA cm^{-2}	FF	$Eff.$ / %	R (+/-2 V)
240	0.64	1.9	0.36	0.44	1714	0.41	9.5	0.36	1.4	213
195	0.69	1.6	0.34	0.38	526	0.59	6.1	0.50	1.8	231
124	0.61	1.5	0.30	0.27	87	0.62	4.2	0.41	1.1	72
52	0.47	1.8	0.30	0.25	71	0.58	3.1	0.41	0.7	58

For the untreated devices, the highest efficiency is observed for the thickest device, but the overall efficiency is low. The low rectification values reflect bad diode behaviour due to shunts, which become less probable for thicker devices. After the thermal treatment, the devices with a thickness over >100 nm show good diode behaviour. These devices have sufficient high parallel resistance. The efficiency maximum is observed for a thickness of 195 nm. For the thicker device, the Isc is increasing, but losses in Voc and FF are observed.

The short circuit current is increasing with the active layer thickness. This is also reflected in the photocurrent spectra for the annealed devices, see Figure 2.8.
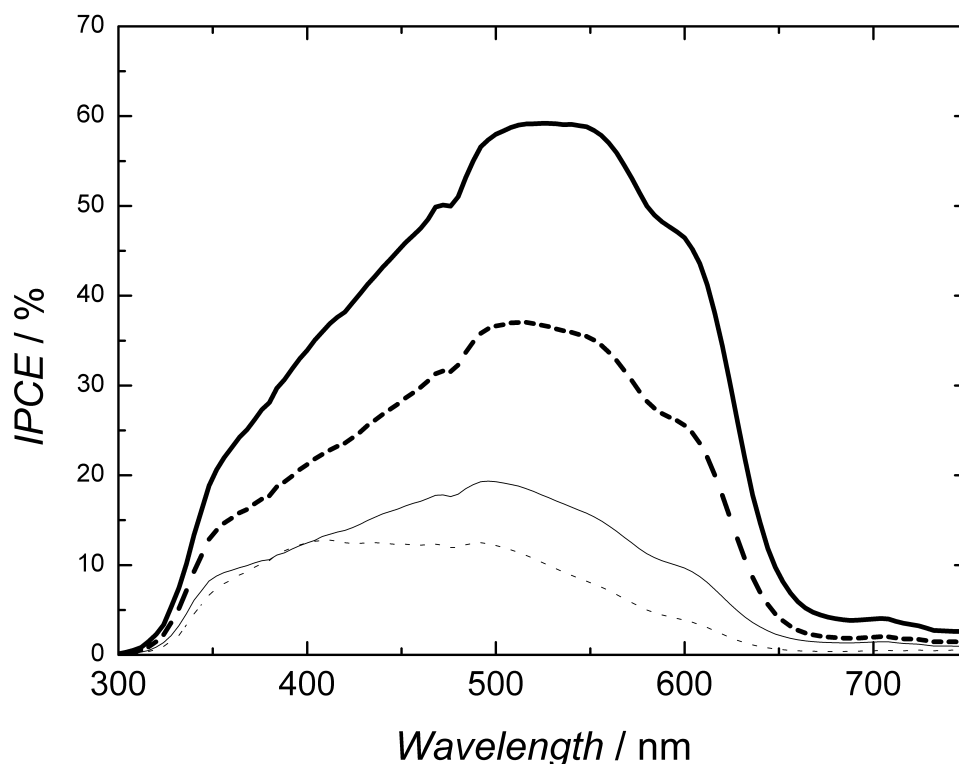
Figure 2. 8: Thickness dependence of the IPCE spectra for P3HT: PCBM 1:2 devices, spin cast from chlorobenzene and thermally treated, 5′ 120°. 240 nm for the thick full line, 195 nm for dashed line, 124 nm for the thin line and 52 nm for the dotted line.

P3HT: PCBM blend devices allow generally higher thicknesses compared to MDMO-PPV. This observation might be assigned to the higher charge carrier mobility in the P3HT phase. The increased thickness lead to increased absorption and consequently to higher external quantum efficiencies. In contrast, P3HT: PCBM device show a lower Voc after the post production treatment in the range of 600 mV. The diode behaviour of these devices is excellent, what is reflected in the extraordinary high FF.
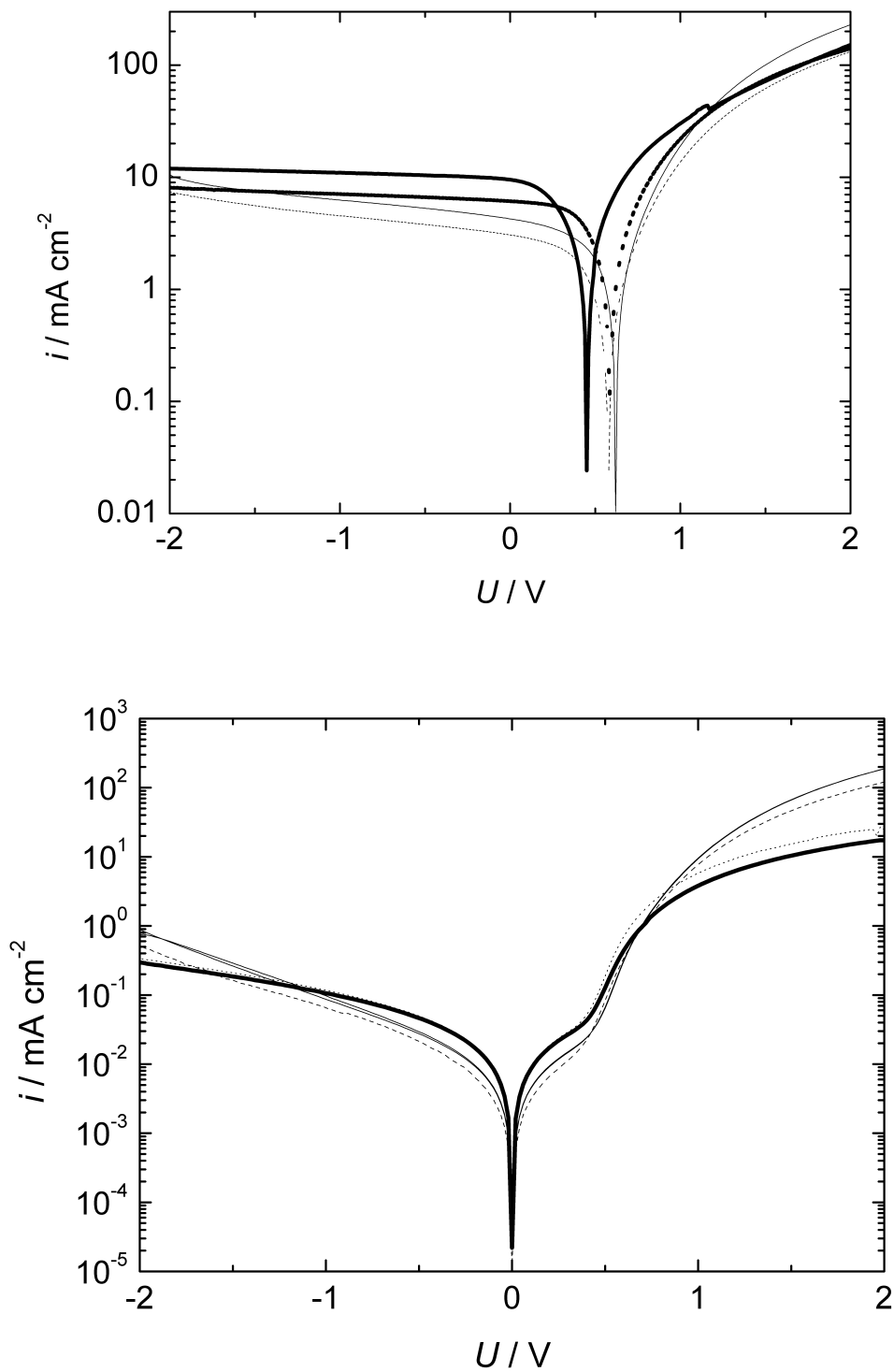
Figure 2. 9: I-V characteristics as a function of active layer thickness is shown for P3HT: PCBM 1:2 devices, spin cast from chlorobenzene and thermally treated, 5′ at 120 °. Active layer thickness are 240 nm (thick full line), 195 nm (dashed line), 124 nm (thin line) and 52 nm (dotted line).

2.4 References

[1] C. W. Tang, *Applied Physics Lett*ers 1986, **48**, 183

[2] D. Wöhrle, D. Meissner *Advanced Materials* 1991, **3**, 129

[3] G. Yu, J. Gao, J.C. Hummelen, F. Wudl, A. J. Heeger, *Science* 1995**, 270**, 1789

[4] M. Granström, K. Petritsch, A. C. Arias, A. Lux, M.R. Andersson, R. H. Friend, *Nature* 1998, **395**, 257

[5] H. Antoniadis, B. R. Hsieh, M. A. Abkowitz, S. A. Jenekhe, M. Stolka, *Synthetic Metals* 1994, **62**, 265

[6] J. J. M. Halls, C. A. Walsh, N. C. Greenham, E. A. Marseglia, R. H. Friends, S. C. Moratti, A. B. Holmes, *Nature* 1995, **376**, 498

[7] G. Yu, A. J. Heeger, *Journal of Appied Physics* 1995, **78**, 4510

[8] S. A. Jenekhe, S. Yi, *Applied Physics Letters* 2000, **77**, 2635

[9] A. J. Breeze, A. Salomon, D. S. Ginley, B. A. Gregg, H. Tillmann, H. H. Hoerhold, *Applied Physics Letters* 2002, **81**, 3085

[10] S. E. Shaheen, C. J. Brabec, N. S. Sariciftci, F. Padinger, T. Fromherz, J. C. Hummelen, *Applied Physics Letters* 2001, **78**, 841

[11] J. J. Dittmer, E. A. Marseglia, R. H. Friend, *Advanced Materials* 2000, **12**, 1270

[12] B. O. Reagan, M. Graetzel, *Nature* 1991, **353**, 737

[13] N. C. Greenham, X. Peng, A. P. Alivisatos, *Physical Review B* 1996, **54**, 17628

[14] H. Hoppe, N. S. Sariciftci, D. Meissner, *Molecular Crystalls Liquid Crystals* 2002, **385**, 113

[15] C. J. Brabec, F. Padinger, J. C. Hummelen, R. A. J. Janssen, N. S. Sariciftci, *Synthetic Metals* 1999, **102**, 861

[16] S. E. Shaheen, R. Radspinner, N. Peyghambarian, G. E. Jabbour, *Applied Physics Letters* 2001, **79**, 2996

[17] N. S. Sariciftci, D. Braun, C. Zhang, V. I. Srdanov, A. J. Heeger, G. Stucky, F. Wudl, *Applied Physics Letters* 1993, **62**, 585

[18] J. J. M. Halls, K. Pichler, R. H. Friend, C. S. Moratti, A. B. Holmes, *Applied Physics Letters* 1996, **68**, 3120

[19] T. Stuebinger, W. Bruetting, *Journal of Applied Physics* 2001, **90**, 3632

[20] A Haugeneder, M. Neges, C. Kallinger, W. Spirkl, U. Lemmer, J. Feldmann, U. Scherf, E. Harth, A. Guegel, K. Muellen*, Physical Review B* 1999, **59**, 15326

[21] M. Theander, A. Yartsev, D. Zigmantas, V. Sundstroem, W. Manno, M. R. Andersson, O. Inganaes, *Physical Review B* 2000, **61**, 12957

[22] M. G. Harrison, J. Gruener, G. C. W. Spencer, *Physical Review B* 1997, **55**, 7831

[23] L.A.A. Pettersson, L. S. Roman, O. Inganas, *Journal of Applied Physics* 1999, **86,** 487

[24] J. Ronstalski, D. Meissner, *Solar Energy Materials and Solar Cells* 2000, **63**, 37

[25] V. Dyakonov, *Physica E* 2002, **14**, 53

[26] I. D. Parker, *Journal of Applied Physics.* 1994, **75**, 1656

[27] D. Meissner, J. Ronstalski, *Synthetic Metals* 2001, **121**, 1551

[28] B. A. Gregg, M. C. Hanna, *Journal of Applied Physics.* 2003, **93**, 3605

[29] N. Koch, A. Kahn, J. Ghijsen, J. J. Prieaux, S. Schwartz, R. L. Johnson, A. Elschner, *Applied Physics Letters* 2003, **82**, 70

[30] G. Greczynski, Th. Kugler, M. Keil, W. Osikowicz, M. Fahlman, W. R. Salanck*, Journal of Electron Spectroscopy and Related Phenomena* 2001, **121**, 1

[31] J. S. Kim, M. Granstrom. R. H. Friend, N. Johansson, W. R. Salaneck, R. Daik, W. J. Feast, F. Cacialli*, Journal of Applied Physics* 1998**, 84**, 6859

[32] C. J. Brabec, N. S. Sariciftci, J. K. Hummelen, *Advanced Functional Materials.* 2001, **11**, 15

[33] P. Schilinsky, C. Waldauf, C. J. Brabec, *Applied Physics Letters* 2002, **81**, 3885

[34] F. Padinger, R. Rittberger, N. S. Sariciftci, *Advanced Functional Materials.* 2003, **13**, 85

[35] C. J. Brabec, A. Cravino, D. Meissner, N. S. Sariciftci, T. Fromherz, T. Rispens, L. Sanchez, J. C. Hummelen, *Advanced Functional Materials.* 2001, **11**, 374

[36] C. J. Brabec, S. E. Shaheen, C. Winder, N. S. Sariciftci, P. Denk, *Applied Physics Letters.* 2002, **80**, 1288

[37] L. S. Hung, C. W. Tang, M. G. Mason, *Applied Physics Letters* 1997, **70**, 151

[38] G. E. Jabbour, Y. Kaxabe, S. E. Shaheen, J. F. Wang, M. M. Morrell, B. Kippelen, N. Peyghambarian, *Applied Physics Letters* 1997, **71**, 1762

[39] ASTM E 892

[40] Peter Würfel, "Physik der Solarzelle", Spektrum Verlag, 2000

[41] V. D. Mihailetchi, P. W. M. Blom, J. C. Hummelen, M. T. Rispens, *Journal of Applied Physics* 2003, **94**, 6849

[42] C. M. Ramsdale, J. A. Barker, A. C. Arias, J. D. MacKenzie, R. H. Friend, N. C. Greenham*, Journal of Applied Physics.* 2002, **92**, 4266,

[43] H. Frohne, S. Shaheen, C. J. Brabec, D. Mueller, N. S. Sariciftci, K. Meerholz, *Chem Phys Chem* 2002, **9**, 796

[44] H. Kim, S. H. Jin, H. Suh, K. Lee, *Proceedings of the SPIE 2003*, in press

[45] A. Gadisa, M. Svensson, M. Andersson, O. Inganäs, *Applied Physics Letter* 2004, **84**, 1609

[46] P. Peumans, S. Uchida, S. Forrest, *Nature* 2003, **425**, 158

[47] H. Hoppe, M. Niggeman, C. Winder, A. Hirsch, J. Kraut, R. Hiesgen, D. Meissner, N. S. Sariciftci, *Advanced Functional Materials* 2004, in press

[48] J. K van Duren, J. Loos, F. Morrissey. C. M. Leewis. K. P. H. Kivits, L. J. van Ijzendoorn, M. T. Rispens, J. C. Hummelen, R. A. J. Janssen, *Advanded Functional Materials* 2002, **12**, 665

[49] T. Martens, J. D'Haen, T. Munters, Z. Beelen, L. Goris, J. Manca, M. D'Olieslaeger, D. Vanderzande, L. De Schepper and R. Andriessen, *Synthetic Metals* 2003, **138**, 243

[50] A. Cravino, N. S. Sariciftci, *Nature Materials* 2003, **2**, 360

[51] A. Cravino. N. S. Sariciftci, *Journal of Material Chemistry* 2002, **12**, 1931

[52] U. Stalmach, B. de Boer, C. Videlot, P. F. van Hutten, G. Hadziioannou, *Journal of The American Chemical Society.* 2000, **122**, 5464

[53] B. de Boer, u. Stalmach, P. F. van Hutten, C. Melzer, V. V. Krasnikov, G. Hadziioannou, *Polymer* 2001, **42**, 9097

[54] J. J. M. Halls, A. C. Arias, J. D. MacKenzei, W. Wu, M. Inbasekaran, E. P. Woo, R. H. Friend, *Advanced Materials* 2000, **12**, 498

[55] A. C. Arias, N. Cocoran, M. Banach, R. H. Friend, J. D. MacKenzuie, W. T. S. Huck, *Applied Physics Letters.* 2002, **80**, 1695

[56] M. Drees, K. Premaratne, W. Graupner, J. R. Heflin, R. M. Davis, D. Marciu, M. Miller, *Applied Physics Letters.* 2002, **81**, 4607

[57] M. Drees, R. M. Davis, R. Haflin, *Physical Review B* 2004, **69**, 165320

[58] S. A. Jenekhe, X. L. Chen, *Science* 1998, **279**, 1903

[59] T. Kietzke, D. Neher, J. Landfester, R. Montenegro, R. Guenter, U. Scherf, *Nature Materials* 2003, **2**, 408

[60] J. K. van Duren, J. Loos, F. Morrissey. C. M. Leewis, K. P. K. Kivits, L. J. van Ijzendoorn, M. T. Rispens, J. C. Hummelen, R. A. J. Janssen, *Advanced Functional Materials* 2002, **12**, 665

[61] J. M. Kroon, M. M. Wienk, W. J. H. Verhees, J. C. Hummelen, *Thin Sold Films* 2002, **403-404**, 223

[62] M.Al-Ibrahim, H. K. Roth, S. Sensfuss, *Applied Physics Letters* 2004, **85**, 1481

[63] V. D. Mihaliletchi, J. K. J. van Duren, P. W. M. Blom, J. C. Hummelen, R. A. J. Janssen, J. M. Kroon, M. T. Rispens, W. J. H. Verhees, M. M. Wienk, *Advanced Functional Materials* 2003, **13**, 43

[64] J. K. J. van Duren, V. D. Mihailetchi, P. W. M. Blom, T. van Woudenbergh, J. C. Hummelen, M. T. Rispens, R. A. J. Janssen, M. M. Wienk, *Applied Physics Letters* 2003, **94**, 4477

[65] I. Riedel, J. Parisi, V. Dyakonov, L. Lutsen, D. Vanderzande, J. C. Hummelen, *Advanced Functional Materials* 2004, **14**, 38

[66] E. A. Katz, D. Faiman, S. M. Tuladhar, J. M. Kroon, M. M. Wienk, T. Fromherz, F. Padinger, C. J. Brabec, N. S. Sariciftci, *Journal of Applied Physics 2001*, **90** , 5343

[67] H. Hoppe, N. Arnold, N. S. Sariciftci, D. Meissner, *Solar Energy Materials and Solar Cells* 2003, **80**, 105

[68] R. D. McCullough, P. C. Ewbank, *Handbook of Conducting Polymers*, Chapter 9, p. 225, edited by T. A. Skotheim, R. L. Elsenbaumer, J. R. Reynolds, 1998, Marcel Dekker Inc.

[69] H. Sirringhaus, P. J. Brown, R. H. Friend, M. M. Nielsen, K. Bechgaard, B. M. W. Langeveld-Voss, A. J. H. Spiering, R. A. J. Janssen, E. W. Meijer, P. Herwig, D. M. De Leeuw, *Science* 1999, **401**, 685

[70] A. Mozer, N. S. Sariciftci, *Chemical Physics Letters* 2004, **389**, 438

[71] K. E. Aasmundtvei, E. J. Samuelson, W. Mammo, M. Svensson, M. R. Anderson, L. A. A. Pettersson, O. Inganaes, *Macromolecules* 2000, **33**, 5481

3. Photoinduced Absorption Spectroscopy

Photoinduced absorption (PIA) spectroscopic techniques are widely used to identify photoexcited species. Generally, PIA can be measured in two different ways.

- Transient photoinduced absorption, where the sample is excited by a short light pulse and photoinduced changes are probed in the time domain.[1,2,3,4]
- Photomodulation PIA technique, where the sample is excited by a modulated continuous wave (cw) light source and the probe is detected in the frequency mode by a lock-in-amplifier.[5,6,7]

For this thesis, generally photomodulation spectroscopy is used and the application of this technique will be discussed in this chapter.

3.1. Steady State PIA

3.1.1 Principles

Figure 3.1 shows a schematic setup of a photomodulation PIA setup, as it is used for most experiments in this thesis. Experimental details will be given later. The specimen is excited across its band gap by the pump beam. Generally, a cw laser is used. The pump is modulated periodically. Photoexcited states are created in the sample by the pump beam. The density of the photoexcited species modulates with the modulation frequency of the pump. Changes in the transmittance of the specimen, induced by the photoexcited states, are detected with the cw probe light. The probe beam is spectrally resolved by a monochromator and measured by a diode detector. The detector signal is amplified and detected by a two channel lock-in amplifier. The reference signal for the lock-in amplifier is the modulation frequency.

The main unit of a lock in amplifier is the phase sensitive detector (PSD). The PSD detects only signals modulating with the frequency of the reference input. This is mathematically achieved by multiplying the signal input V_{in} and reference signal V_{ref}, giving the output signal V_{PSD} of the phase sensitive detector. The basic equation for the PSD is shown in equation 3.1.

$$V_{PSD} = V_{in} * V_{ref} = |V_{in}| * \sin(\varpi_{in} * t - \theta_{in}) * |V_{ref}| * \sin(w_{ref} t - \theta_{ref}) =$$
$$= \frac{1}{2} * |V_{in}| * |V_{ref}| * \{\cos[(\omega_{in} - \omega_{ref}) * t + \theta_{in} - \theta_{ref}] - \cos[(\varpi_{in} + \varpi_{ref}) * t - \theta_{ref} - \theta_{un}]\} \qquad 3.1$$

ω_{in} is the frequency of the input signal, ω_{ref} is the frequency of the reference signal and θ the phase of the signal.

The output signal V_{PSD} is filtered by a low pass filter, as a consequence only the first cosinus term for $\omega_{in} \approx \omega_{ref}$ will contribute to the PSD output signal X (in phase signal).

In a second PSD, the input signal is multiplied with the reference signal, shifted for 90°, giving the output signal Y. Signals at the frequency ω_{ref}, but a phase shift of 90°, will contribute to the output signal Y (out of phase signal).

The total output signal can be regarded as complex number and is alternatively described by a radius R and phase φ, with $R = (X^2+Y^2)^{0.5}$ and φ= arctan (Y/X).

Figure 3. 1: Schematic scheme for a photomodulation setup in transmission geometry.

The measured photoinduced signal ΔT_m may consist of several contributions.

- New absorptions can be observed from photoexcited species. The photoinduced absorption signal is $-\Delta T_{PIA} \sim N*\alpha*d$, whereas N is the number of photoexcited states, α their absorption cross-section and d the film thickness.

- Photobleaching ΔT_{PB}. The sample can become more transparent. The ground state is depopulated as a consequence of the high pump beam

- Luminescence ΔT_L can be induced by the pump excitation. This contribution can be corrected by subtracting the luminescence, which is determined in a separate measurement.

- Stark effect or electroabsorption ΔT_{EA} can occur in the region of the band-band absorption, in the case charges are created. These charges are modulating with the pump and cause an alternating electric field, which causes the Stark effect. The spectrum for the Stark effect is the first derivative of the groundstate absorption

The photoinduced spectrum is than calculated by equation 3.2

$$-\frac{\Delta T}{T} = \frac{-(\Delta T_{PIA} + \Delta T_{PB} + \Delta T_L - \Delta T_L)}{T} = \frac{-(\Delta T_m - \Delta T_L)}{T} \qquad (3.2)$$

Additional information is got from the signal dependence on the modulation frequency ω and the pump power I.

The dependence of the photoinduced signal on the pump modulation frequency can be used to estimate the recombination time of the observed species.[8,9,10,11,12] Epshtein et al have introduced recently the analysis for dispersive dynamics[9,10], as it is observed in amorphous systems like conjugated polymers. The frequency response is described by equation 3.3.

$$R(\varpi) = \frac{R_0}{1 + (i\varpi\tau)^\alpha} \qquad (3.3)$$

Where R(ω) is the complex frequency response, R_0 the steady-state response at zero frequency, τ the mean lifetime and α the dispersion factor. The dispersion factor describes the distribution of lifetimes and vary between 0 for the broadest inhomogeneous distribution and 1 for a homogeneous distribution.

The in-phase (X, dT_x) and out-of-phase frequency (Y, dT_y) response are fitted simultaneously by equation 3.4 and 3.5, respectively.

$$X = R_0 \frac{1 + (\varpi\tau)^\alpha \cos(\frac{\pi\alpha}{2})}{1 + 2(\varpi\tau)^\alpha \cos(\frac{\pi\alpha}{2}) + (\varpi\tau)^{2\alpha}} \qquad (3.4)$$

$$Y = R_0 \frac{(\varpi\tau)^\alpha \sin(\frac{\pi\alpha}{2})}{1 + 2(\varpi\tau)^\alpha \cos(\frac{\pi\alpha}{2}) + (\varpi\tau)^{2\alpha}} \qquad (3.5)$$

Generally, the in phase component X is decreasing with ω, whereas Y shows a maximum. The pump power dependence $\Delta T \sim I^{\alpha}$ can be used to determine the recombination behaviour of the detected states. $\alpha = 1$ for first order kinetic (monomolecular type recombination), $\alpha = 0.5$ second order kinetic (bimolecular type recombination).

3.1.2 Experimental Setup

For a schematic view of the setup, see Figure 3.1. As pump sources, an Ar^{+} laser, INNOVA 400, at the wavelength of 476 nm or 514 nm is used, typically in a power range between 40 and 100 mW. The illumination spot on the sample is around $4mm^2$.Alternatively, diode lasers with a wavelength at 664 nm, $I_{out} = 45$ mW, or 685 nm, $I_{out} = 30$ mW, is used. The pump beam is modulated by a mechanical chopper, Standford SR 540, with a frequency between 5- 4000 Hz. The samples are mounted in a homemade N_2 cold finger cryostat or a He continuous flow cryostat Oxford CF 204, Oxford Instruments plc, respectively. As probe, a halogen lamp with a power of 120 W is used. The light beam is focused on the sample and on the entrance of the monochromatic unit. The monochromator consists of a turret with 3 gratings, which are blazed at 300, 1000 and 2000 nm. In front of the monochromator is an additional set of cut-off filters to block the pump excitation and higher order from the gratings. The detector is mounted on the monochromator exit slit. It is a sandwich diode detector, consisting of Si for the VIS and NIR <1100 nm and an InGaAsSb for the range between 1100 and 2200 nm. The signal is amplified and detected by a lock in amplifier, Standford Model SR 830.

3.2 Photophysics of MDMO-PPV and MDMO-PPV: PCBM

In Figure 3.2, the photoluminescence of MDMO-PPV and its blend with PCBM is shown. The pristine material shows a strong luminescence with peaks at 600 and 650 nm. The addition of a small amount of the fullerene derivative PCBM (3.3 % w/w) quenches the photoluminescence by approximately a factor of 10. Further addition of PCBM (33.3 % w/w) leads to a quenching of a factor > 100. No photoluminescence from PCBM is detected (peak at 750 nm) for films cast from chlorobenzene.
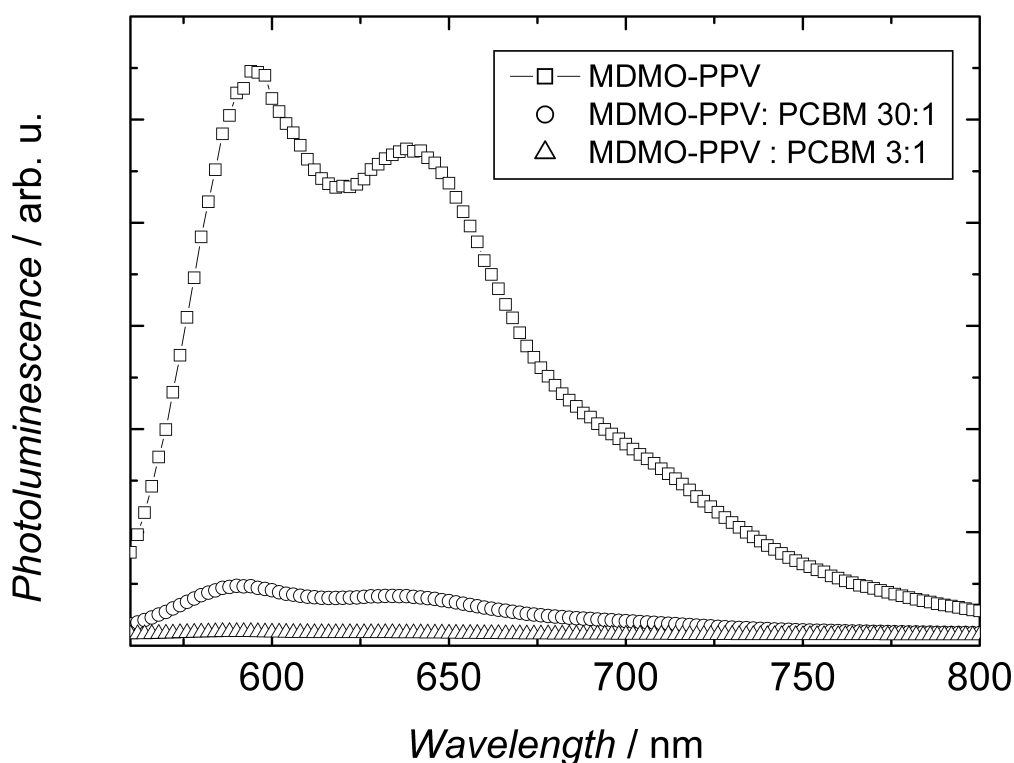

Figure 3. 2: Photoluminescence of pristine MDMO-PPV (squares), blends of MDMO-PPV: PCBM 30:1 (circles) and 3:1 (triangles) blends, samples are cast from chlorobenzene solutions. Samples are excited at 476 nm with 40 mW at room temperature.
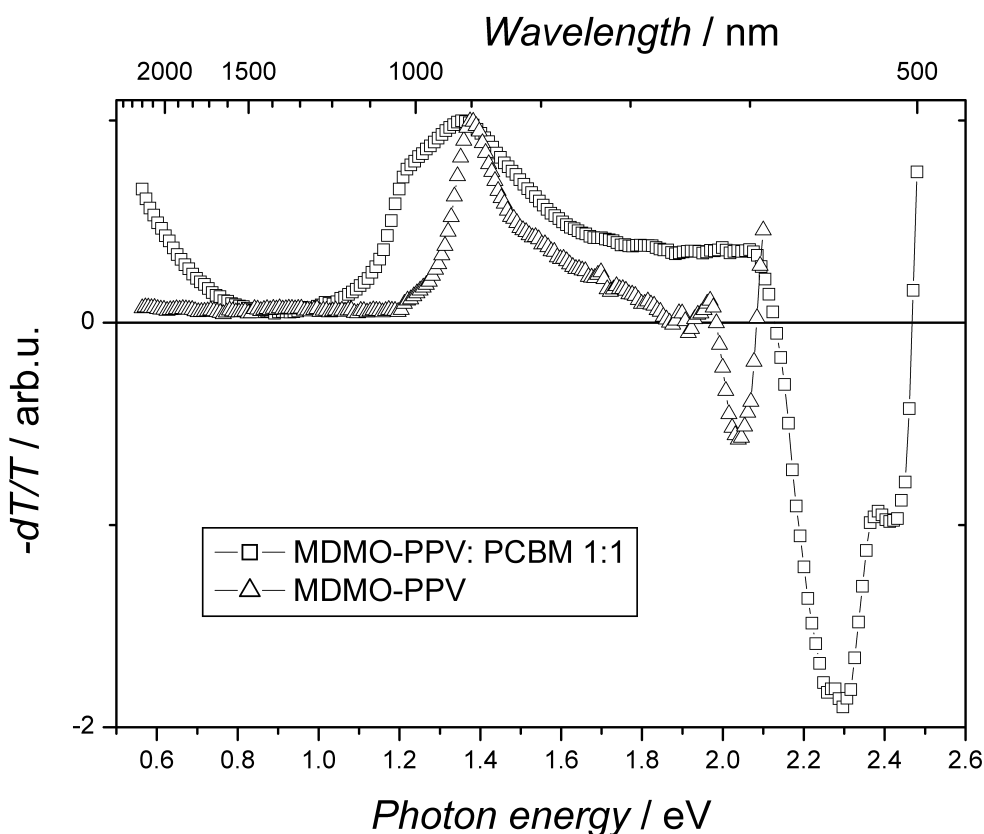
Figure 3. 3: Comparison of PIA spectra of MDMO-PPV (triangle) and MDMO-PPV: PCBM 1.1 blend (squares), excited at 476 nm at 100 K. Spectra a normalized at their maximum for comparison.

Figure 3.3 shows the PIA spectra of a pristine MDMO-PPV film and MDMO-PPV: PCBM 1:1 blend in comparison. The PIA of MDMO-PPV shows a single absorption peak at 1.4 eV (890 nm), which is assigned to a $T_1 \rightarrow T_n$ excitation of the polymer.[13,14] The features around 2 eV are most probable uncompensated photoluminescence of MDMO-PPV.

The MDMO-PPV: PCBM blend shows two photoinduced absorption peaks, a broad one on between 1.1 and 2.1 eV, and a second one < 0.6 eV. These two peaks are assigned to the sub band gap polaronic absorption (HE, LE), for the energy diagram see Figure 1.3. The strong negative signal around 2.3 eV is assigned to photobleaching. The origin of the broad HE polaron absorption will be discussed later.

Strong indications are found for photoinduced charge transfer as the dominant de-excitation pathway for photoexcitation in MDMO-PPV: PCBM blends.[6,7,15] The polymer photoluminescence and the triplet state of the polymer are quenched in blends with PCBM. Further, polaronic transition of MDMO-PPV are found in the blend.

Figure 3.4.a shows the PIA spectrum (in and out of phase) of a MDMO-PPV: PCBM 1:1 film at 16 K, recorded with a modulation frequency of 330 Hz. At this chosen frequency, both components are of similar magnitude and show mirror image like features.

Figure 3.4.b shows the PIA at a modulation frequency of 2970 Hz. The in-phase (X) component of the high energy absorption decreases by approximately one order of magnitude and shrinks to
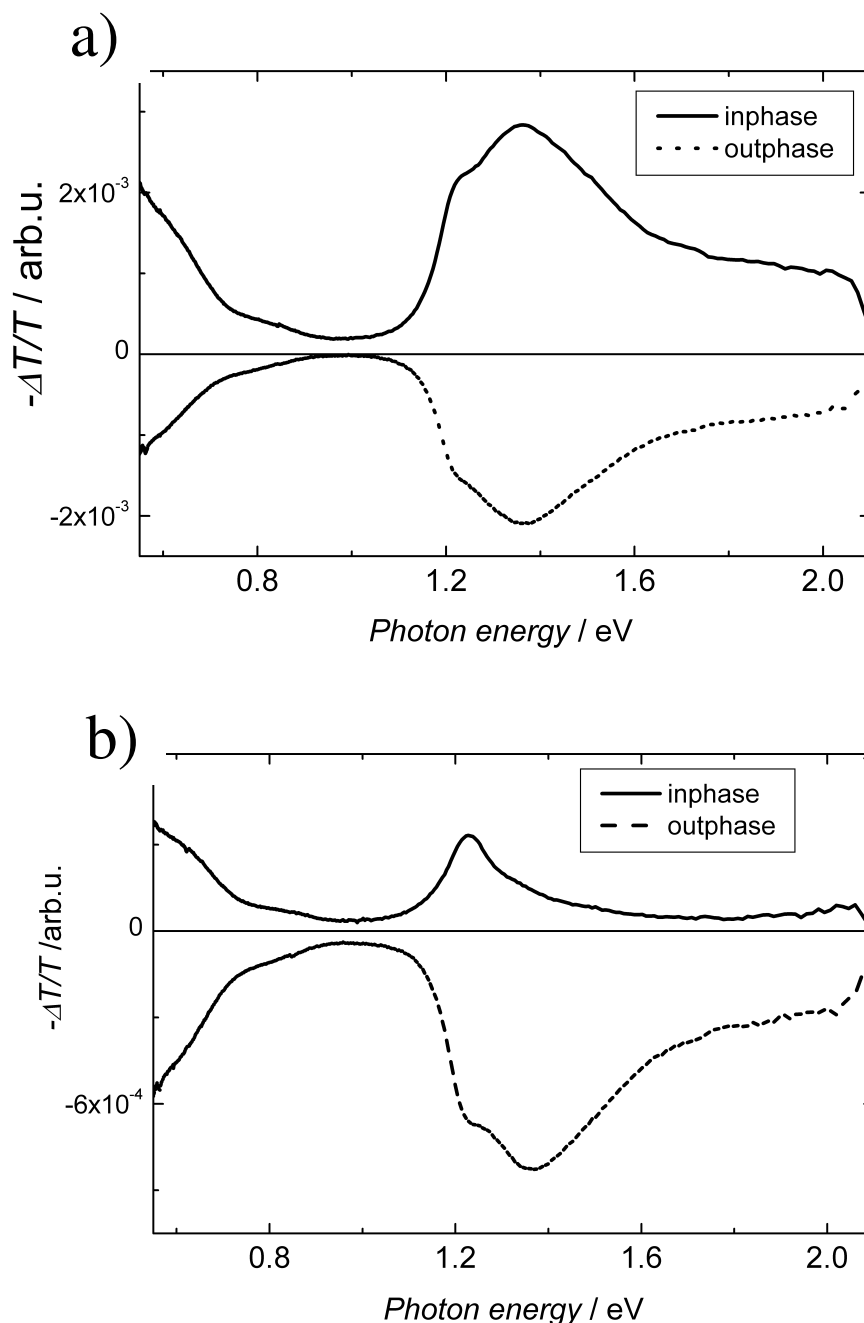

Figure 3. 4: a) Photoinduced absorption spectra at 16K of MDMO-PPV/PCBM acquired at a) 330 Hz and b) 2970 Hz. In both spectra in-phase (solid line) and out-of-phase (dashed line) components are plotted.

a small peak around 1.24 eV. The shape of the out-of-phase part (Y) remains unchanged (Figure 3.4.b).
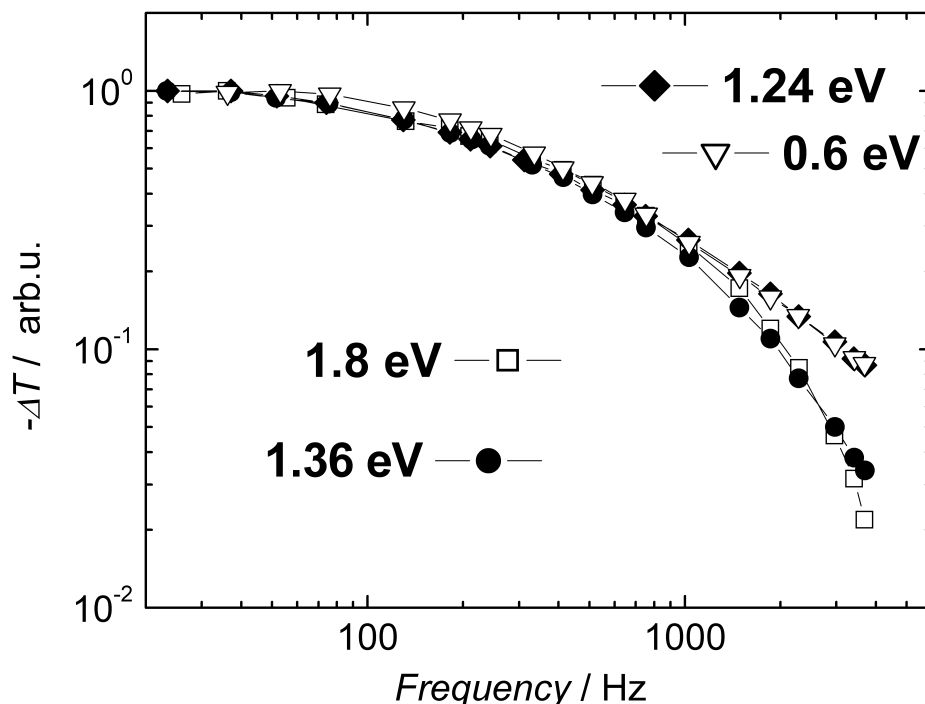

Figure 3. 5: Modulation frequency dependence of the PIA signal recorded at 0.6 eV, 1.24 eV, 1.36 eV, and 1.8 eV. Measurements were performed at 16 K normalized at the lowest recorded modulation frequency.

In Figure 3.5, the frequency dependencies of several features in the spectrum are shown (0.6 eV, 1.2 eV, 1.36 eV, 1.8 eV). For better comparison, the curves are normalized at the lowest modulation frequency. By increasing the modulation frequency, the PIA signal at 1.36 eV and 1.8eV are decreasing more than the signals at 0.6 eV and 1.24 eV. This is equivalent to a slower decay of the species causing the 1.8 and 1.36 eV PIA as compared the species causing the 1.2 and 0.6 eV PIA. This finding contradicts the assumption that the peak between 1.1 eV and 2.1 eV originates from only one type of photoexcited species.

The recombination process at T< 40 K is known to be tunnelling dominated. Lifetimes up to hours are observed in CP: fullerene blends.[16]

Recently, Beljonne et al[17] calculated the influence on the optical signature of polarons by interchain interaction in CP. Figure 3.6.a and 3.6.b shows schematically the energy diagram for a polaron on a isolated chain and for a delocalised polaron on a co-facially aggregated dimer of

two five-unit PPV oligomers separated by four angstrom. For such aggregates, the polaronic levels are split and a new absorption (C3) is possible.

One may conclude, that the photoinduced absorptions in MDMO-PPV: PCBM blends are originating from localized and delocalised polarons. The delocalised polarons show a longer lifetime compared to isolated chain polarons, at least at the temperature of 16 K. As a consequence, the signals become easier over-chopped in photomodulation experiments and are not detectable at high modulation frequencies.
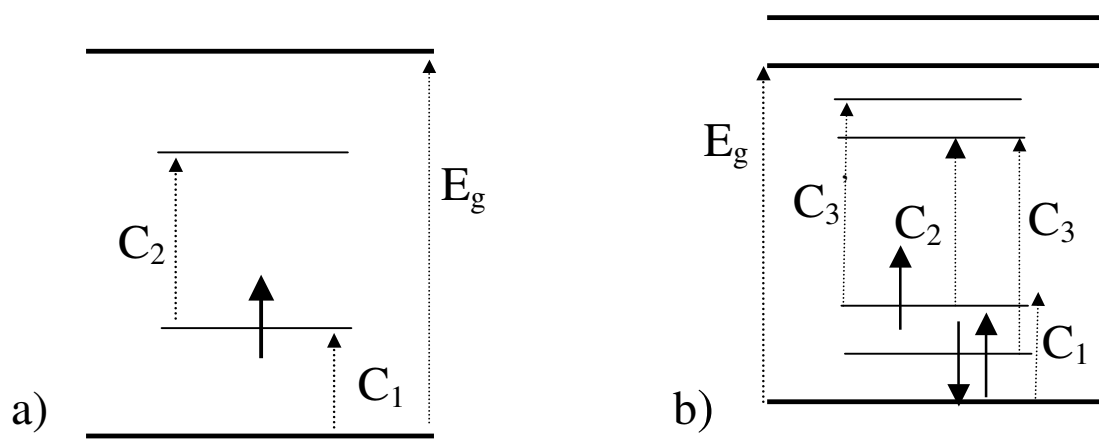

Figure 3. 6: Allowed optical transitions in a localized (intramolecular) polaron and b) delocalised (on two conjugated segments, intermolecular) polaron. Energetic positions of different levels are only schematic Thick lines are indicating states of the neutral molecule, thin lines additional states of the polaron. Dashed arrows are indicating optical transitions.

3.3 Electric field effects on the photoexcitations.

The influence of an electric field on the photoexcitations in organic materials and conjugated polymers was investigated by photoluminescence and pump-probe experiments by several groups.

For the photoluminescence, field induced quenching was observed.[18,19,20] This effect is generally assigned to electric field assisted exciton dissociation.

In steady state pump-probe experiments, triplets are the primarily detected species in pristine conjugated polymers.[21] Upon applying an electric field and charge injection, faster decay of the triplets was found.[22] This effect was assigned to the interaction of injected charges with the triplets. Furthermore, Zenz et al showed in ps pump probe experiments[23] the hexaphenylene triplet signal increasing due to the effect of an external electric field. The increased triplet signal

was assigned to the formation of additional triplets by recombination of polarons, which are formed by field induced breaking of excitons.

Fewer studies are known on the photophysical behaviour of conjugated polymer: fullerene blends under bias electric field. Liess et al[24] found in C_{60} doped conjugated polymer films with low C_{60} concentration enhancement of the photoinduced polaronic signal under bias. This effect was attributed to enhanced dissociation of excitons due to tunnelling of the negative charge to the fullerenes. Further, faster decay of the fullerene anion photoinduced signals under the influence of the electric fields was found.

In this thesis, a detailed study of the steady state photoinduced absorption in conjugated polymer/fullerene bulk heterojunction solar cells with high fullerene concentration is presented. Photoinduced absorption was measured either in transmission/absorption with thin, transparent electrodes or in reflection/absorption with thick, reflecting electrodes. Significant enhancement of the photoinduced polaronic absorption signal by applying an external field of several Volts/ 100 nm is observed. At higher positive voltages (forward bias, injection regime), the photoinduced signal is reduced again due to recombination with injected charges. The temperature dependence of this effect is discussed in comparison with the temperature dependence of the current-voltage characteristics of the devices. Furthermore, we analysed the charge carrier lifetimes as a function of the applied field using a dispersive recombination model. This analysis clearly shows the shortening of the average lifetime of the photoexcited polarons under applied electric field.

3.3.1 Experimental

The device structure and the light beam pathways for the optical measurements are shown in Figure 3.7. As top electrode, 0.6 nm of LiF and subsequently a layer of Au or Al were evaporated. LiF is known to improve the electron injection between Al or Au and organic materials.[25,26] Au and Al show similar behaviour as top electrode material in conjugated polymer/fullerene bulk heterojunction devices.[27] 30 nm of Au or Al were used as top electrodes for semi-transparent devices. Whereas thin Au devices show good stability, thin Al devices show degradation after a short time period. All electrodes with a thickness over 60 nm show sufficient stability and were used for spectroscopic measurements in reflection/absorption geometry. The active area of the device is approx. 2x4 mm².
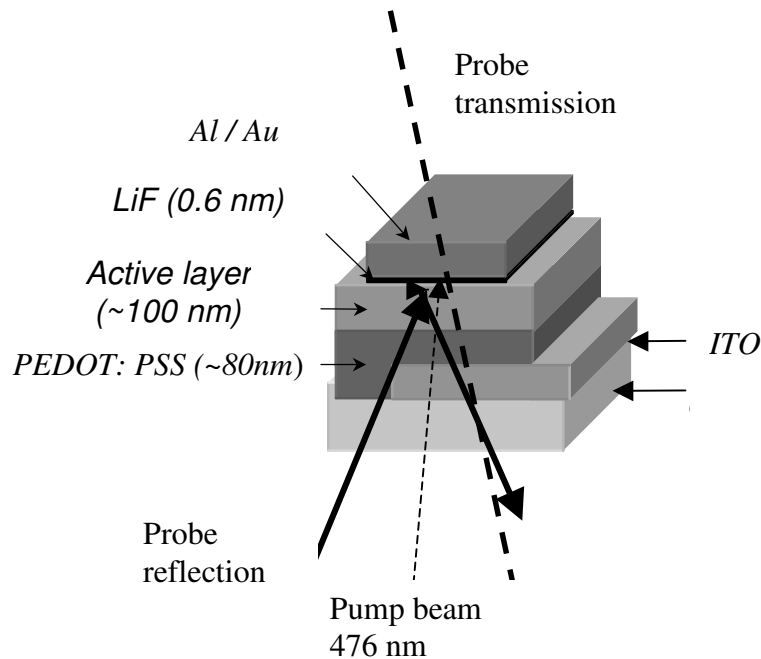
Figure 3. 7: The device structure of a bulk heterojunction photovoltaic cell and optical beam paths for the pump-probe experiments in transmission and reflection geometry are shown. The 476 nm line of an Ar^{+} laser, modulated with a mechanical chopper, was used as pump beam. It illuminated the sample through the ITO electrode. For the transmission measurements, the probe beam entered through a semitransparent top electrode. For the reflection measurements, the probe beam entered from the ITO side and was reflected at the metal electrode.

Photoinduced absorption spectra (PIA) were measured in two different setups: in transmission geometry with the semi-transparent electrodes and in reflection geometry with devices with reflecting back contacts. In both setups, the 476 nm line of an Ar^{+} laser was used as pump, typically chopped at 73 Hz, and with a power between 40 and 100 mW on a spot diameter of approx. 2 mm. Under this illumination conditions, a current of 7-20 mA in the area of the laser spot of approx. 3-4 mm² is induced. The devices absorb roughly 50 % of the incident light in the active layer and show quantum efficiency for the current extraction of 1. As probe, a tungsten-halogen lamp was used. In the transmission setup, the monochromator was set after the sample, in the reflection setup the monochromator was in front of the sample; in this case an additional 1.8 eV cut-off filter was used in front of the detector. The probe was measured with a Si-InGaAsSb sandwich detector or a N_2 cooled Ge detector in transmission and reflection geometry setups, respectively, and recorded with a lock-in amplifier. The PIA spectra were corrected for the photoluminescence.

The DC bias was applied between the ITO and Al electrode.

3-11

3.3.2 Results

Photoinduced absorption spectra from MDMO-PPV: PCBM devices, recorded at 80 K are compared in Figure 3.8. The photovoltaic devices were measured under open circuit conditions, corresponding to the flat band condition. The photoinduced spectra of such blends are well known and show the polaronic absorption of MDMO-PPV with a maximum at 1.3 eV, assigned to the high-energy (HE) polaronic transition and a peak arising below 0.6 eV, assigned to the low energy polaronic (LE) transition, which is around 0.3- 0.4 eV.[3-5] No differences in the spectral positions of the PIA bands were observed, showing the possibility to measure photoinduced absorption in device structures.
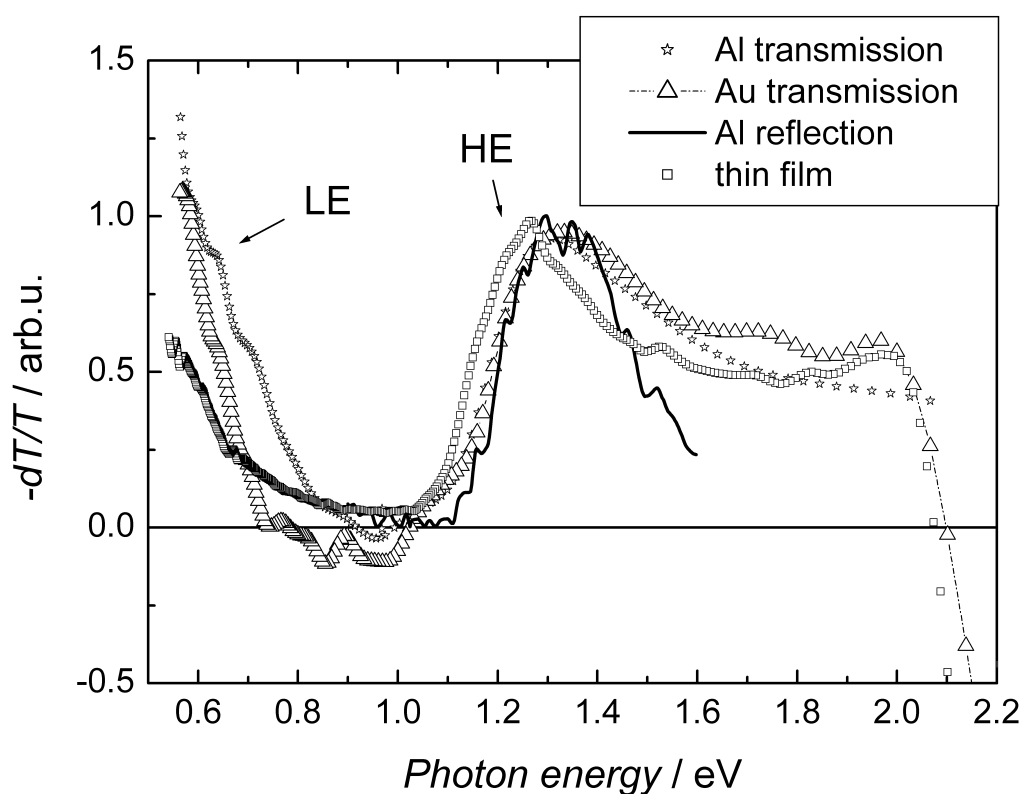

Figure 3. 8: Photoinduced absorption (PIA) spectra of MDMO-PPV: PCBM blend at 80 K, normalized to the peak maximum of the HE polaron peak. Spectra were measured in the different device geometries and thin film on glass. The photovoltaic devices were measured under open circuit conditions.

Figure 3.9 shows the photoinduced spectra, measured in transmission in a photovoltaic device with a thin Al top electrode, under different external bias voltages. An increase of the photoinduced signal of a factor 2-3 is observed upon applying an external voltage of +/- 3V. The open circuit potential at this temperature is approx. 1V. The corresponding field strength is 1x

10^5 V cm^{-1} at short circuit, 2×10^5 V cm^{-1} at +3 V and 4×10^5 V cm^{-1} at $-$3V. Constant electric field drop over the active layer is assumed.
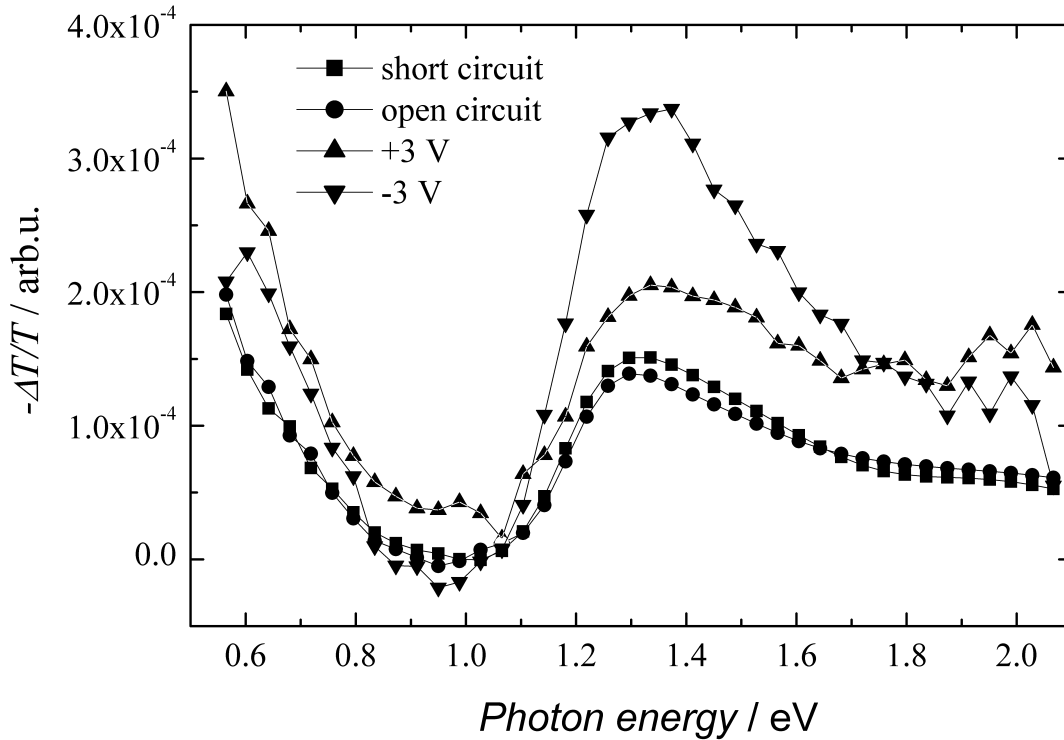

Figure 3. 9: Photoinduced absorption at 80 K of a photovoltaic device in transmission with a thin Al electrode under open circuit, short circuit and positive and negative applied bias.

Figure 3.10a shows the photoinduced signal at 1.25 eV as a function of the external applied voltage at different temperatures. At low temperature, the photoinduced signal is increasing symmetrically around a voltage of ~ 1 V, what is close to the open circuit potential of these devices. The open circuit potential can be used as a measure for the built in field. The PIA signal shows a minimum around this field free case. Generally, the open circuit voltage of MDMO-PPV: PCBM bulk heterojunction photovoltaic devices shows an increase with the light intensity and saturation for higher illumination intensities. The threshold for this saturation is around the solar illumination intensity. Under the illumination conditions in this experiments the cells operate at high intensities, far beyond the threshold of this saturation. The temperature dependence of the open circuit voltage in the saturation regimes shows a shift with temperature from 1 V below 100 K down to 800 mV at room temperature.[28,29] Such small variations are beyond the resolution of the photoinduced absorption measurements.
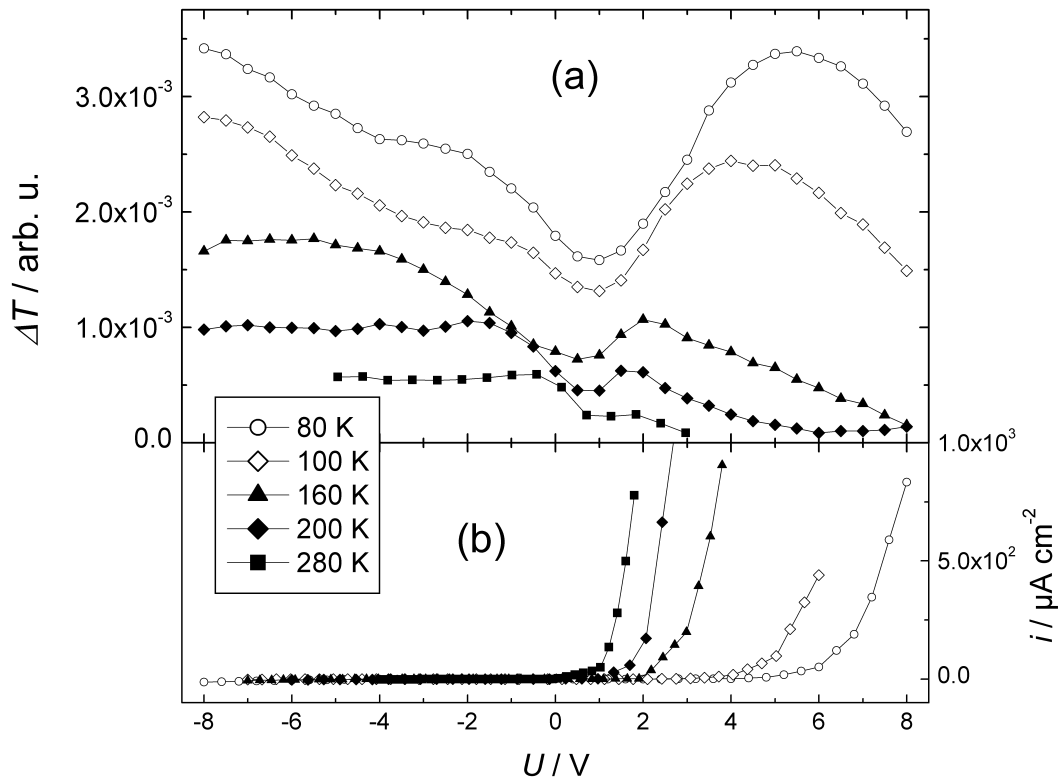
Figure 3. 10: PIA at 1.25 eV in reflection geometry on a device with 60 nm Al back electrode at different temperature, (b) I-V curve in the dark of the corresponding device.

For higher applied voltages, an asymmetry is observed; the signal shows a maximum in forward bias and is decreasing again for higher positive voltages. The voltage, where this maximum occurs, is decreasing with increasing temperature. At the highest measured temperature of 280 K, no maximum but a saddle point is observed for positive voltage and the PIA vs. voltage curve becomes completely asymmetric. Furthermore, at temperatures above 160 K the curve flattens for higher negative voltages.

For the same device, current voltage curves in the dark were recorded, shown in Figure 3.10b. The I-V curves of the devices show a rectification and good diode behaviour. At 280 K, an onset for the current injection at 1 V is observed. This onset for the forward bias charge injection is steadily shifting for lower temperature to a value of ~ 6 V at 80 K. This onset shift corresponds remarkably with the shift of the maximum of the photoinduced signal in forward bias.

Table 3.1: Calculated mean polaron lifetimes τ_0 and dispersion factors α for different applied voltages.

Applied Voltage /V	τ_0 / ms	α
-6	0.29	0.62
-4	0.32	0.64
-2	0.38	0.69
0	0.51	0.7
V_{oc}	0.53	0.72
+2	0.43	0.69
+4	0.37	0.66

Figure 3.11 shows the fitted chopping frequency dependence for a device with thin Au top electrode at 80 K and different bias voltages. For comparison, the in-phase curves have been normalized to the steady state value at low frequency and the out-of-phase values have been normalized to their maximum. Table 3.1 sums up the determined lifetimes and dispersion factors. For positive as well as negative applied bias voltages, the in phase component become more flat and the out of phase component shifts its maximum to higher chopping frequencies. The calculated mean lifetime is decreasing from 3.3 ms down to 1.8 ms for negative bias voltages.
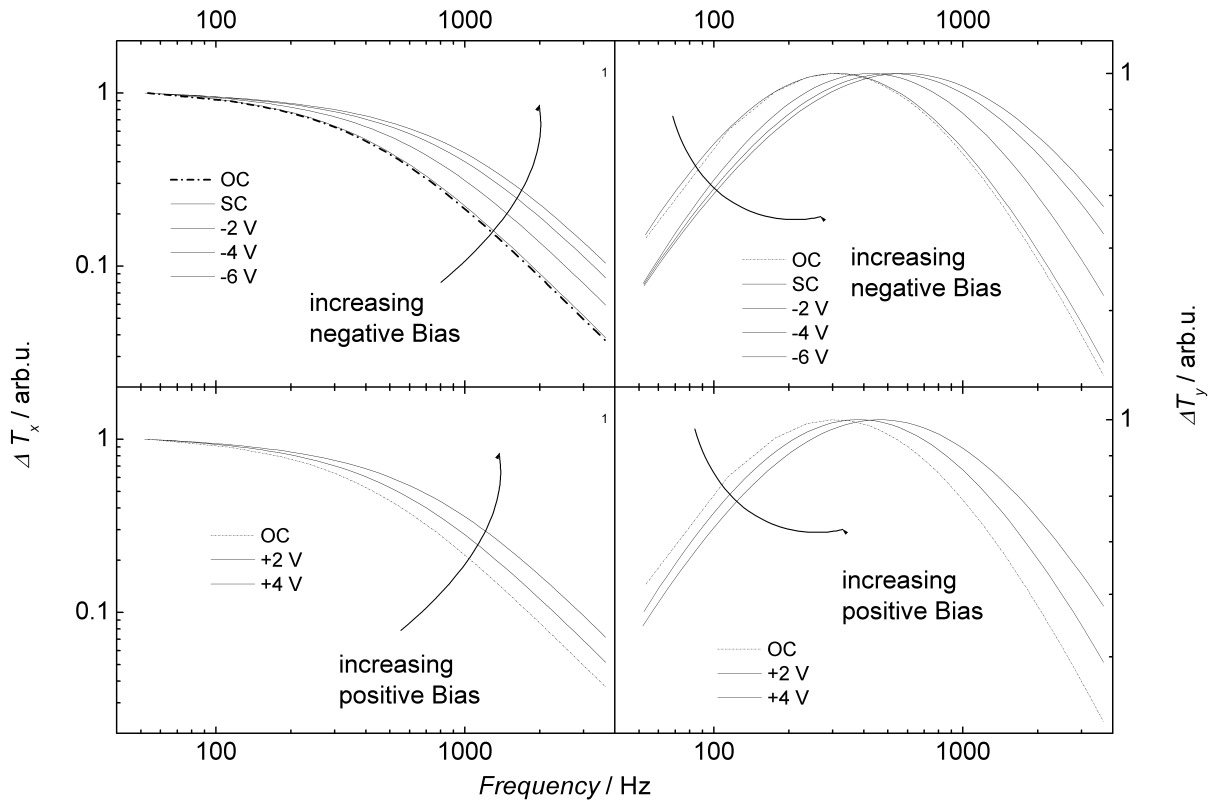
Figure 3. 11: Fitted dependence of the PIA signal on the chopping frequency at 1.3 eV at different bias voltage, normalized to the low frequency part for the in phase component (X) and to the maximum for the out of phase component (Y). Measurement is done in transmission with a thin Au electrode. (a) in-phase component (b) out-of-phase component for short circuit (SC) and increasing negative Bias (c) in-phase phase component and (d) out-pf-phase component for increasing positive Bias. The open circuit (OC) case is shown for comparison. The "in-phase" curves are normalized to the steady state value at low chopping frequencies, the "out-of-phase" curves to their maximum.

3.3.3. Discussion

The photoinduced signal under steady state conditions is given by the following equation 3.6:

$$dT = n * \sigma * \tau \tag{3.6}$$

Where dT is the photoinduced signal, n is the number of photoexcitation generated per time, σ is the absorption cross section of the photoexcitations and τ their lifetime. In our measurements, positive polarons on the conjugated polymer are observed. The change in the photoinduced signal by the electric field should now be assigned to a change in one of these quantities.[22] For σ, we don't expect any change due to the action of the electric field.[24] Furthermore, we don't see any change in the spectra by applying a voltage and can rule out significant Stark effect on the photoinduced signal. Also for the number of photo-generated polarons, no significant change can be expected, since the quantum efficiency for the photoinduced charge transfer is close to unity. We measured at 80 K a decrease of the lifetime by applying an electric field, see Figure 3.11 and

Table 3.1. This decrease in the lifetime reflects the collection of the charge carriers at the electrode as additional relaxation pathways for the charge carriers. The maximum lifetime is observed under open circuit conditions, what is close to flat band conditions. Under these conditions, we presume that most of the photoinduced charge carriers recombine in the bulk and a few are reaching the electrodes by simple diffusion processes. Upon applying an external bias voltage, more charge carriers are drifting to the electrodes under the action of this bias field and recombine at the electrodes. This decrease of lifetimes seems to be in contrast with the increased signal for the photoinduced charge carriers under applied bias. This is not so by taking into account the persistent charge carriers. These charge carriers are not observable in modulation experiments.

The existence of such persistent charge carriers was observed at low temperature by light induced electron spin resonance.[30] These persistent charge carriers show lifetimes in the range of seconds and longer at low temperatures and can therefore not be detected by the modulation techniques we use in our PIA experiments. The origin of these persistent charge carriers is deep trap states with a low probability of thermally activated recombination. However, these deeply trapped persistent charge carriers will be influenced by the electric field, escape from the traps and will drift towards the electrodes. We propose therefore electric field assisted enhanced recombination of long living charge carriers as a reason for the increase in the photoinduced signal reported here. The lifetime of these persistent charge carriers is too long to be detected by the modulation technique, but under the influence of the electric field they can be liberated, recombine and become detectable for the modulation experiment.

For higher positive voltages, the photoinduced signal is decreasing again. The onset for this decrease is shifting to smaller voltages at higher temperatures. This point is coinciding with the onset for current injection into the device. Both effects, the turning point of the PIA vs. voltage and the current injection show the same temperature behaviour. We assign the decrease of the photoinduced signal at higher positive bias voltages to recombination of the photoexcitations with injected charge carriers, resulting lowering the PIA signal.

3.3.4. Conclusion

We studied the electric field effect on the photoinduced charge carrier recombination in conjugated polymer/ fullerene bulk heterojunction solar cells by means of photoinduced modulation spectroscopy. The magnitude of the photoinduced spectra is increasing by a factor of two to three upon applying an electric field on the order of 10^5 V/cm. We assign this increase to

the accelerated recombination of persistent charge carriers, which can than be detected by the modulation spectroscopy, otherwise they are invisible for the modulation spectroscopy. A decrease of the mean lifetime of the photoexcited charge carrier is observed due to this applied field.

For higher applied voltages, the photoinduced signal is decreasing due to injected charge carriers. The onset for this current injection coincides with the turning point for the PIA spectra vs. voltage and is shifted to higher voltages at lower temperature.

3.4 References

[1] B. Kraabel, V. I. Klimov, R. Kohlman, S. Xu, H. L. Wang, D. W. McBranch, *Physical Review B* 2000, **61**, 8501

[2] E. Peeters, A. M. Ramos, S. Meskers, R. A. J. Janssen, *Journal of Chemical Physics* 2000, **112**, 9445

[3] S. C. J. Meskers, P. A. van Hal, A. J. H. Spiering, J. C. Hummelen, A. F. G. van der Meer, R. A. J. Janssen, *Physical Review B* 2000, **61**, 9917

[4] P. B. Miranda, D. Moses, A. J. Heeger, *Physical Review B* 2001, **64**, 081201

[5] M. Wohlgennant, W. Graupner, G. Leising, Z. V. Vardeny, *Physical Review Letters* 1999, **82**, 3344

[6] M. Wohlgenannt, Z. V. Vardeny, *Synthetic Metals* 2002, **125**, 55

[7] X. Wei, Z. V. Vardeny, N. S. Sariciftci, A. J. Heeger, *Physical Review B* 1996, **53**, 2187

[8] G. Dellepiane, C.Cuniberti, D. Comoretto, G. F. Musso, G. Figari, A. Piaggi, A. Borghesi, *Physical Review B* 1993, **48**, 7850

[9] O. Epsthein, G. Nakhmanovich, Y. Eichen, and E. Ehrenfreund, *Physical Review B* 2001, **63**, 125206

[10] O. Epshtein, Y. Eichen , E. Ehrenfreund, M. Wohlgenannt, Z. V. Varedeny, *Physical Review Letters* 2003, **90**, 046804

[11] M. Wohlgenannt, W. Graupner, G. Leising, Z. V. Vardeny, *Physical Review B* 1999, **60**, 5321

[12] M. Westerling, C. Vijila, R. Österbacka, H. Stubb, *Chemical Physics* 2003, **286**, 315

[13] L. Smilowitz, N. S. Sariciftici, R. Wu, C. Gettinger, A. J. Heeger, F. Wudl, *Phsical Review B* 1993, **47,** 13835

[14] H. S. Woo, S. C. Graham, D. A. Halliday, D. D. C. Bradley, R. H. Friend, *Physical Review B* 1992, **46**, 7379

[15] C. J. Brabec, V. Dyaknov, N. S. Sariciftci, W. Graupner, G. Leising, J. C. Hummelen, *Journal of Chemical Physics* 1998, **109**, 1185

[16] N. A. Schultz, M. C. Scharber, C. J. Brabec, N. S. Sariciftci, *Physical Review B* 2001, **64**, 245210

[17] D. Beljonne, J. Cornil, H. Sirringhaus, P. J. Brown, M. Shkunov, R. H. Friend and J. L. Bredas, *Advanced Functional Materials* 2001, **11**, 1

[18] V. I. Arkhipov, H. Bässler, M. Deussen, E. O. Gobel, R. Kersing, H. Kurz, U. Lemmer, and R. F. Mahrt, *Physical Review B* 1995, **52**, 4932

[19] A. Haugeneder, U. Lemmer, and U. Scherf, *Chemical Physics Letters* 2002, **351**, 354

[20] M. C. Vissenberg and M. J. M. de Jong, *Physical Status Solidi B* 1998, **205**, 347

[21] H. S. Woo, S. C. Graham, D. A. Halliday, D. D. C. Bradley, R. H. Friend, P. L. Burn, and A. B. Holmes, *Physical Review B* 1992, **46**, 7379

[22] A. S. Dhoot, D. S. Ginger, D. Beljonne, Z. Shuai, and N. C. Greenham, *Chemical Physics Letters* 2002, **360**, 195

[23] C. Zenz, G. Cerullo, G. Lanzani, W. Graupner, F. Meghdadi, G. Leising, and S. De Silvestri, *Physical Review B* 1999, **59,** 14336

[24] M. Liess, Z. V. Vardeny, and P. A. Lane, *Physical Review B* 1999, **59**, 11053

[25] L. S. Hung, C. W. Tang, and M. G. Manson, *Applied Physics Letters* 1997 **70**, 151

[26] C. J. Brabec, S. E. Shaheen, C. Winder, N. S. Sariciftci, and P. Denk, *Applied Physics Letters* 2002, **80**, 1288

[27] C. J. Brabec, A. Cravino, D. Meissner, N. S. Sariciftci, T. Fromherz, T. Rispen, L. Sanchez, and J. C. Hummelen, *Advanced Functional Materials* 2001 **11**, 374

[28] V. Dyakonov, *Physica E* 2002, **14**, 53

[29] E. A. Katz, D. Faiman. S. M. Tuladhar, J. M. Kroon, M. M. Wienk, T. Fromherz, F. Padinger, C. J. Brabec, and N. S. Sariciftci, *Journal of Applied Physics* 2001, **90**, 5343

[30] N. Schultz, M. C. Scharber, C. J. Brabec, and N. S. Sariciftci, *Physical Review B* 2001, **64**, 245210

4. Low Band Gap Polymers

4.1 Band Gap Tuning of Conjugated Polymers

Conjugated polymers are 1-dimensional atomic systems. Rudolf Peierls predicted already in the year[1] in the year 1956 the instability of such systems. Peierls predicted in his theorem the lifting of the bond length degeneracy, leading to significant bond length alternation. As a result, one dimensional systems show a significant band gap.

The first conductive polyacetylene was reported by Shirakawa et al much later in 1977.[2]

In the case of trans-polyacetylene, the band gap is around 1.4 eV.

The intrinsic band gap of conjugated polymers is generally ascribed to four contributions related to the conjugated polymer backbone.[3,4] A schematic picture is shown in Figure 4.1. Additional, intermolecular interactions can further influence the band gap in the solid state.
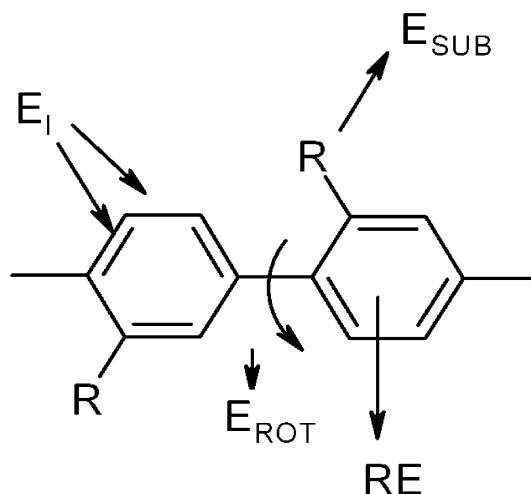

Figure 4. 1: Relation of the chemical structure and the conformation with the band gap is show. As example, poly-para-phenylene PPP is shown. E_l is the contribution from the bond length alternation, RE the aromatic energy, E_{ROT} the contribution from tilting between adjacent rings and E_{SUB} the influences from substituents.

The individual factors and their impact on the synthesis of low band gap polymers will be discussed in the following:

- *Bond length alternation*: The origin of a Peierls gap is directly related to the bond length alternation. Figure 1.1 shows the potential energy as a function of the bond length alternation. Two distinct minima can be seen. In the case of conjugated polymers with a non-degenerate ground state, like most polyaromatic conjugated polymers are, these two minima have different energy values. The two minima correspond to an aromatic and a quinoid form. For a detailed discussion see chapter 1.1.
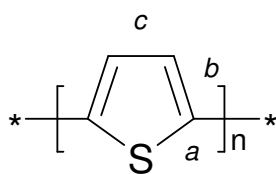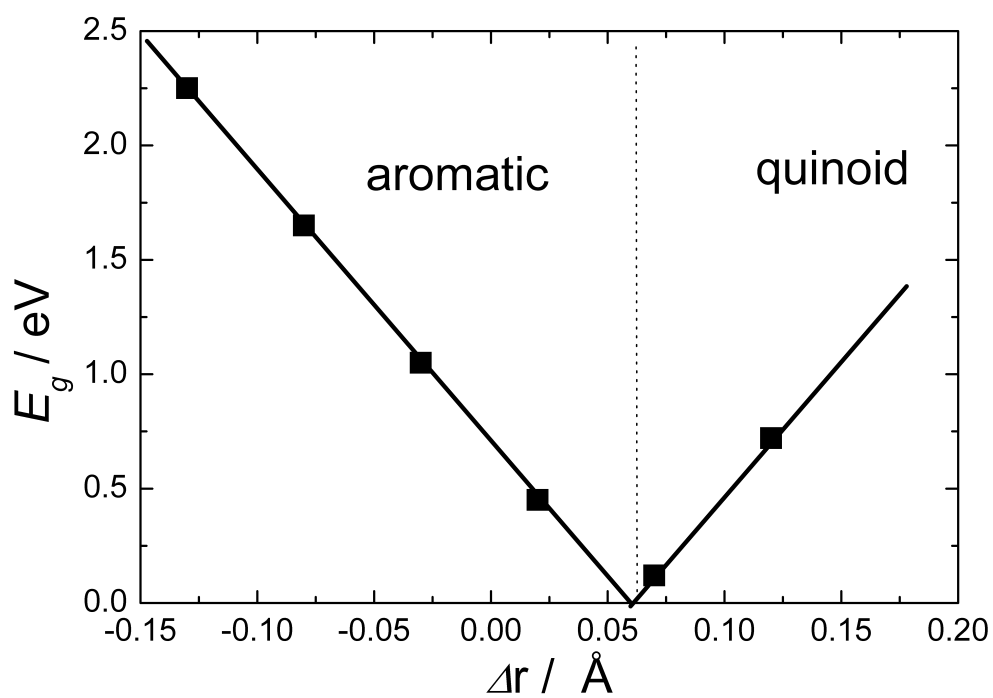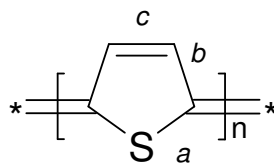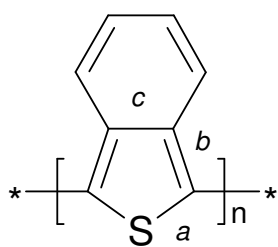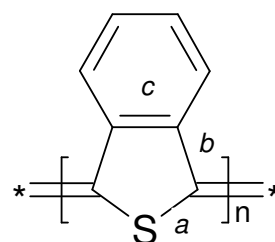
Figure 4. 2: Band gap as a function of the bond length alternation (Δr) (diagram drawn after Lit.5). Δr is defined as the difference between C-C bonds parallel to the chain axis and C-C bonds inclined with respect to the axis. Lower part shows the aromatic and quinoid form of poly-thiophenes (PT) and poly-isothianaphtene (PITN).

Manipulating the bond length alternation was shown to be a powerful tool to manipulate the band gap. Figure 4.2 shows the band gap as a function of the bond length alternation, as calculated for a poly-thiophene backbone.[5] Changes of the bond length alternation are equivalent to the change from an aromatic character to a quinoid one. The band gap shows a minimum at $\Delta r = 0.06$ Å. At this point, the band gap is very small.

This concept could be realized in poly-isothianaphtenes (PITN´s). [6,7,8,9] PITN´s have a band gap of 1.0 eV. The parent structure poly-thiophene has a band gap of ~ 2.0 eV. The lower part of Figure 4.2 shows the resonant structures of PT and PITN. In PT, the aromatic structure is favoured as compared to the quinoid. In PITN, the aromaticity is an interplay between the thiophene and benzene ring. The thiophene and benzene ring cannot preserve aromaticity in the same resonant structure. Since the six-ring is aromatic, the [c] bond is shorter than in the PT case. This stabilizes the quinoid form of the PT part.[10,11]

- *Aromaticity:* Most conjugated polymers have aromatic units as monomers; the aromaticity is preserved in the polymer structure. The aromaticity energy is defined as the energy difference between the aromatic structure and a hypothetic reference structure, consisting of isolated double bonds. Aromaticity leads to a confinement of the π-electron on the ring and competes with the delocalisation. Further, it leads to a stabilisation of the binding orbitals in the monomer. The inherent HOMO-LUMO gap of the monomer is increased.

- *Conjugation length:* The longer the conjugation on the backbone, the smaller the band gap. It was generally found that the band gap is decreasing with increasing conjugation length, approaching a finite value for infinite conjugation length.[12] Torsion between the adjacent rings partially interrupts the conjugation and leads to an increase of the band gap.

- *Substituent effects:* Substituents can change the energetic position of the HOMO or LUMO level, respectively, via mesomeric or inductive effects. Electron donating groups raise the energetic position of the HOMO. Electron withdrawing groups lower the energetic position of the LUMO.

Intermolecular interactions: Conjugated polymers show in the solid state generally a red shifted absorption as compared to the solution phase. This is attributed to an increased interaction between the chains. Furthermore, mesoscopically ordered phases of conjugated polymers could occur. Such phases lead to a significant decrease of the band gap as compared to the disordered phases.

For example, bulky side chains can hinder intermolecular interactions between the backbones. The regio-stereochemistry has an important influence on the formation of mesoscopic ordered

phases. As example, regioregular substituted poly-3-alkylthiophenes show in general a lower band gap compared to their regiorandom counterparts.[13,14]
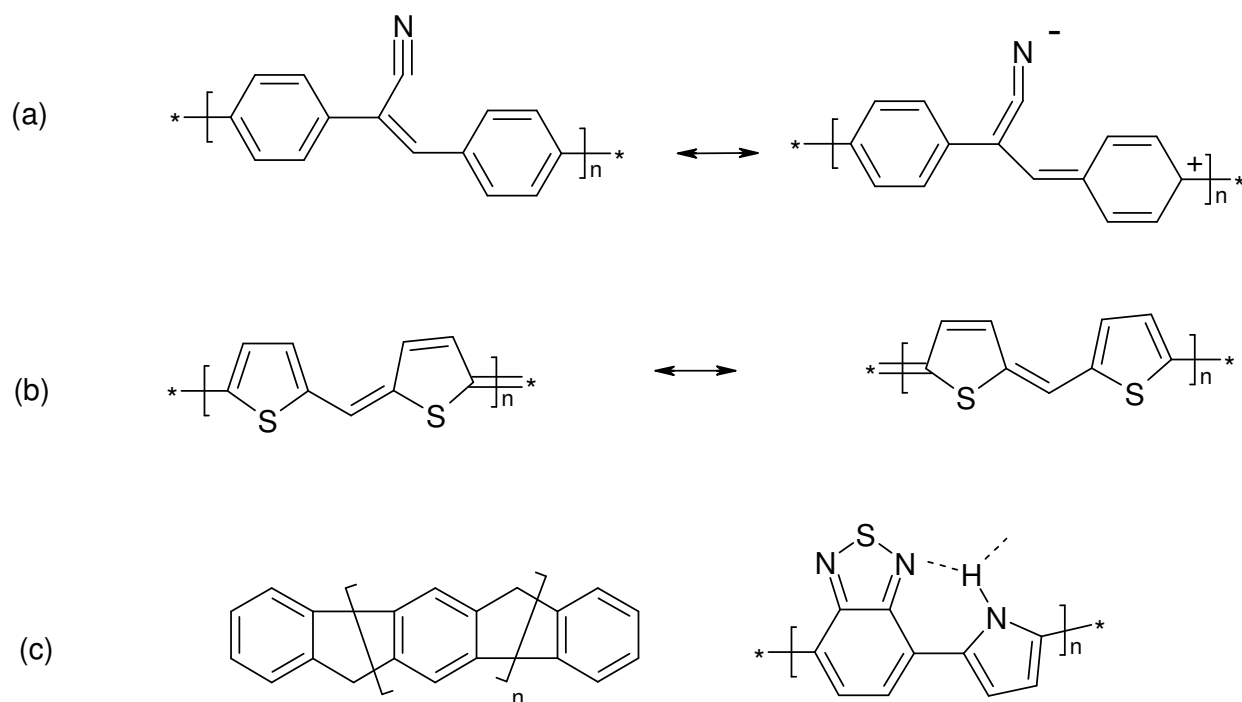

Figure 4. 3: (a) shows the resonant stabilization in a push-pull polymer. Only two resonant structures are shown of the example cyano- phenylene vinylene. (b) shows the stabilization of the quinoid form in poly-methine-thiophene. (c) shows the planarization of the conjugated backbone by either a chemical bond (ladder type poly phenylene, to the left) or by a H-bonding linkage between pyrrole N-H and 2,1,3, benzothiadiazole (to the right).

Different concepts have been proposed and realized to influence the band gap of conjugated polymers:[15]

- *Push-pull polymers* have altering electron rich (donor) and electron poor units (acceptor). Interaction between these two units stabilizes the quinoid, low band gap, form.[16,17] Also, electron donating and electron withdrawing substituents are used to form donor and acceptor units, respectively.[18,19] A schematic drawing for such resonant stabilization is shown in Figure 4.3a.

- Introduction a *methine group* between the rings can lead to a significant decrease of the band gap.[20,21,22] By this approach, the double bond character of the bridging bond leads to a more flat structure and hinders angular rotation between the rings. Further, quinoid character is induced in every second unit. Figure 4.3b shows the resonant structure for poly methine thiophene.

- *Planarization* of the conjugated backbone increases the conjugation length. This can be achieved by either a bridge via a chemical bond (ladder type polymers)[23],[24] or by a zwitterionic structure.[25] For examples see Figure 4.3c.

4.2 Low Band Gap Polymers for Bulk Heterojunction Solar Cells

Due to better theoretical understanding, [5,26,27] and much synthetic effort,[28,29,30,31], several new polymers have been proposed as possible low band gap polymers. In the following, CP´s with a band gap 2 eV (absorption edge > 640 nm) will be considered as low band gap polymer for bulk heterojunction solar cells.

The most interesting and promising materials are benzodiazathiole[32,33,34,35,36,37] push-pull copolymers, isothianaphtene polymers[38] and copolymers[39],[40] or EDOT-based copolymers[41]. For examples see the Figure 4.4 and Table 4.1.

Table 4. 1: material and photovoltaic parameters for several low band gap polymers used in bulk heterojunction devices , chemical structures see Figure 4.4

Materials	V_{oc} / V	I_{sc} / mA cm^{-2}	FF	*Efficiency / %*	*Absorption edge / nm*
EDOT-PPV: PCBM	0.28	0.73[1]	0.28	--	800
PTV: PCBM	0.41	1.4	0.30	0.18[b]	800
PFD-DBT: PCBM	1.04	4.66	0.46	2.2[2]	650
P3HT: PCBM	0.56	9.3	0.6	3.5[3]	650
PEDOT-EHIITN: PCBM	0.13	1.0	0.34	0.06[c]	1100
PTPTB: PCBM	0.72	3.1	0.37	1[c]	750

---

[1] Measured with a halogen lamp
[2] AM 1.5 simulated illumination, 100 mW cm^{-2}
[3] AM 1.5 simulated illumination, 80 mW cm^{-2}

PFDTBT

TTF-PTV

EDOT-PPV

PTPTB

PEOPT

Figure 4. 4: Poly-[2,7-(9-(2éthylhexyl)-9hexyl-fluorene)-alt-5,5-(4´,7´,di-2-thienyl-2´,1´,3´-benzothiadiazole] (PFDTBT) EDOT-PPV, (3,4-ethylenedioxythiophene-*N*-2´ethylhexyl-4,5-dicarboxylic-imide-benzo[c]thiophene (PEDOT-EHI-ITN), poly(3-(4-(1´´,4´´,7´´-trioxaoctyl)phenyl)thiophene (PEOPT), poly N-dodecyl-2,5-bis(2´thienyl)-pyrrole- (2,1,3-benzothiadiazole) (PTPTB), poly- (3´,4´-ethylenedioxy)- thienyl-(2´cyano) vinylene-alt-1,4-(2,5,di-decyloxyl)-phenylene-(1´-cyano)-vinylene EDOT-PPV, TTV-PTV

4.3 PEOPT-a Polythiophene with a Tuneable Band Gap

Polythiophenes are a versatile class of conjugated polymers and have been investigated for a wide range of applications.[42] For some 3-alkyl-substituted thiophenes, a thermally activated absorption shift was observed.[43] This shift was attributed to a conformational change of the polymer backbone, induced by a side chain ordering. Longer effective conjugation length by decreased steric hindrance and increased interchain interactions leads to a reduction of the HOMO-LUMO gap. X-ray diffraction studies on a wide range of phenyl-substituted thiophenes proved the occurrence of ordered crystalline phases in this class of polymers.[44,45]

In the absorption, a significant redshift is observed, which is attributed to the occurrence of crystalline phases.

The recently discovered postproduction treatment in bulk heterojunction photovoltaic devices using poly-3-hexylthiophene is partially explained by such effects .[42]

4.3.1. Optical Properties

The regioregular poly-3-(4´-(1´´,4´´,7´´-trioxaoctyl)phenyl)thiophene PEOPT[46,47] (Figure 4.2) shows the specific case that both, the non-crystalline and partially crystalline phases, are metastable and the non-crystalline phase can be transferred into the partially crystalline one easily. This transformation can be seen by eye due to the colour change from orange to blue, going from the non-ordered to the ordered phase. The band gap is changing from the non-ordered to the ordered phase from 2.1 to 1.75 eV, see for the absorption and emission spectrum Figure 4.5.

The non-ordered form shows a single absorption peak, whereas the ordered form shows several shoulders at the low energy side end, which are typical vibronic satellites for crystalline phases in conjugated polymers.[66] The photoluminescence is shifted for the different phases coincidently with the absorption. Interestingly, a strong solvatochromism can be observed. The absorption spectra in good solvents like chloroform resemble the orange phase, whereas the absorption spectra in benzene, a relative poor solvent for PEOPT, shows shoulders to the low energy end, typically for the ordered phase.
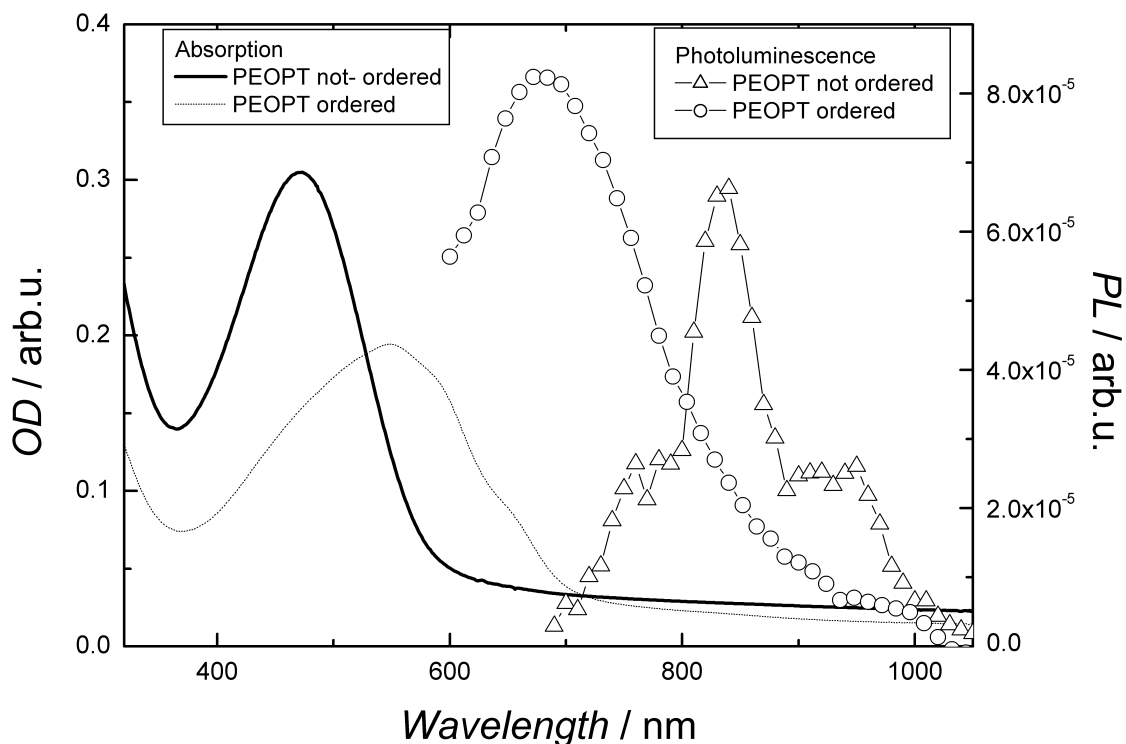
Figure 4. 5: Optical absorption and photoluminescence of PEOPT films in the non-ordered and ordered form. The photoluminescence is measured at 100 K and excitation at 488 nm.

The two phases of PEOPT are observed also in blends with PCBM.

The orange phase is got by spin casting from chloroform. This can be transferred to blue phase by heat treatment at 100 ° C for ten minutes or by treatment with chloroform vapour. Furthermore, the blue phase is got by spin casting from solvents like chlorobenzene or toluene. Drop casting lead generally to the blue phase.[48]

4.3.2 Photophysical Properties

The change in the nanoscopic order of the polymer shows corresponding changes in the photophysics and the interaction of the excited state with fullerene. Figure 4.6 shows the photoinduced absorption spectra of the pristine material in the ordered and non-ordered phase, and the corresponding spectra in the blends with the PCBM.

The non-ordered material shows spectra as observed for many conjugated polymers.

In the pristine material, a single excited state absorption peak is observed below the band gap, which is generally assigned to a $T_1 \rightarrow T_n$ transition.[49] This peak is quenched in the mixture with

fullerene and two new absorption transitions are observed, which are assigned to the polaronic state absorptions of the polymer cation.
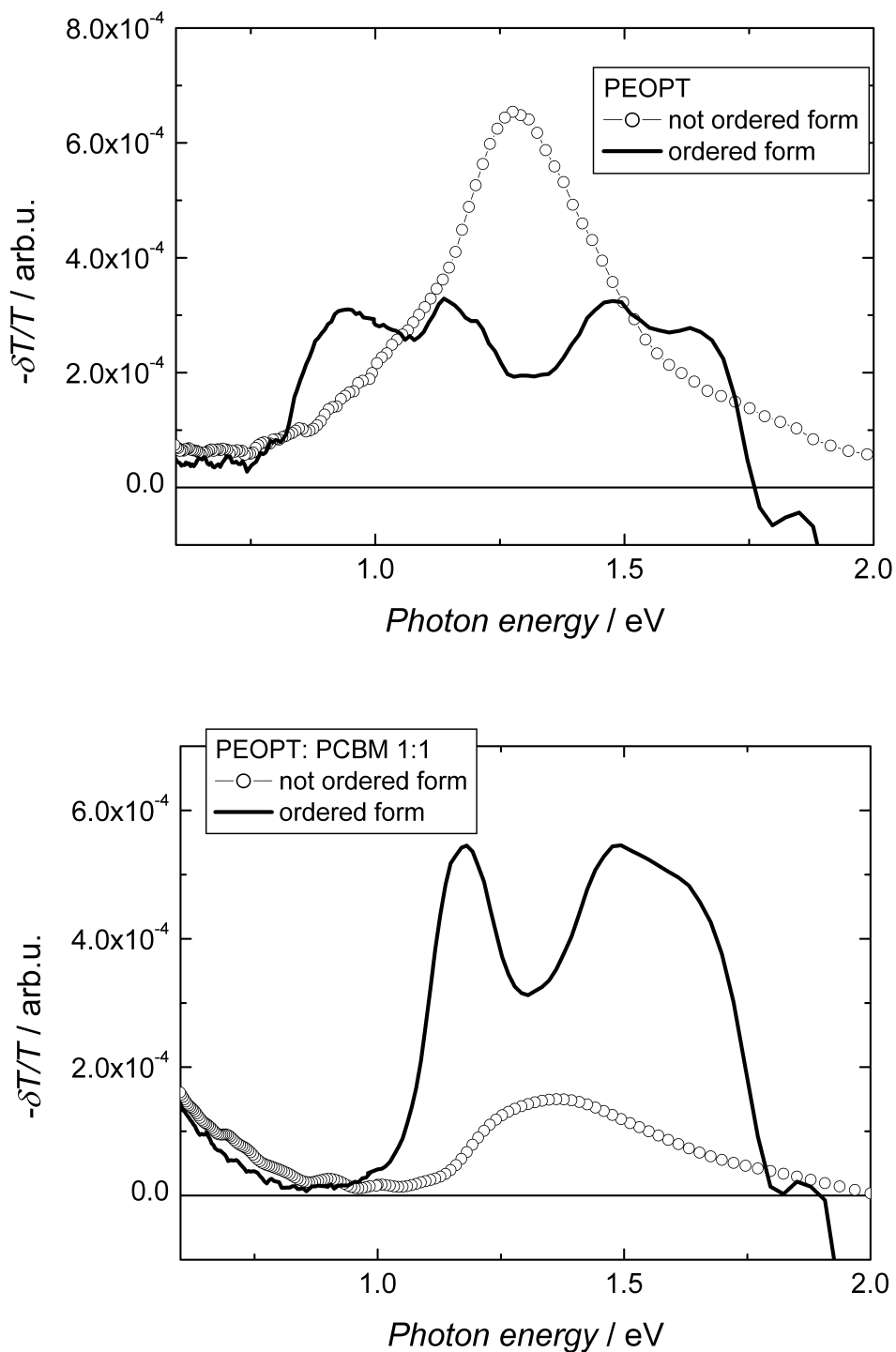

Figure 4. 6: Photoinduced Absorption spectra of PEOPT in the non-ordered and ordered phase (upper graph); Photoinduced Absorption Spectra of PEOPT: PCBM 1:1 blends with the polymer in the ordered and non-ordered phase (lower graph); spectra were recorded at 100 K and excitation at 488 nm.

The photoinduced absorption spectra of the ordered from is much more complicated. In the pristine material, see Figure 4.6, a complicated pattern with peaks at 1.5, 1.2 and 0.9 eV is observed. By addition of fullerene acceptor, for the PIA spectra see Figure 4.6, the low energy peak at 0.9 eV is quenched, and a new peak is arising below 0.6 eV. In the blend with PCBM, all transitions are assigned to polaronic absorption. The splitting of the high energy polaron peak was attributed to the existence of two-dimensional delocalised[50] charged photoexcitations. Recent calculations by Beljonne et al.[51] showed interacting chains may give rise to splitting of the polaronic levels. Figure 3.6 shows a schematic Figure for the one-excitation levels for a polaron on a single chain and for a polaron with co-facial interaction with an adjacent chain. This splitting, which will be heavily dependent on the interchain coupling of the polarons, is presumably much stronger in the ordered phase of the PEOPT and thus can explain this observed splitting in the high energy photoinduced absorption band. We specifically compare our experimental Figure 4.6 with the theory of Beljonne et al., calculated for charged polarons, since the efficient photoinduced electron transfer results in charged polarons on the polymer backbone in the blends with fullerenes.

4.3.3 Photovoltaic Devices

Figure 4.7 shows the photocurrent action spectra of photovoltaic devices of PEOPT in its two forms. The spectra of the ordered form are extended to the red as compared to the disordered form, confirming the lower band gap of the ordered form.

As shown by the photoinduced absorption experiments, interaction of the photoexcited PEOPT with PCBM leads to efficient charge creation. Photovoltaic devices of PEOPT with fullerene acceptor have been demonstrated in bilayer with C_{60} as evaporated acceptor layer well as for bulk heterojunction blends with PCBM. The photocurrent of both forms can be significantly enhanced forming bilayer devices with C_{60}.[52] Blending of the two distinct forms of PEOPT with PCBM fullerene acceptor in bulk heterojunction type photovoltaic devices resulted in solar cells with short circuit responses up to 0.5 mA/cm2 (see Figure 4.8). In the ordered phase of PEOPT, however, the quality of the films were poor and the devices lost both in short circuit current and open circuit voltage as compared to the non-ordered phase.
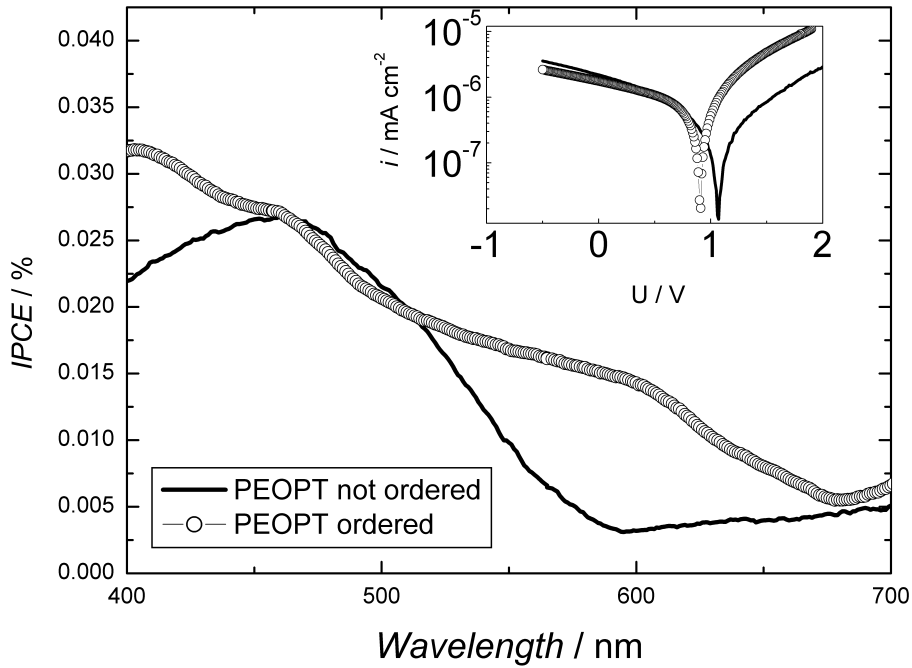
Figure 4. 7: Photocurrent spectra of a photovoltaic cell of pristine PEOPT in the orange (not-ordered) and blue (ordered form). Inset show the I-V curve, following values were measured: ordered phase V_{oc} = 0.91 V, I_{sc} = 1.9 μA cm^{-2}, FF = 0.30; not-ordered phase V_{oc} = 1.06 V, I_{sc} = 2.2 μA cm^{-2} and FF = 0.24.
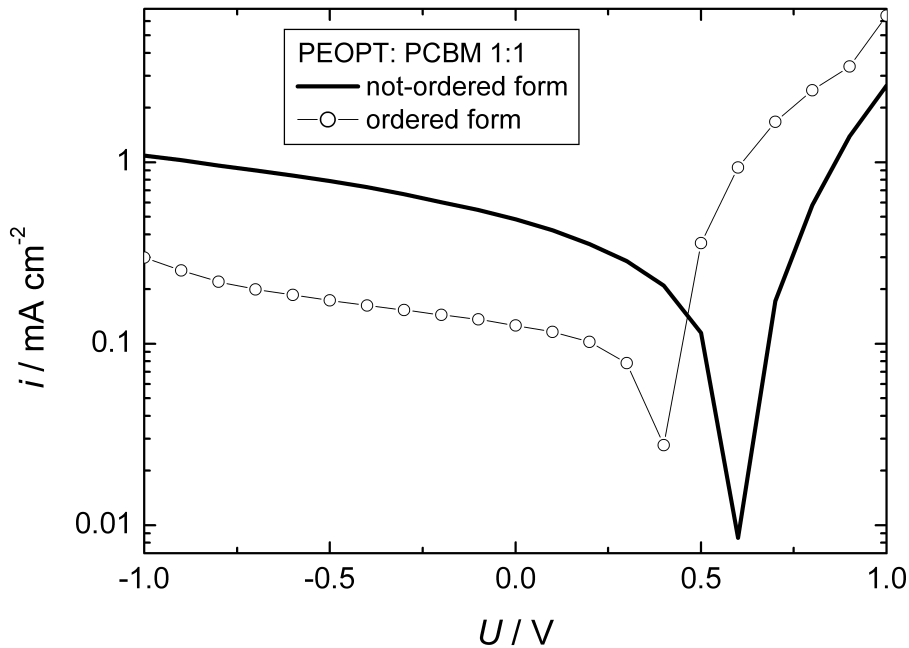

Figure 4. 8: Current- Voltage curve of PEOPT: PCBM 1:1 diodes with the polymer in the ordered and non-ordered form, under illumination from a solar simulator; for the non-ordered polymer, V_{oc} = 0.62 V, I_{sc} = 0.480 μA cm^{-2} and FF = 0.28; for the ordered form polymer V_{oc} = 0.38 V, I_{sc} = 125 μA cm^{-2} and FF = 0.49; films were spin cast from chloroform, top contact Al without LiF.

4.4 PTPTB- a Novel Low Band Gap Polymer[53]

PTPTB, consisting of alternating electron-rich N-dodecyl-2,5-bis (2´-thienyl)pyrrole (TPT) and electron-deficient 2,1,3-benzothiadiazole (B) units, for the chemical structure see Figure 4.4, was synthesized for the application as electron donor polymer in bulk heterojunction solar cells. The material shows an optical band gap of 1.7 eV, which is in good agreement with the value determined by electrochemical voltage spectroscopy of 1.8 eV.[54] A reversible oxidation is found with an onset at +0.54 V vs. Ag/Ag$^+$. No reversible reduction is found. Spectroscopic investigation of blends of PTPTB with fullerene acceptor PCBM demonstrates photoinduced charge transfer. The polymer photoluminescence is quenched and polaronic transitions occur in the blend due to photoexcited charges on the polymer backbone.[91,55]

Figure 4.9 shows the I-V curves and the photocurrent spectra, in comparison with the optical absorption, of a bulk heterojunction device from PTPTB / PCBM (1:3 wt ratio). In the dark the current-voltage curve shows a rectification ratio of about 10^2 at +/- 2V. Under simulated AM 1.5 illumination, a strong photoeffect is observed.

The spectral photocurrent peaks at 600 nm,[56] coinciding with the absorption maximum. The onset of the photocurrent is around 750 nm, demonstrating the low band gap nature of PTPTB and the efficient photon harvesting.
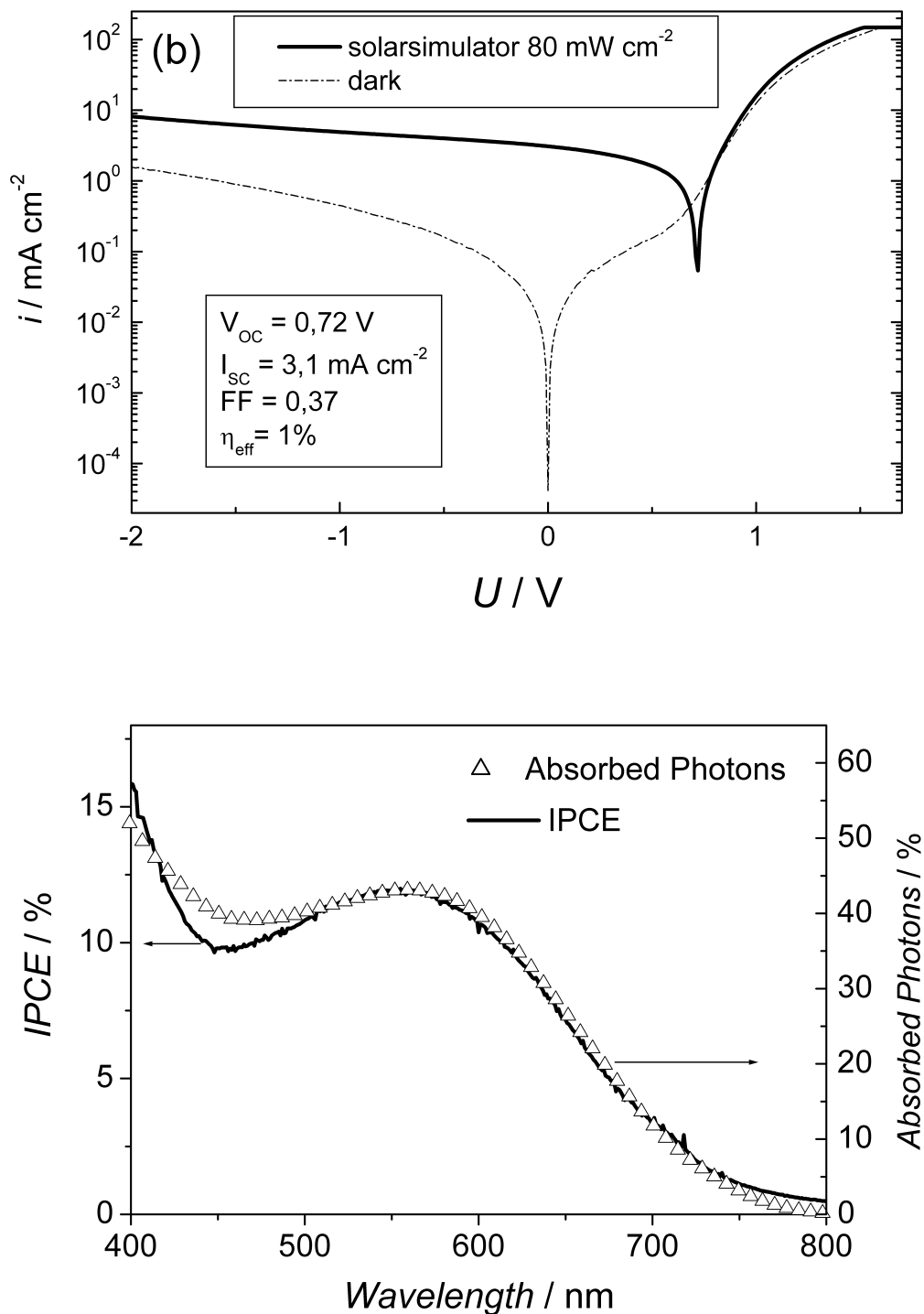
Figure 4. 9: Photocurrent spectra IPCE of a photovoltaic device with PTPTB: PCBM 1:3 as active layer in comparison with the thin film transmission spectrum, thickness of the active layer is approx. 100 nm (upper graph). Current voltage curve under illumination from a solar simulator with 80 mW cm^{-2} and in the dark from the same device (lower graph).

The open circuit voltage of 0.72 V is just 0.1 V less than the highest values observed for

MDMO-PPV/fullerene devices although the band gap of PTPTB is reduced by approx 0.5 eV as

compared to MDMO-PPV. The position of the HOMO level of PTPTB is close to that reported .for HOMO of MDMO-PPV. Since the energetic position for the positive charge is mainly determined by the HOMO of the donor and the energetic position for the negative charge by the LUMO of the fullerene, this explains the similar values for the open circuit voltage between MDMO and PTPTB based solar cells. The energetic splitting between the donor HOMO and the acceptor LUMO is the thermodynamic maximum, which can be got from this photovoltaic device and can be lowered by several reasons, for example low parallel resistance of the device. Instead, the offset between the LUMO levels of the donor and acceptor is lower in the case of PTPTB and PCBM with approx. 0.4 eV instead of MDMO-PPV/PCBM with approx. 1 V. This offset is required for the charge separation, but is on the other hand also an energetic loss. The short circuit current I_{SC} is measured with 3 mA cm^{-2} and the fill factor FF is calculated to be 0.37. From these values, the power conversion efficiency $\eta_{AM1.5}$ is calculated with ~ 1 %. While the short circuit current of the device is already high, the overall efficiency of the device is limited by the low fill factor. Generally, low FF can be induced by high series resistances or by small shunt resistances. For PTPTB/PCBM devices we find serial resistances below 10 Ohm cm^{-2}, which cannot explain the low FF. Therefore, the low FF is expected to originate from a small parallel shunt resistance in the device. Most likely, the low molecular weight of the polymer, determined with 5-16 aromatic units by size exclusion chromatography, causes the low film forming quality and the many pinholes that lead to nanoshorts.[57]

4.5 Thienylene Vinylene based polymer TTV-PTV

Thienylene vinylene based oligomers[58,59,60,61] and polymers[62,63] have been studied in the last years as promising candidate for low band gap materials. Optical absorption onsets < 1.5 eV have been reported for such material systems.[64]

Here, a novel thienylene vinylene (PTV-TTF) polymer with a tetrathiafulvalene condensed to the thiophene ring is presented. For the structure, see Figure 4.4. Its electrochemical and photophysical properties are investigated and, in combination with device results, are discussed for its suitability for solar cells.

4.5.1 Optical and Electrochemical Properties

The optical absorption of PTV-TTF, see Figure 4.10, shows a maximum around 630 nm and an onset around 850 nm (E_G = 1.5 eV). The photoluminescence is weak and shows a broad maximum at 800 nm and a relatively sharp peak at 670 nm, for the spectra see Figure 4.10 as

well. The origin of the 670 nm peak in the photoluminescence is unclear. The absorption and photoluminescence spectra are overlapping. A similar effect was reported for poly-(2,5-thienylene vinylene) films.[65] The photoluminescence of PTV-TTF is preserved in blends with PCBM, see Figure 4.10.

Cyclovoltammetry of a PTV-TTF film on ITO glass shows an irreversible oxidation and a reversible reduction. The onset for the oxidation is at $E_{ox} = 0.49$ V vs NHE and for the reduction at $E_{red} = -0.97$ V vs NHE. The electrochemical band gap of 1.46 eV is in good agreement with the optical one. From these electrochemical potentials, energy values for the HOMO with 5.24 eV and for the LUMO with 3.78 eV are determined.

The LUMO of PTV-TTF shows only a small energy offset to PCBM LUMO. Therefore, the energetic possibility for photoinduced electron transfer from PTV-TTF to PCBM is unclear.
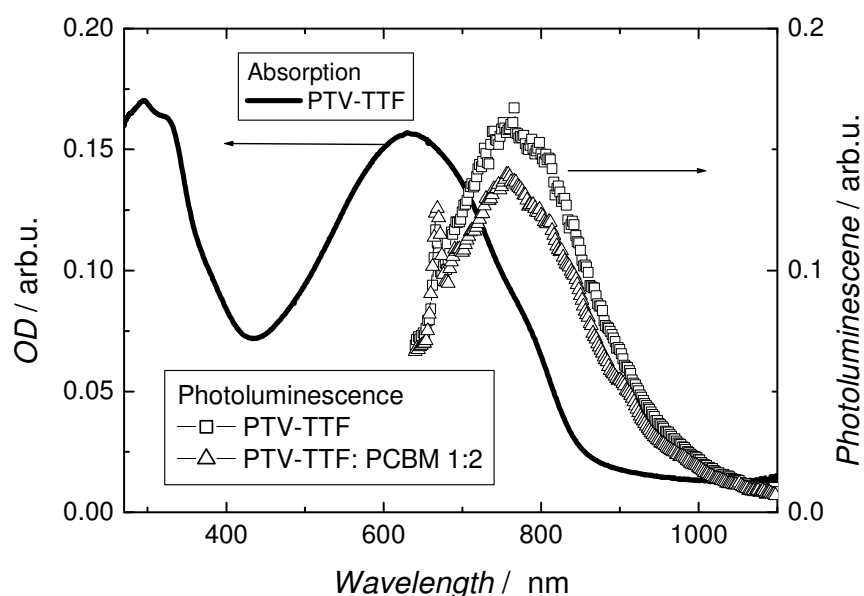

Figure 4. 10: Absorption and photoluminescence of a PTV-TTF thin film. In comparison, the photoluminescence of a PTV-TTF: PCBM 1:2 blended film. Photoluminescence spectra were recorded at 80 K, excitation with 40 mW at 514 nm.

4.5.2 Photophysical Properties

The PIA spectrum of PTV-TTF, see Figure 4.11, shows a peak at 1.35 eV with a shoulder at 1.2 eV. In the near infrared region between 1.0 and 0.6 eV, a significant offset without any distinct feature is observed. The modulation frequency dependences of the PIA at 1.38 and 1.22 eV are weak and no crossing of the in and out-of-phase is observed. This indicates relatively short lifetimes ($\tau < 0.1$ ms) with a broad inhomogeneous distribution. No model could be found to fit this modulation dependence satisfactorily.
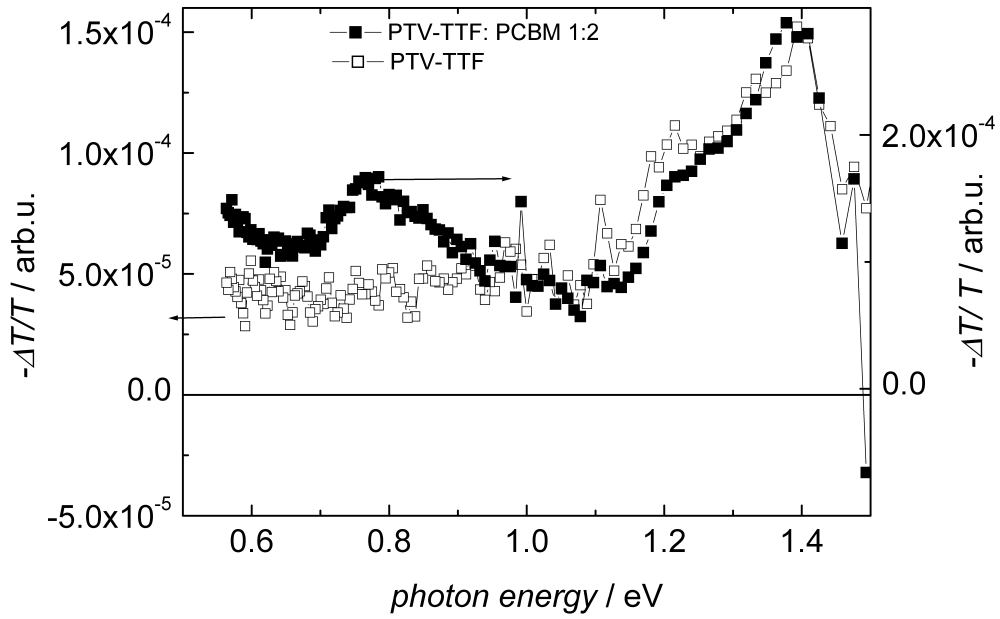
Figure 4. 11: PIA spectrum of PTV-TTF and PTV-TTF: PCBM 1:2 thin films, drop cast on glass. Spectra were recorded at 20 K, illumination at 514 mW with 40 mW.
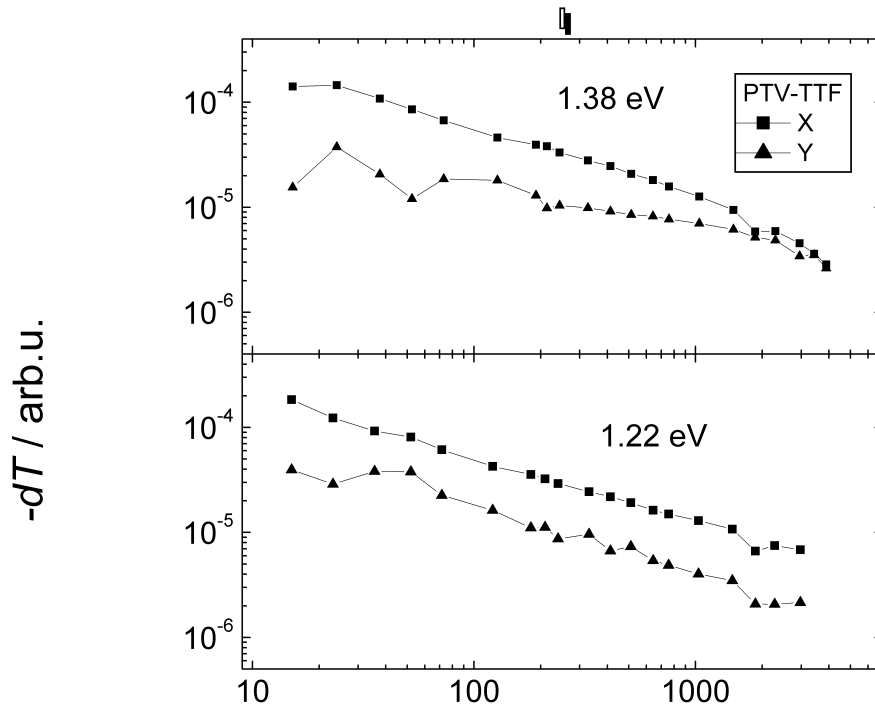

Figure 4. 12: Modulation frequency dependence of the PIA of PTV-TTF at 1.38 eV (upper part) and 1.22 eV (lower part), measurements were done at 20 K, illumination 40 mW. Lines are guide for the eyes.

PIA spectrum of a PTV-TTF: PCBM blend film is shown in Figure 4.11. The 1.4 eV PIA of the pristine polymer is preserved in the blend, but additionally, two new absorption peaks at 0.8 and <0.55 eV are observed.

The modulation frequency dependences, see Figure 4.13, show differences for the 1.4 eV and the new absorption at 0.8 and <0.55 eV. The peak at 1.46 eV could be fitted by the dispersive recombination model with a mean lifetime of $\tau = 0.7$ ms. The lifetime shows a broad distribution ($\alpha = 0.64$). The two low energy peaks show a weaker dependence on the modulation frequency, what indicates shorter lifetimes. Their dependence could not be fitted satisfactorily, the lines in the graph are guide for the eye. Interestingly, also the shoulder at 1.24 eV shows a distinct modulation frequency dependence as the 1.46 eV peak.
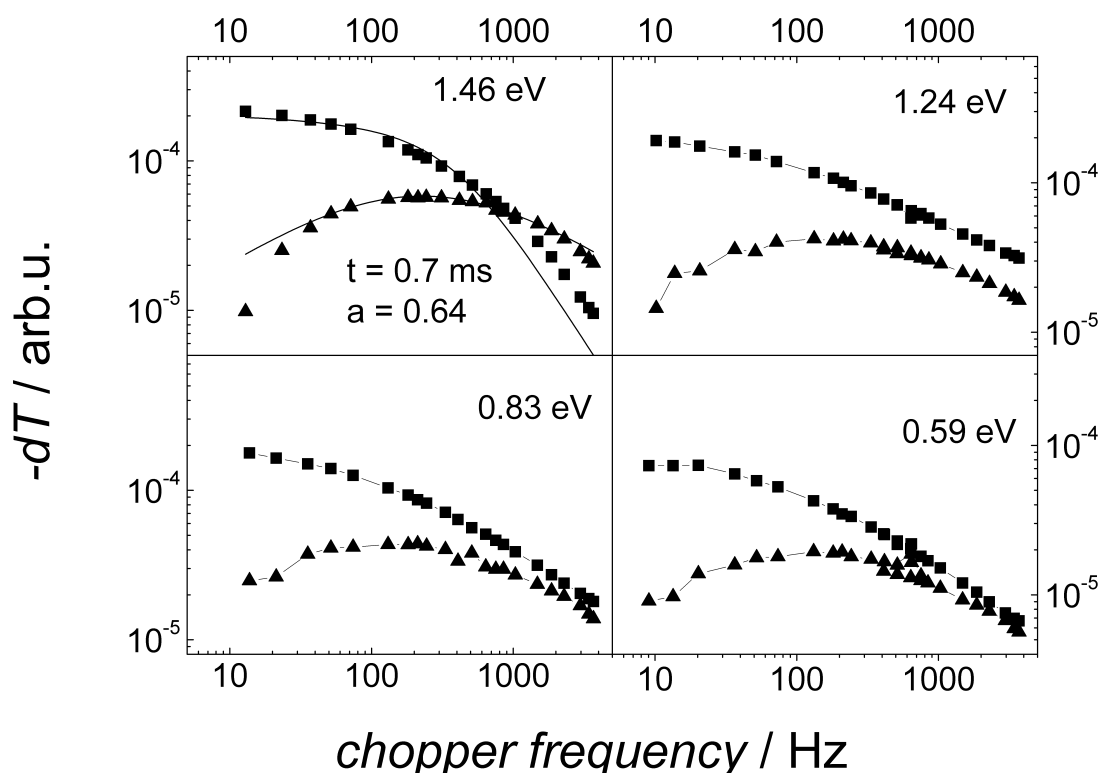

Figure 4. 13: Modulation frequency dependence of the PIA of PTV-TTF: PCBM 1:2 at 1.46 eV, 1.24 eV, 0.83 eV and 0.59 eV measurements were done at 20 K, illumination 40 mW. For 1.46 eV, an excited state lifetime of 0.7 ms and a dispersion factor of $\alpha = 0.64$ is calculated. For the other measurements, the fitting procedure does not lead to a satisfying result. Lines are guide for the eyes.

Excited state interactions between oligo- thienylene vinylenes and fulleropyrrolidines MP-C_{60} in solution were investigated by Apperloo et al.[66] The PIA spectra for PTV-TTF and blend with PCBM will be compared with spectra for hexyl-substituted *dodec*a thienylene vinylene (12TV): MP-C_{60} mixed solution. The optical absorption of 12TV in CH_2Cl_2 shows a maximum at 2.11

eV, as compared for PTV-TTF in chlorobenzene solution 2.06 eV. In solid state, the absorption maximum is shifted to 1.96 eV.

PIA of 12 TV and MP-C$_{60}$ in the non-polar solvent toluene shows a peak at 1.42 eV. This peak is assigned to a T$_1$→T$_n$ absorption of triplet excited 12TV. In the more polar solvent o-dichlorobenzene, two additional peaks at 0.46 and 1.00 eV are observed besides the 1.42 eV peak. These two new absorptions are assigned to the 12TV radical cation. This assignment is confirmed by in-situ electrochemical absorption measurements.[67] Further, for poly-thienylene vinylene polaron absorptions were determined by Lane et al by Photoinduced Absorption Detected Magnetic Resonance with 1.1 eV and 0.4 eV.[68]

Apperloo et al determined that the triplet and the charge separated state of 12TV possess comparable energies. It is therefore assumed that the triplet state of 12TV and charge separated state can be formed and observed simultaneously.[67]

In the PIA, for both materials a peak at 1.4 eV is observed. This peak was assigned to a T$_1$→T$_n$ absorption. Further, the 0.8 eV and <0.55 eV peaks are comparable with the cation absorption of 12TV at 1 eV and 0.46 eV and therefore assigned to the polaron absorption of PTV-TTF. Similar to the optical absorption, a redshift is observed for the positive polaron.

In blends of PTV-TTF and PCBM, the coexistence of triplets and charge separated state is concluded. The quantum efficiency for the charge separation is unclear.

4.5.3 Photovoltaic Devices from PTV-TTF

Pristine PTV-TTF shows non-favourable film forming properties, no electro-optical characterization could be obtained.

In combination with PCBM, thin films of sufficient quality can be spin cast from chlorobenzene solution. The I-V characteristics shows good diode behaviour with a rectification factor R(+/-2V) = 250, see for the I-V characteristics Figure 4.14. Under illumination, a photovoltaic effect is observed with a power conversion efficiency of 0.13 % under solar simulated light. This is comparable with literature values reported poly-(thienylene vinylene) based bulk heterojunction devices. [69]

The photocurrent spectrum, see Figure 4.15, shows peaks at 350 and 650 nm, corresponding to PCBM and PTV-TTF absorption, respectively. The onset for the photocurrent is around 850 nm, corresponding to the absorption onset of PTV-TTF.
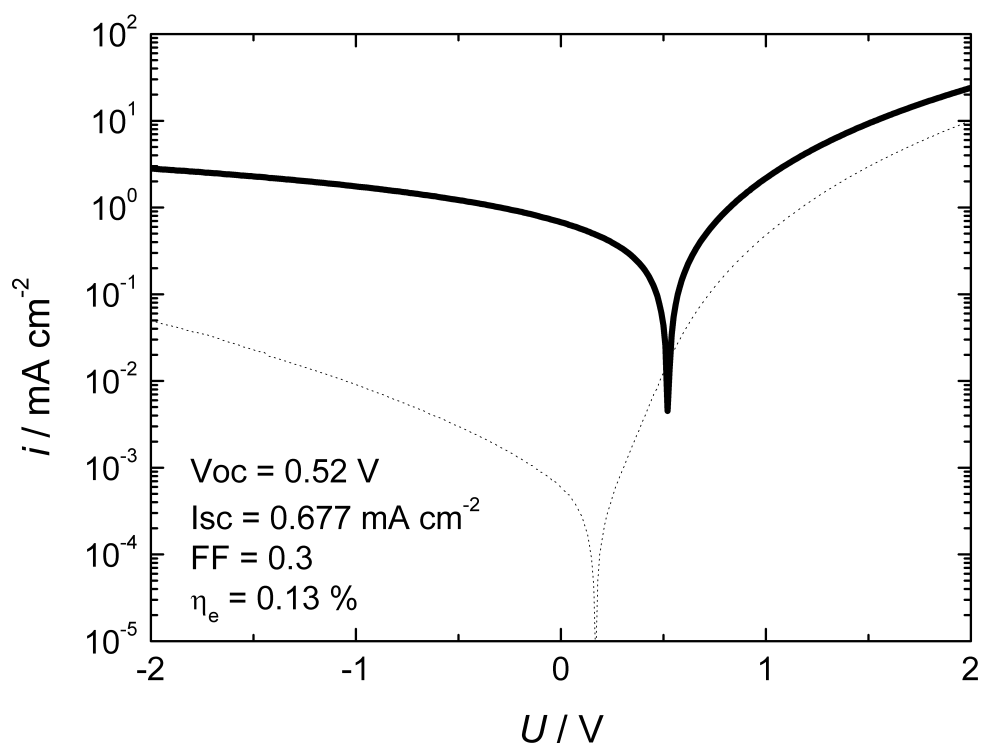
Figure 4. 14: Current –Voltage characteristics for a PTV-TTF: PCBM 1:2 device, spin coat from chlorobenzene, in the dark (dotted line) and under illumination from a solar simulator with 80 mW cm^{-2}. Active area thickness is approx. 50 nm.
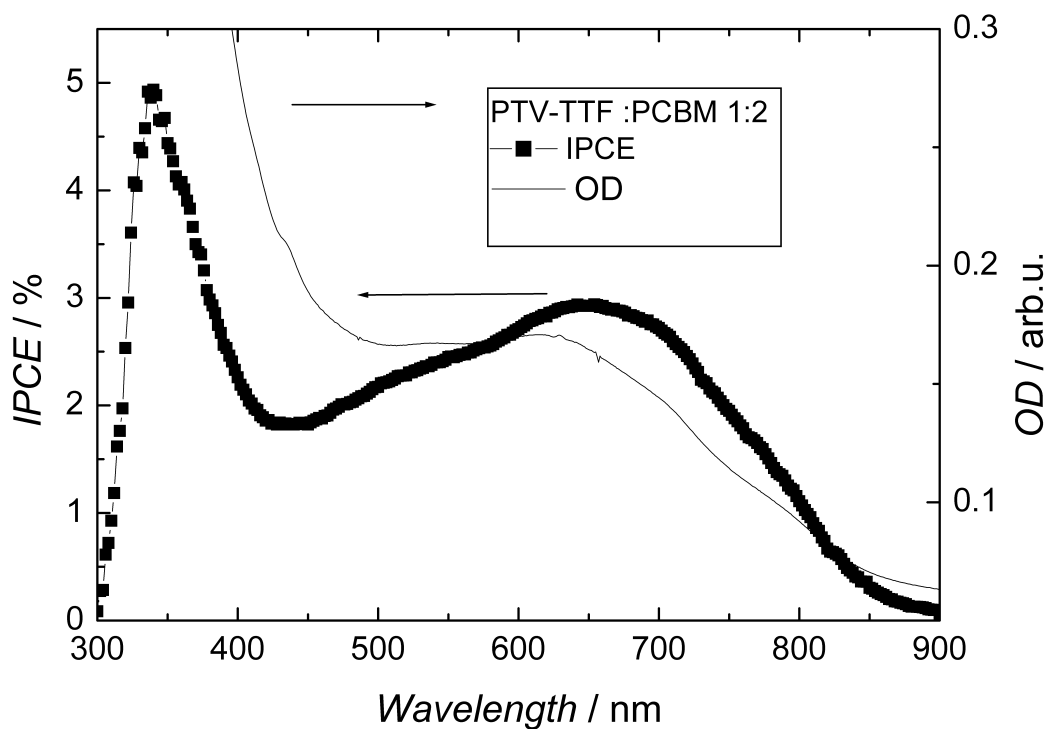

Figure 4. 15: Photocurrent spectrum of a PTV-TTF: PCBM 1:2 device, in comparison the optical absorption spectrum of a film, prepared under same conditions, on glass.

4.6 References

[1] R. E. Peierls, Quantum Theory of Solids, Oxford University Press, London 1955

[2] H. Shirakawa, E. J. Louis, A. G. MacDiarmid, C. K. Chiang, A. J. Heeger, Journal of The Chemical Society, Chemical Communication 1977, 578

[3] J. Roncali, *Chemical Review.*1997, **97**, 173

[4] R. Kiesboms et.al, "Synthesis of Electric and Optical Properties of Conjugated Polymer in Handbook of Advanced Electronic and Photonic Material and Devices 8, p 38-47 edited by Hari Singh Nalwa, (2000)

[5] J. L. Bredas, A. J. Heeger, F. Wudl, *Journal of Chemical Physics* 1986, **85**, 4673

[6] F. Wudl, M. Kobayashi, A. J. Heeger, *Journal of Organic Chemistry* 1984, **49**, 3382

[7] M. Kobayashi, N. Colaneri, M. Boysel, F. Wudl, A. J. Heeger, *Journal of Chemical Physics* 1985, **82**, 5717

[8] H. Meng, Y. Cheng, F. Wudl, *Macromolecules* 2001, **34**, 1810

[9] I. Polec, A. Henckens. L. Goris, M. Nicolas, M. A. Loi, P. J. Adriaensens, L. Lutsen, J. V. Manca, D. Vanderzande, N. S. Sariciftci, *Journal of Polymer Science A* 2003, **41**, 1034

[10] G. Zerbi, M. C. Magnoli, I. Hoogmartens, R. Kiebooms, R. Carleer, D. Vanderzande, J. Gelan, *Advanced Materials* 1995, **7**, 1027

[11] C. Quattrocchi, R. Lazzaroni, J. L. Brédas, R. Kieboom D. Vanderzande, J. Gelan, *Journal fo Physical Chemistry* 1995, **99**, 3932

[12] H. Meier, U. Stalmach, H. Kolshorn, *Acta Polymerica* 1997, **48**, 379

[13] R. D. McCullough, R. D. Lowe, M. Jayaraman, D. L. Anderson, *Journal of Organic Chemistry* 1993, **85**, 904

[14] T. D. Chen, R. D. Rieke, *Journal of The American Chemical Society* 1998, **8**, 25

[15] M. Pomerantz, in *Handbook of Conducting Polymers*, edited by T. A. Skotheim, R. L. Elsenbaumer, J. R. Reynolds, Marcel Dekker, Inc. New York, Basel, Hong Kong, 1998, 277

[16] A. Ajayaghosh, *Chemical Society Review* 2003, **32**, 181

[17] G. Brocks, A. Tol, *Journal of Physical Chemistry* 1996, **100**, 1838

[18] M. Dietrich, J. Heinze, G. Heywang, F. Jonas, *Journal of Electranalytic Chemistry* 1994, **369**, 87

[19] Q. Pei, G. Zuccarello, M. Ahlskog, O. Inganäs, *Polymer* 1994, **35**, 1347

[20] S. A. Jenekhe, *Nature* 1986, **322**, 345

[21] H. Aota, T. Reikan, A. Matsumoto, M. Kamachi, *Chemical Physics Letters* 1998, **335**

[22] M. Hanack, S. Döttinger, *Synthetic Metals* 1996, **79**, 43

[23] U. Scherf, K. Müllen, *Synthesis* 1992, 23

[24] Y. Yao, J.J.S. Lamba, H. M. Tour, *Journal of The American Chemical Society* 1998, **120**, 2805

[25] T. W. Brockman, J. M. Tour, *Journal of The American Chemical Society* 1995, **117**, 4437

[26] J. L. Bredas, *Advanced Materials* 1995, **7**, 263

[27] A. Dkhissi, F. Louwet, L. Groenendaal, B. Beljonne, R. Lazzaroni, J. L. Bredas, *Chemical Physics Letters* 2002, **359**, 466

[28] L. B. Groenendaal, F. Jonas, D. Freitag, H. Pielartzik, J. R. Reynolds, *Advanced Materials* 2000, **12**, 481

[29] C. Aribizzani, M. Castellani, C. G. Cerrroni, M. Mastagostino, *Journal of Electroanalytic Chemistry* 1997, **423**, 23

[30] M. Castellani, R. Lazzaroni. J. L. Bredas, S. Luzzati, *Synthetic Metals* 1999, **101**, 175

[31] A. Cravino, H. Neugebauer, S. Luzzati, M. Castellani, A. Petr, L. Dunsch, N. S. Sariciftci, *Journal of Physical Chemistry B* 2002, **106**, 3583

[32] A. Dhanabalan, P.A. van Hal, J.K.J. van Duren, R. A. J. Janssen, *Synthetic Metals* 2001 **121**, 2175

[33] A. Dhanabalan, J.K.J. van Duren, P.A. Van Hal, J.L.J. van Dongen, R.A.J. Janssen, *Advanced Functional Materials* 2001, **11**, 255

[34] M. Svensson, F. Zhang, S. C. Veenstra, W. J. H. Verhees, J. C. Hummelen, J. M. Kroon, O. Inganäs, M. R. Andersson, *Advanced Materials* 2003, **15**, 988

[35] Y. Teketel, F. Zhang, M. Svensson, J. C. Hummelen, M. R. Andersson, O. Inganäs. *Thin Solid Films* 2004, **449**, 152

[36] Q. Hou, Y. Xu, W. Yang, M. Yuan, J. Peng, Y. Cao, *Journal of Materials Chemistry* 2002, **12**, 2887

[37] Q. Zhou, Q. Hou, L. Zheng, X. Deng, G. Yu, Y. Cao, *Applied Physics Letter*, 2004, **84**, 1653

[38] L. Goris, M. A. Loi, A. Cravino, H. Neugebauer, N. S. Sariciftci, I. Polec, L. Lutsen, E. Andries, J. Manca, L. De Schepper, D. Vanderzande, *Synthetic Metals* 2003, **138**, 249

[39] A. Cravino, M. A. Loi, M. C. Scharber, C. Winder, H. Neugebauer, P. Denk, H. Meng, Y. Chen, F. Wudl, N. S. Sariciftci, *Synthetic Metals* 2003, **137**, 1435

[40] S. E. Shaheen, D. Vangeneugden, R. Kiebooms, D. Vanderzande, T. Fromherz, F. Padinger, C. J. Brabec N. S. Sariciftci, *Synthetic Metals* 2001, **121**, 1583

[41] K. Colladet, M. Nicolas, L. Goris, L. Lutsen, D. Vanderzande, *Thin Solid Films* 2004, **451-452**, 7

[42] H. Sirringhaus, N. Tessler, R. H. Friend, *Science* 1998, **280**, 1741

[43] K. Yoshino, S. Nakajima, Dae-Hee-Park. R. Sugimoto, *Japanese Journal of Applied Physics Part 2* 1988, *27, 715*

[44] H. J. Fell, E. J. Samuelson, M. R. Andersson, J. Als-Nielsen, G. Grübel, J. Mardalen, *Synthetic Metals* 1995, **73**, 279

[45] K. E. Aasmundtvei, E. J. Samuelsen, W. Mammo, M . Svensson, M. R. Andersson, L. A. A. Pettersson, O. Inganäs, *Macromolecules* 2000, **33**, 5481

[46] M. R. Andersson, O. Thomas, W. Manno, M. Svensson, M. Theander, O. Inganäs, *Journal of Materials Chemistry* 1999, **9**, 1933

[47] C. J. Brabec, C. Winder, M. C. Scharber, N. S. Sariciftci, J. C. Hummelen, M. Svensson, M. R. Andersson, *Journal of Chemical Physics* 2001, **15**, 7235

[48] C.J. Brabec, C.Winder, M.Scharber, N.S. Sariciftci, M.R.Andersson, O.Inganäs, J.C.Hummelen *Material Research Symposium Proceedings* 2000, **598**, B 3.24.1-6

[49] X. Wei, Z. V. Vardeny, N. S. Sariciftci, A. J. Heeger, *Physical Review B* 1996, **53**, 2187

[50] R. Österbacka. C. P. An, X. M. Jiang, Z. V. Vardeny, *Science* 2000, **287**, 839

[51] D. Beljonne, J. Cornil, H. Sirringhaus, P. J. Brown, M. Shkunov, R. H. Friend, J. L. Bredas, *Advanced Functional Materials.* 2001, **11**, 229

[52] L. S. Roman, W. Manno, L. A. A. Pettersson, M. R. Andersson, O. Inganäs, *Advanced Materials* 1998, **10** , 774

[53] part of this work was already presented in: C. Winder, Diplomarbeit, Universität Linz, 2001

[54] D. Muehlbacher, H. Neugebauer, A. Cravino, N. S. Sariciftci, J.K.J. van Duren, A. Dhanabalan, P. van Hal, R. A.J. Janssen, J.K. Hummelen, *Molecular Crystals and Liquid Crystals.* 2002, **385**, 85

[55] J.K.J. van Duren, A. Dhanabalan, P.A. van Hal, R. A. J. Janssen, *Synthetic Metals.* 2001**121**, 1587

[56] C. J. Brabec, C. Winder, N. S. Sariciftci, H. C. Hummelen, A. Dhanabalan, P. A. van Hal, R. A. J. Janssen, *Advanced Functional. Materials* 2002, **12**, 709

[57] C. Winder, G. Matt, J. C. Hummelen, R. A. J. Janssen, N. S. Sariciftci, C.J. Brabec, *Thin Solid Films* 2002, **403-404**, 373

[58] N. Ono, H. Okumura, T. Murashima, *Heteroatom Chemistry* 2001, **12**, 414

[59] J. Roncali, I. Jestin, P. Frère, E. Levillain, D. Stievenard, *Synthetic Metals* 1999, **101**, 667

[60] C. Martineau, P. Blanchard, D. Rondeau, J. Delaunay, J. Roncali, *Advanced Materials* 2002, **14**, 283

[61] D. Rondeau, C. Matrineau, P. Blanchard, J. Roncali, *Journal of Mass Spectrometry* 2002, **37**, 1081

[62] H-Q. Xie, C. M. Liu, J. S. Guo, *European Polymer Journal* 1996, **32**, 1131

[63] Z. Guijiang, L. Junchao, Y. Cheng, *Synthetic Metals* 2003, **485**, 135

[64] I. Jestin, P. Frère, E. Levillain, J. Roncali, *Advanced Materials* 1999, **11**, 134

[65] A. J. Brassett, N. F. Colaneri, D. D. C. Bradley, R. A. Lawrence, R. H. Friend, H. Murata, S. Tokito, T. Tsutsui, S. Saito, *Physical Reviev B* 1990, **41**, 10586

[66] J. J. Apperloo, C. Matrineau, P. A. van Hal, J. Roncali, R. A. J. Janssen, *Journal of Physical Chemistry B* 2002, **106**, 21

[67] J. J. Apperloo, J. M. Raimundo, P. Frère, J. Roncali, R. A. J. Janssen, *Chemistry, A European Journal* 2000, **6**, 1698

[68] P.A. Lane, X. Wei, Z. V. Vardeny, *Physical Review Letters* 1996**, 77**, 1544

[69] A. Henckens, M. Knipper, I. Polec, J. Manca, L. Lutsen, D. Vanderzande, *Thin Solid Films* 2004, **451**, 572

5. Electron Acceptor Polymer

In this chapter, conjugated polymers are presented which have electron accepting properties. Such materials are cheap alternatives for C_{60} based acceptors. Further, absorption range, electron affinity and solubility are important parameter, which can be tuned much easier and over a larger range as compared to C_{60}. Ellen Moons recently reviewed properties and device applications of conjugated polymer blends.[1]

A wide range of electron acceptor polymers has been presented in the literature. Most of them contain electron-withdrawing groups like cyano, nitro or halogen substitutions. These substitutions lower the electron density in the polymer backbone and stabilize therefore the negative charge. Most prominent materials, which were presented for photovoltaic applications, are MEH-cyano-PPV,[2,3] showing in combination with polythiophenes 1.8 % conversion efficiency, polyfluorene-2,1,3-benzoethiadazole copolymers[4,5,6] and poly-(benzamidazobenzo phenanthroline) BBL.[7,8,9]

5.1 Poly(*p*-Phenylene vinylene) Fluorinated Copolymer

The polymer copoly- 2,3,5,6-tetrafluoro-1,4-phenylene vinylene-2,5-dioctyloxy-1,4-phenylene vinylene, TFPV-DOPV, was synthesized at the university of Bari, group of Prof. Gianluca Farinola, and provided to the University of Linz. The ratio of the tetrafluoro substituted and dialkoxy substituted monomers is TFPV: DOPV 60:40. The monomers are randomly distributed in the chain. The synthesis is performed *via* the Stille cross-coupling reactions, as described in the literature.[10,11,12]

5.1.1 Photophysical and Electrochemical Properties

The polymer is tested as possible donor as well as acceptor material. The chemical structure and the absorption-emission of a thin solid film are shown in Figure 5.1. The absorption coefficient at the maximum λ_{max} = 450 nm is $1.3* 10^5$ cm $^{-1}$, see Figure 5.1. The absorption is slightly blue-shifted compared to parent homopolymer dialkoxy-substituted para-phenylene vinylene PDOPV (λ_{max} = 460 nm), but red-shifted in comparison with the poly-tetrafluoro-phenylene vinylene PTFPV(λ_{max} = 335 nm). Interestingly, the photoluminescence maximum (λ_{max} = 660 nm) is red-shifted in comparison to PDOPV (λ_{max} = 580 nm) and PTFPV (λ_{max} = 530 nm). This large Stoke shift in solid state is assigned to an increased interchain interaction in the copolymer.[11]

This is further confirmed by the large redshift of the photoluminescence from $CHCl_3$ solution (λ_{max} = 530 nm) to solid state (λ_{max} = 660 nm).[11]
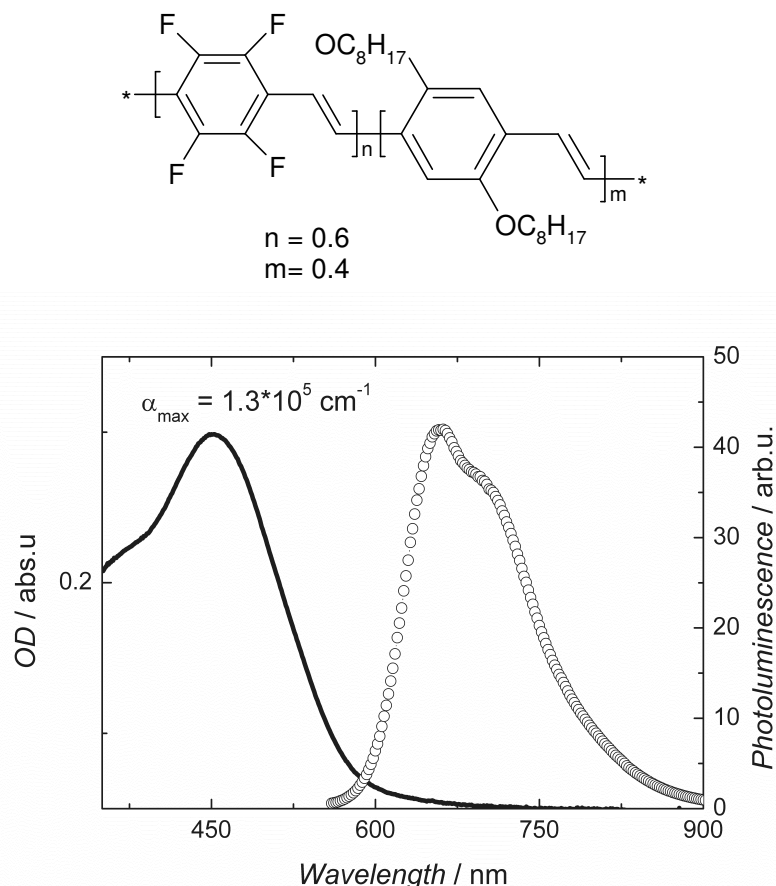

Figure 5. 1: Chemical structure of copoly- 2,3,5,6-tetrafluoro-1,4-phenylene vinylene-2,5-dioctyloxy-1,4-phenylene vinylene, TFPV-DOPV (upper part); optical absorption and photoluminescence of TFPV-DOPV thin film. Photoluminescence is measured at 80 K, excitation with 476 nm and 40 mW (lower part).

Cyclic voltammetric experiments were carried out with a platinum foil working electrode (WE) with a dip-coated film from chloroform solutions (5mg/ml). As a counter electrode (CE) a platinum foil and as a quasi-reference electrode (RE) a silver wire coated with AgCl were used. The electrolyte solution, a 0.1 M Bu_4NPF_6-acetonitril solution, was kept under argon flow to exclude moisture and oxygen during the electrochemical processes. It can be seen that the material is both oxidized and reduced with p-doping/dedoping onset potential at about 0.9 V (HOMO 5.8 eV) and n-doping/dedoping onset potential at about -1.0 V (LUMO 3.9 eV) versus the quasi Ag/AgCl reference electrode.

Infrared spectroelectrochemical studies show the optical signature of positive and negative charges. Both charge carriers show different IRAV bands. Photoinduced infrared active vibration spectroscopy shows predominantly absorption of negative charge carriers.[13]
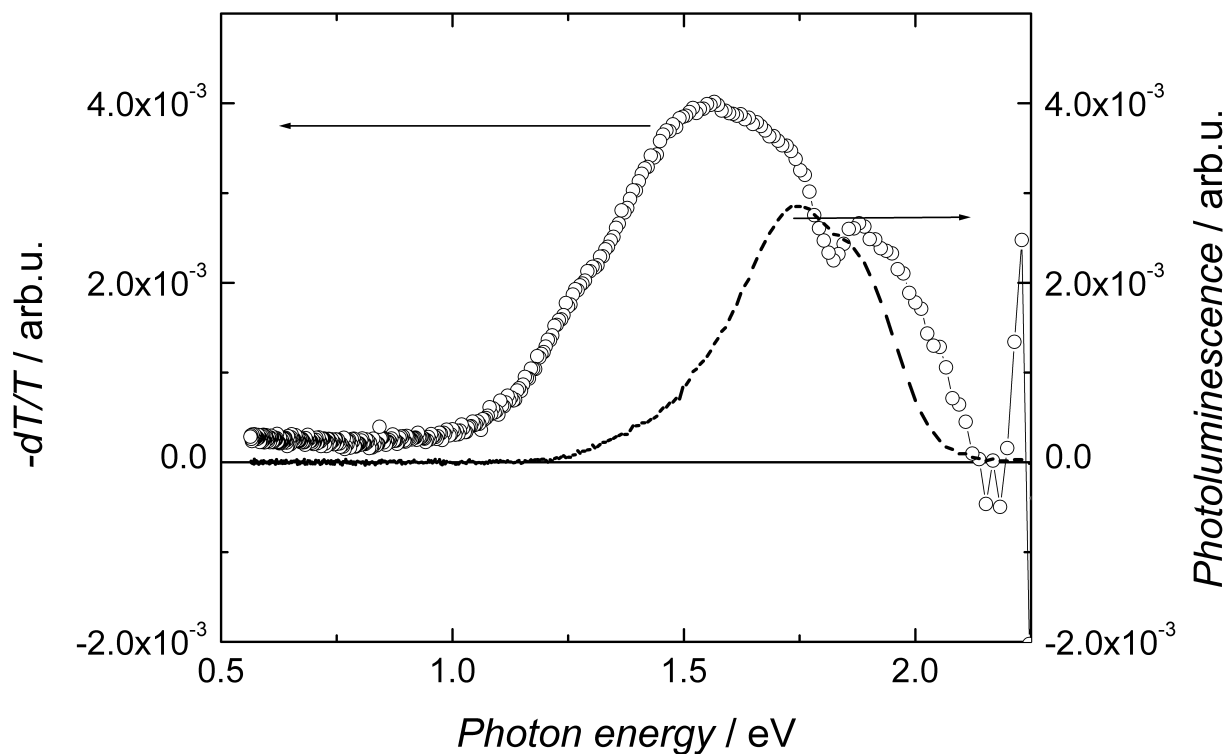
Figure 5. 2: PIA (circles) of TFPV-DOPV drop cast film on glass at 80 K, excitation with 40 mW at 476 nm. Photoluminescence response is shown for comparison (dashed line).

PIA of TFPV-DOPV shows a broad single peak at 1.55 eV, see Figure 5.2. The small dip around 1.75 eV might origin from overcompensated photoluminescence. The photoluminescence response of the film is shown for comparison. In the spectral range between 1.7 and 2.0 eV, it is stronger than the PIA signal.

The modulation frequency dependence, see Figure 5.3, is measured at 1.38 eV. At this energy, the contribution from the photoluminescence is negligible. A well defined ($\alpha = 0.90$) exited state lifetime of $\tau = 0.13$ ms is calculated. The PIA might be attributed to a $T_1 \rightarrow T_n$ transition.
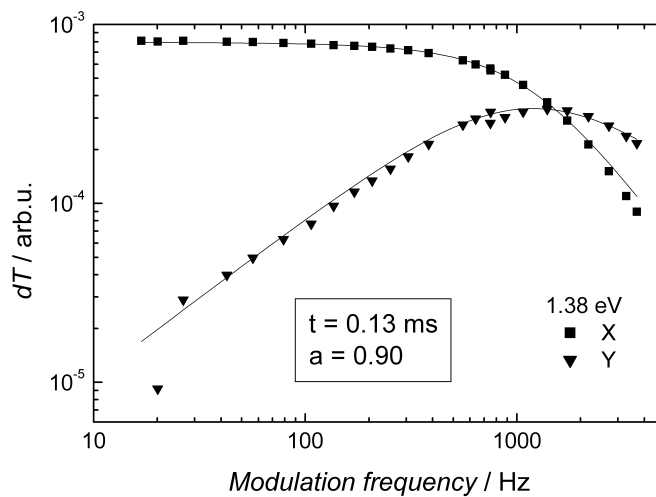
Figure 5. 3: Modulation frequency dependence of the PIA of TFPV-DOPV at 1.38 eV, at 80 K and 40 mW excitation. Fit (thin line) is done by a dispersive recombination model.
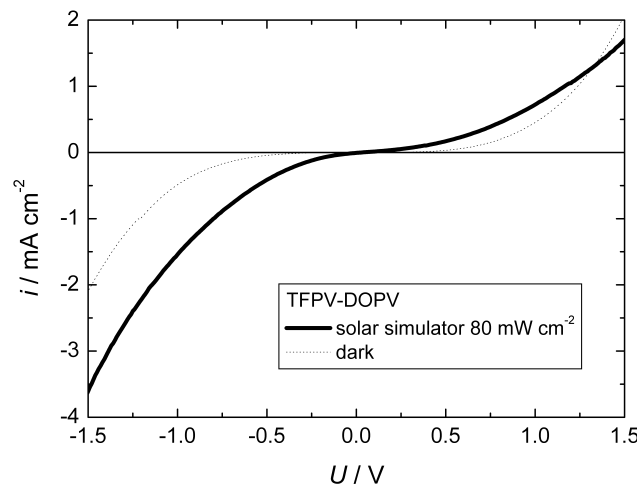
5.1.2 Devices

Figure 5. 4: I-V characteristics of a TFPV-DOPV single layer device, spin cast from chlorobenzene, under solar simulated illumination and in the dark. The active layer thickness is approx. 35 nm.

Figure 5.4 shows the I-V characteristics of a TFPV-DOPV single layer device. No photovoltaic effect is observed, but photoconductivity. Interestingly, the device shows inverse rectification under illumination.

5.1.3 TFPV-DOPV: MDMO-PPV blends

The possibility of reversible reduction and the formation of negative charges under illumination show the electron accepting properties of TFPV-DOPV. Therefore, the material is tested as possible electron acceptor towards MDMO-PPV. A schematic energy diagram is shown in Figure 5.5. It shows a large offset between the MDMO-PPV and TFPV-DOPV levels. This is required for photoinduced charge separation.
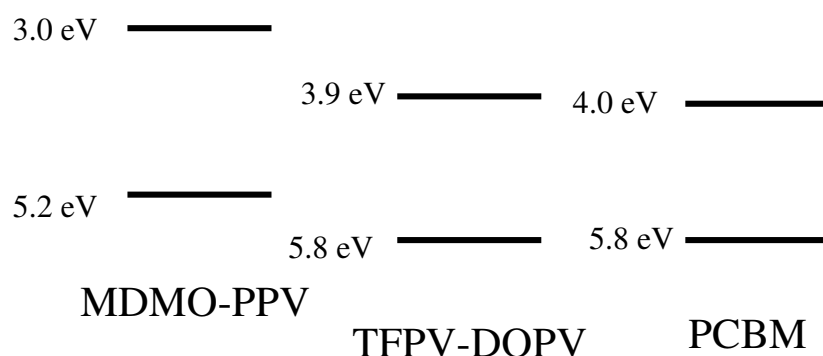
3.0 eV ———

3.9 eV ——— 4.0 eV ———

5.2 eV ———

5.8 eV ——— 5.8 eV ———

MDMO-PPV

TFPV-DOPV   PCBM

Figure 5. 5: Energy levels of HOMO and LUMO of MDMO-PPV, TFPV-DOPV and PCBM, derived from electrochemical measurements in solution. The LUMO level of MDMO-PPV and the HOMO of PCBM are estimated by the optical band gap, since this processes are not observed.

Figure 5.6 shows the photoluminescence for different blends of MDMO-PPV and TFPV-DOPV and the pristine materials. Small additions of TFPV-DOPV quench the MDMO-PPV photoluminescence. The second vibronic peak of MDMO-PPV seems to gain intensity with increasing of TFPV-DOPV concentration, which might be photoluminescence contribution from the latter one. At higher concentration of TFPV-DOPV, only the TFPV-DOPV photoluminescence is observed. Interestingly, the photoluminescence of the 1:1 blend is slightly red shifted compared to pristine TFPV-DOPV. This might be originating from the different environment in the blends as compared to the pristine material. The strong quenching of the MDMO-PPV luminescence shows interaction of the photoexcited state with TFPV-DOPV. Further, the photoluminescence of TFPV-DOPV is solely observed in the blends. Such behaviour is commonly explained by energy transfer. But no increase of the TFPV-DOPV is observed, as would be expected for such interaction.

Further, the MDMO-PPV photoluminescence, peak at 600 nm, shows no overlap with the TFPV-DOPV absorption, which shows its peak at 450 nm. Such an overlap is necessary for efficient energy transfer (see Chapter 1.3).

Alternatively, photoinduced electron transfer form MDMO-PPV to TFPV-DOPV can rationalize the photoluminescence quenching. For the photoexcited state of TFPV-DOPV, no interaction with MDMO-PPV is assumed, since its photoluminescence is not influenced.
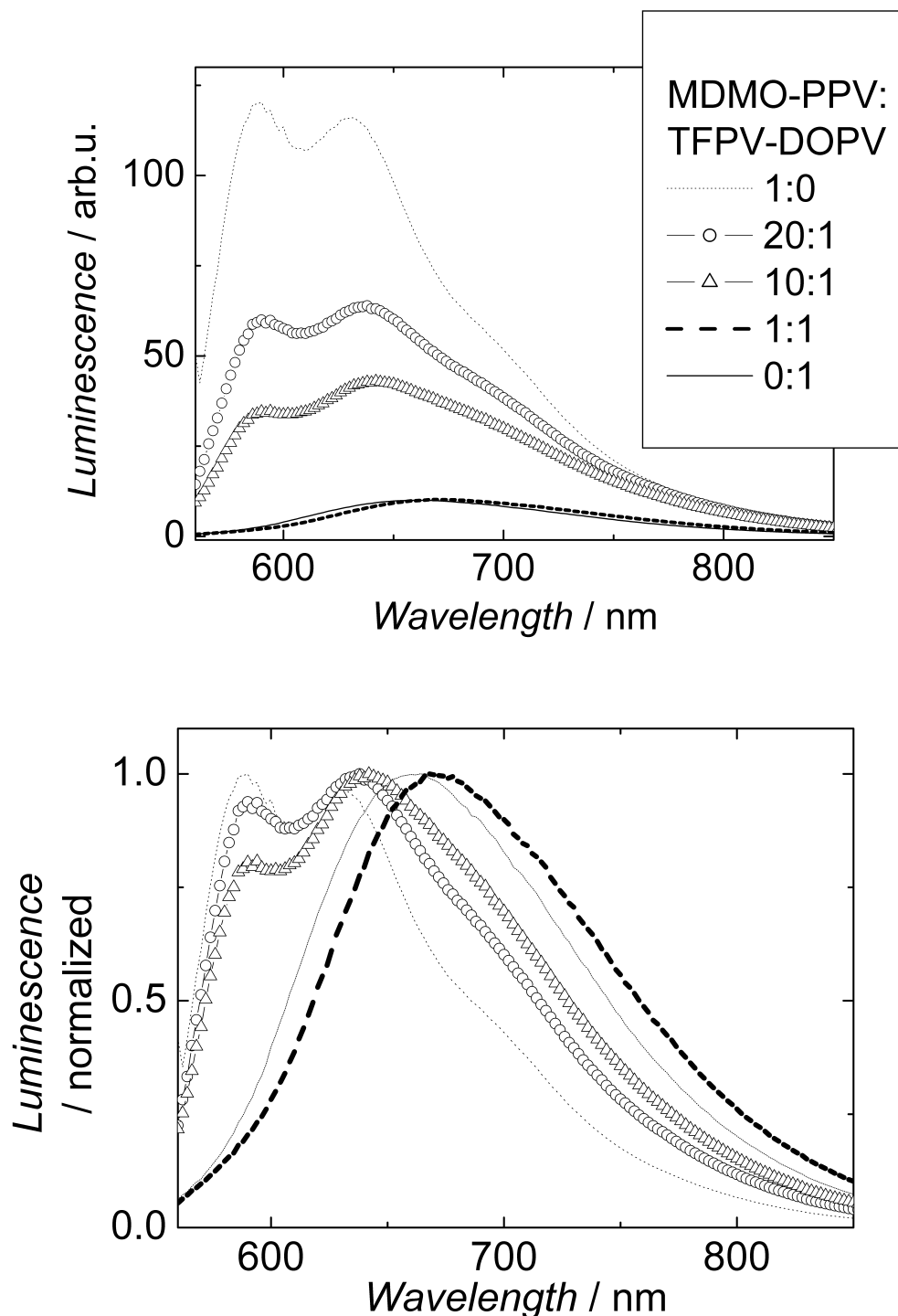

Figure 5. 6: Photoluminescence of MDMO-PPV: TFPV-DOPV blend films (to the right), spincast form chlorobenzene. Measurements are done at room temperature and vacuum $p < 10^{-5}$ mbar, excitation with 40 mW at 476 nm. On the left, the photoluminescence spectra are shown normalized to their maximum.

The PIA of the blend, see Figure 5.7, shows a peak at 1.4 eV with a shoulder at 1.2 eV and a long tail up to 2 eV. A weak absorption feature is observed for probe energies <0.5 eV. In comparison, the PIA spectra of the MDMO-PPV polaron (from MDMO-PPV: PCBM blends) and a calculated spectrum of two the two triplet absorption of MDMO-PPV and TFPV-DOPV is shown. The PIA feature of the polymer blend matches the HE polaron feature of MDMO-PPV. The low energy feature of the polymer blend is much weaker than the low energy absorption of the MDMO-PPV polaron. Alternatively, the PIA of the blend is compared with the triplet features of the pristine material. None of the triplet absorption nor the sum of both match the PIA of the blend. The absorption spectrum in the VIS-NIR spectral range of TFPV-DOPV polaron could not be measured.

From the modulation frequency dependence at 1.38 eV, see Figure 5.8, a broad distributed ($\alpha = 0.68$) and a mean lifetime of $\tau = 0.13$ ms is determined. The laser power dependence is fitted by a power law and shows a gradient of k = 0.53. This indicates bimolecular type recombination behaviour of the photoexcitation, which is expected for charge carriers.
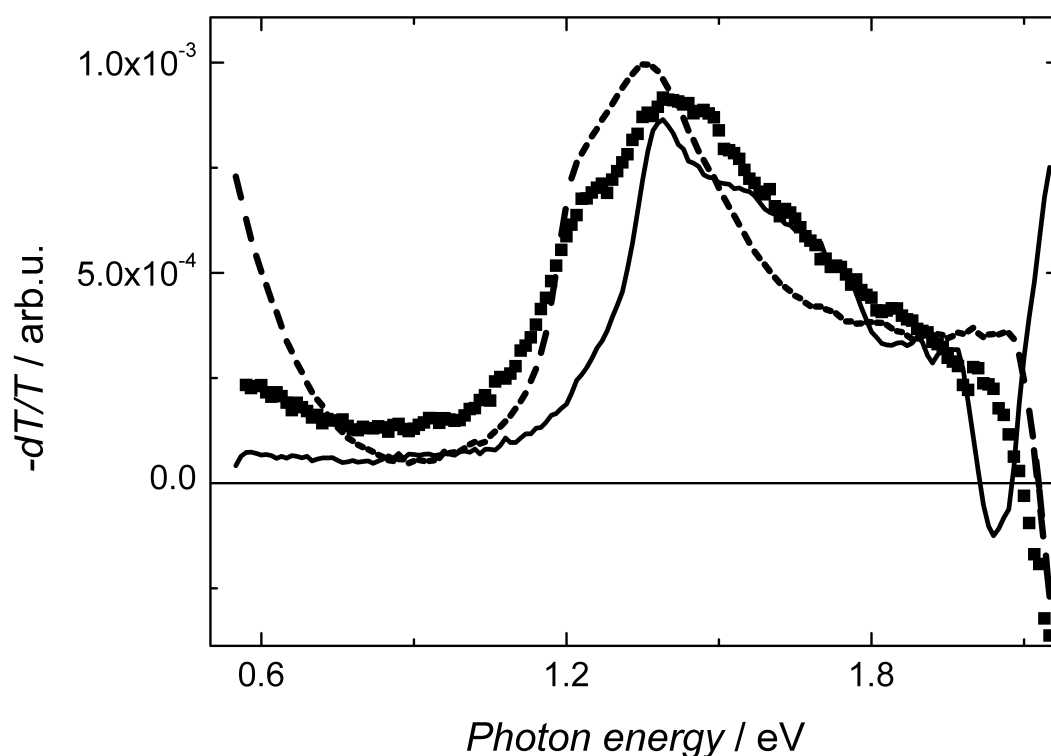

Figure 5. 7: PIA of a TFPV: MDMO-PPV 1:1 (squares) blend film at 80 K, excitation with 40 mW at 476 nm. In comparison the mathematical sum spectrum of TFPV-DOPV and MDMO-PPV triplet (full line), and MDMO-PPV positive polaron (dashed line).
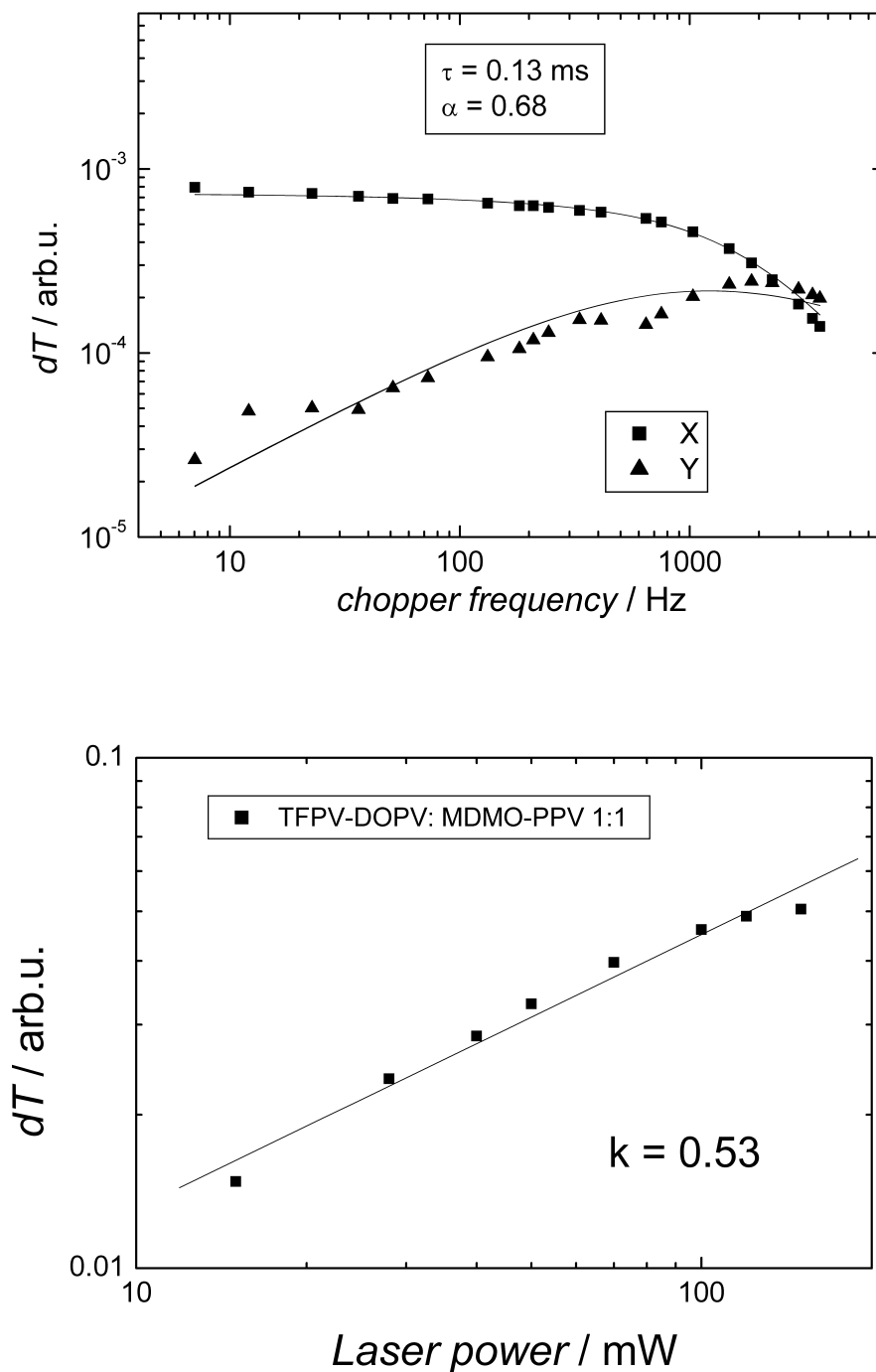
Figure 5. 8: Modulation frequency dependence of the PIA at 1.38 eV (upper graph) of TFPV-DOPV: MDMO-PPV, spin cast from chlorobenzene solution, at 80 K and excitation with 40 mW at 476 nm; lines show fit after a dispersive recombination model. Excitation power dependence of the PIA at 1.38 eV (lower part) for the same film, modulation frequency 37 Hz, is shown. The line show fit after a power law.

In summary, photophysical experiments of TFPV-DOPV: MDMO-PPV blends show strong indications for photoinduced charge transfer. The PIA spectrum of this blend resembles most the absorption of MDMO-PPV polaron. The laser power dependence indicates bimolecular type

recombination. And the lifetime shows a broad distribution, which is typical for polaronic charge carriers in conjugated polymer. Further, the photoluminescence of MDMO-PPV is quenched in blends with TFPV-DOPV.
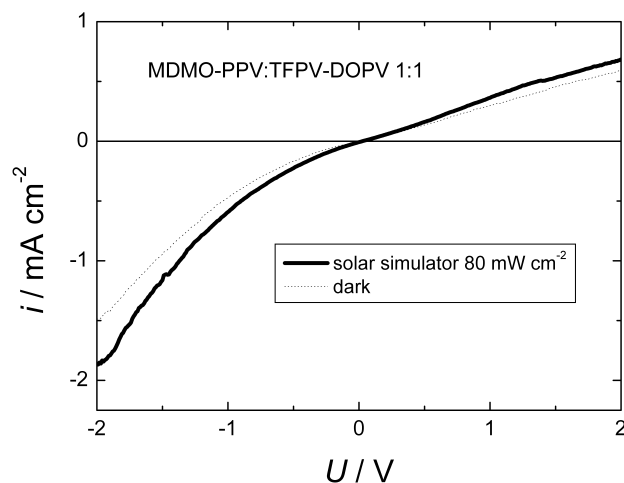

Figure 5. 9: I-V curve of an MDMO-PPV: TFPV-DOPV 1:1 blend device under solar simulated light (full line) and in the dark (dotted line). Active layer thickness is approx. 60 nm.

Figure 5.9 shows the current voltage characteristics of an MDMO-PPV: TFPV-DOPV blend device. No photovoltaic effect is observed. Interestingly, the device shows an inverse rectification. This might originate from a wrong choice of contacts.

5.1.4 TFPV-DOPV: PCBM blend

Blends from TFPV-DOPV and PCBM are investigated to test TFPV-DOPV as possible electron donor material in combination with fullerenes.

The photoluminescence of a blend with a TFPV-DOPV: PCBM 1:3 ratio, see Figure 5.10, shows two peaks at 650 nm and 750 nm, assigned to TFPV-DOPV and PCBM, respectively.
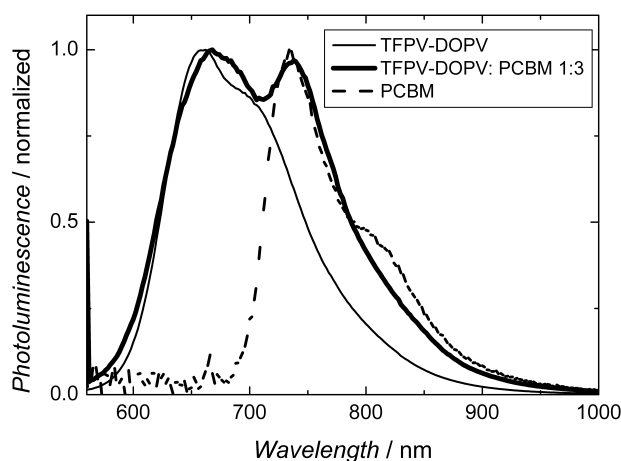

Figure 5. 10: Photoluminescence of TFPV-DOPV: PCBM 1:3 blend (thick line), in comparison with the photoluminescence of the pristine materials. Excitation is at 476 nm and 40 mW, spectra are recorded at 80 K. Spectra are normalized for comparison.

The PIA spectrum of the same blend, see Figure5.11, shows a broad peak between 1 eV and 2.2 eV, with a maximum around 1.6 eV. The PIA of TFPV-DOPV is shown for comparison. The two spectra match well, but the dip around 1.8 eV is not observed in the blend.

For the peak at 1.59 eV, a rather defined lifetime of 0.1 ms, dispersion factor $\alpha = 0.93$, is determined from the modulation frequency dependence, see Figure 5.12. These values are comparable with the pristine material ($\tau = 0.13$ ms, $\alpha = 0.90$) as well. It is therefore assumed, that in blends of TFPV-DOPV and PCBM, the triplet state of TFPV-DOPV is preserved and the predominant photoexcitation.
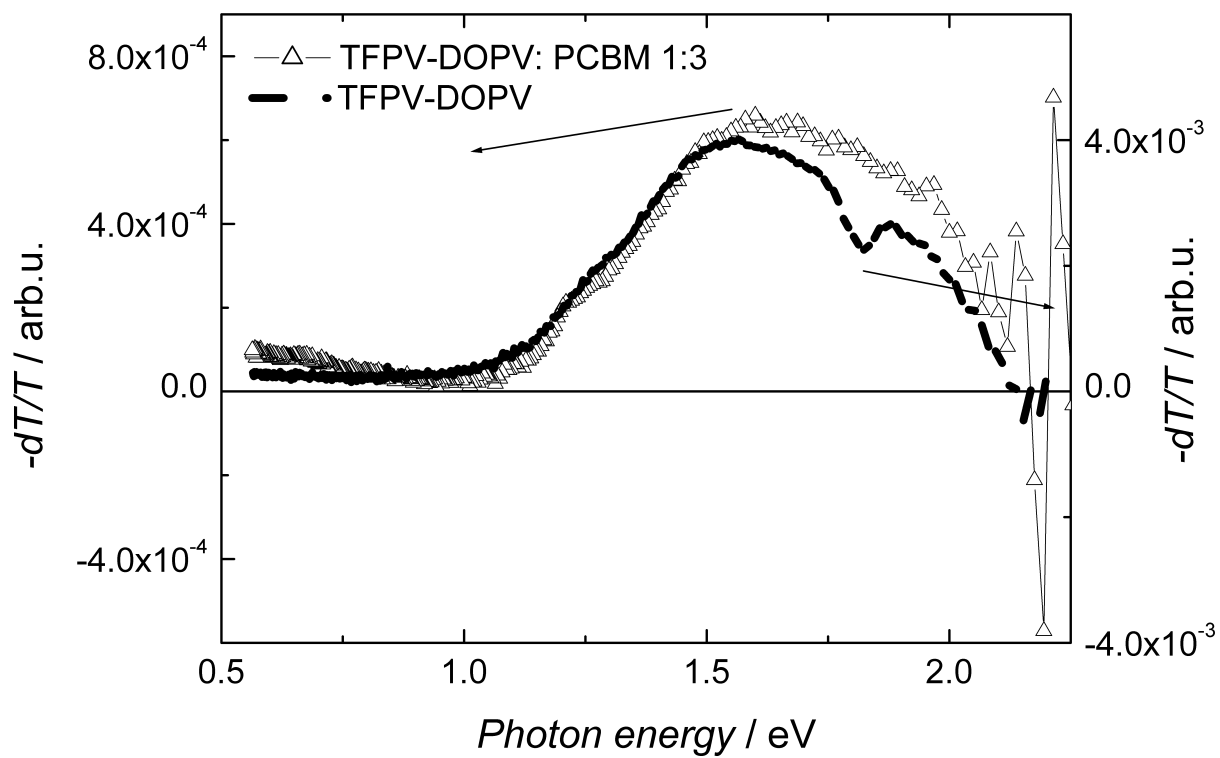
Figure 5. 11: PIA spectrum of TFPV-DOPV: PCBM 1:3 blend, in comparison with the pristine polymer spectrum. Spectra are recorded at 80 K, excitation at 476 nm and 40 mW.
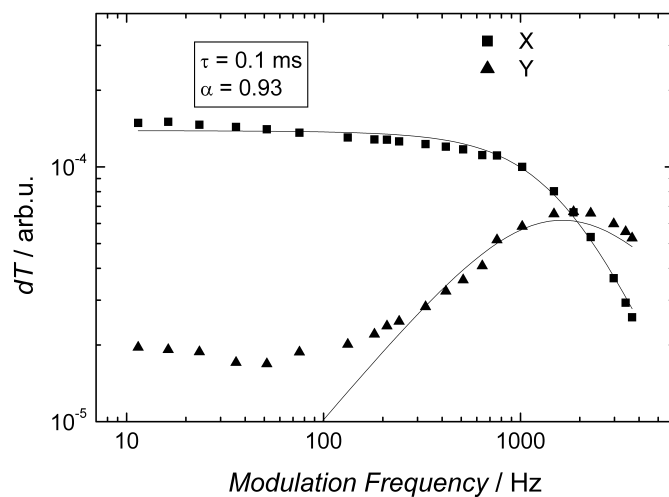

Figure 5. 12: Modulation frequency dependence of the PIA signal at 1.59 eV, excitation at 476 nm and 40 mW. For the fit, only Y values for modulation frequencies >100 Hz are taken into account.

5.2 3-Cyano-substituted poly-hexylthiophene P3CN4HT

Several polythiophenes (PT´s) with an high electron affinity have been proposed in the literature.[14,15,16,17,18] Substitution of PT´s on the 3 or 3,4 position with electron withdrawing groups like cyano, nitro or halogen lowers the electron density in the backbone and increases the electron affinity. For 3,4-Cyanothiophene, HOMO and LUMO levels of 6.7 eV and 3.6 eV are reported.[19] The LUMO is lowered for 0.6 eV as compared to alkyl-substituted PT. The material acts as electron acceptor towards photoexcited MEH-PPV. [19]

Such materials without any solubilizing alkylchain show often poor solubility in common organic solvents. Therefore, a novel cyano substituted alkyl-thiophene poly-(3-cyano,4-hexyl)thiophene P3CN4HT was synthesised at the Patras University and tested for photophysical and device application. For the chemical structure see Figure 5.13.

5.2.1 Optical and Electrochemical Properties

P3CN4HT shows an absorption maximum around 380 nm and an onset around 500 nm. The absorption is clearly blue-shifted compared to regioregular poly-3-hexylthiophene P3HT, see for both spectra Figure 5.13 as well. Further, the absorption of P3CN4HT shows no shoulder at the red end like rr P3HT. Such features are generally indications for ordered phases in the solid state. Sterical hindrance by the 3,4 substitution of the backbone might hinder such structures. Also, thermal annealing at 100° for 5 minutes does not change the absorption spectrum of P3CN4HT. Such procedure was reported to induce ordering in polythiophenes films and lead to a redshift in absorption.

The absorption spectra of P3CN4HT: P3HT blends are linear superposition of the individual component absorption, even at 80 % P3CN4HT content. Thermal annealing shows no significant change. The occurrence of the well structured P3HT absorption shows that the formation of the highly ordered P3HT phase is not hindered in this composition, as observed in P3HT: PCBM blends.

Electrochemical voltage spectroscopy of a P3CN4HT film shows oxidation and reduction at +1.35 eV vs. NHE (HOMO 6.1 eV) and -1.45 eV vs. NHE (LUMO 3.3 eV), respectively. The electrochemical band gap of 2.8 eV is slightly higher as the optical with 2.5 eV.
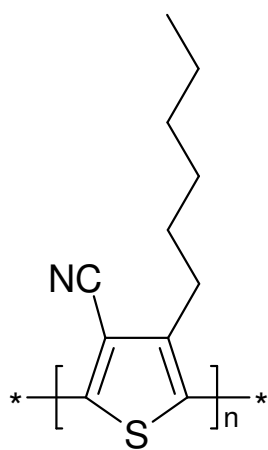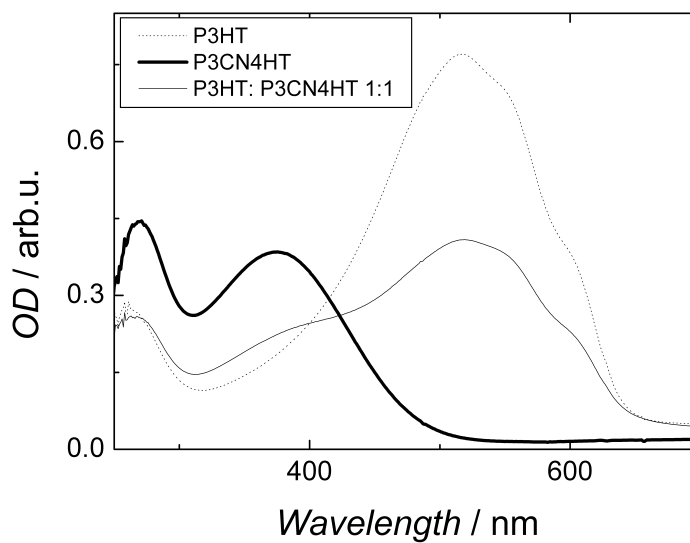
Figure 5. 13: Chemical structure of poly-(3-cyano,4-hexyl)-thiophene P3CN4HT (left), absorption spectrum of P3CN4HT, P3HT and blend of both materials. Films are spincast from 2 % chlorobenzene solutions.

5.2.2 Photophysical and Device Properties

The photoluminescence of P3CN4HT shows its photoluminescence with a peak beyond 560 nm. In blends with P3HT, the photoluminescence of P3CN4HT is quenched below the sensitivity of the setup. Also the P3HT photoluminescence is quenched in the blend by a factor >10.
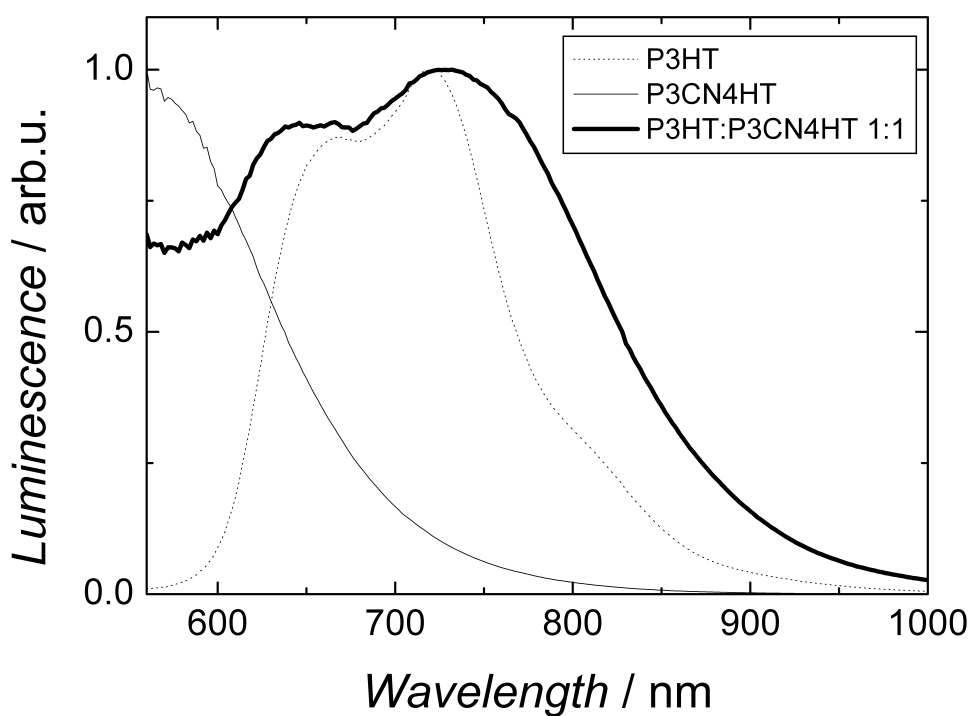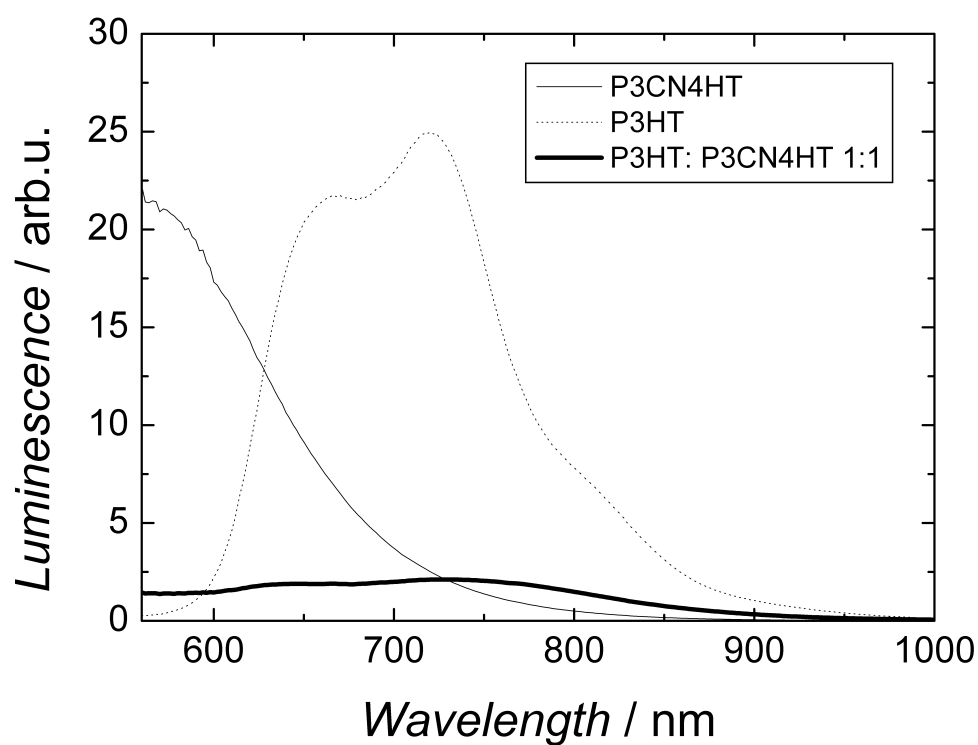
Figure 5. 14: Photoluminescence of P3CN4HT, P3HT and a 1:1 blend from both materials (upper part). On the lower graph, the same spectra, normalized to their maximum. Photoluminescence is recorded at room temperature under vacuum, excitation at 476 nm with 40 mW.

P3CN4HT shows an extraordinary strong single peak PIA absorption at 1.5 eV, see Figure 5.15. Modulation frequency dependence shows a rather defined lifetime of t = 0.2 ms, dispersion factor $\alpha = 0.94$. The excitation power dependence shows a gradient of k = 0.9, indicating primarily first order type recombination. All these facts let conclude that the PIA in P3CN4HT is originating from a $T_1{\rightarrow}T_n$ transition. Triplets were identified earlier in PT and acceptor substituted PT unambiguously.[20,21,22]

Further, blends of P3CN4HT and P3HT are investigated. The PIA shows a rather broad feature with several peaks between 1.8 and 1.2 eV. Further, a weak absorption feature is observed for probe energies <0.8 eV.

For rr- P3HT, a broad photoinduced absorption spectrum is reported between 1 and 1.9 eV. Several peaks are observed at 1.1 eV, assigned to an interchain exciplex, 1.25 eV, assigned to the high energy polaron absorption and at 1.8 eV, assigned to the high energy two dimensional polaron absorption, are reported. [23,24]

The peaks at 1.8 eV and 1.25 eV can be found in the PIA spectrum of the P3HT: P3CN4HT blend. No PIA is observed at 1.1 eV, therefore no interchain exciplex can be observed in the blend. The low energy transition for the polaron and two dimensional polaron are found at 0.35 eV and 0.1 eV. These peaks are beyond the range of the setup, but a PIA < 0.8 eV is observed, which can be attributed to the low energy polaron absorption. The other PIA features in the P3HT: P3CN4HT blend between 1.5 and 1.7 eV might origin from P3CN4HT negative polaron, but its spectrum is not known yet.

Modulation frequency dependence of the blend at 1.44 eV shows rather short lifetime ($\tau = 0.18$ ms) with a wide distribution ($\alpha = 0.50$). Fit is only done with the in phase component since the out of phase signal is rather small and its maximum is out of the measurement range. Excitation power dependence shows a gradient of k = 0.77. No conclusion on the recombination mechanism can be drawn.
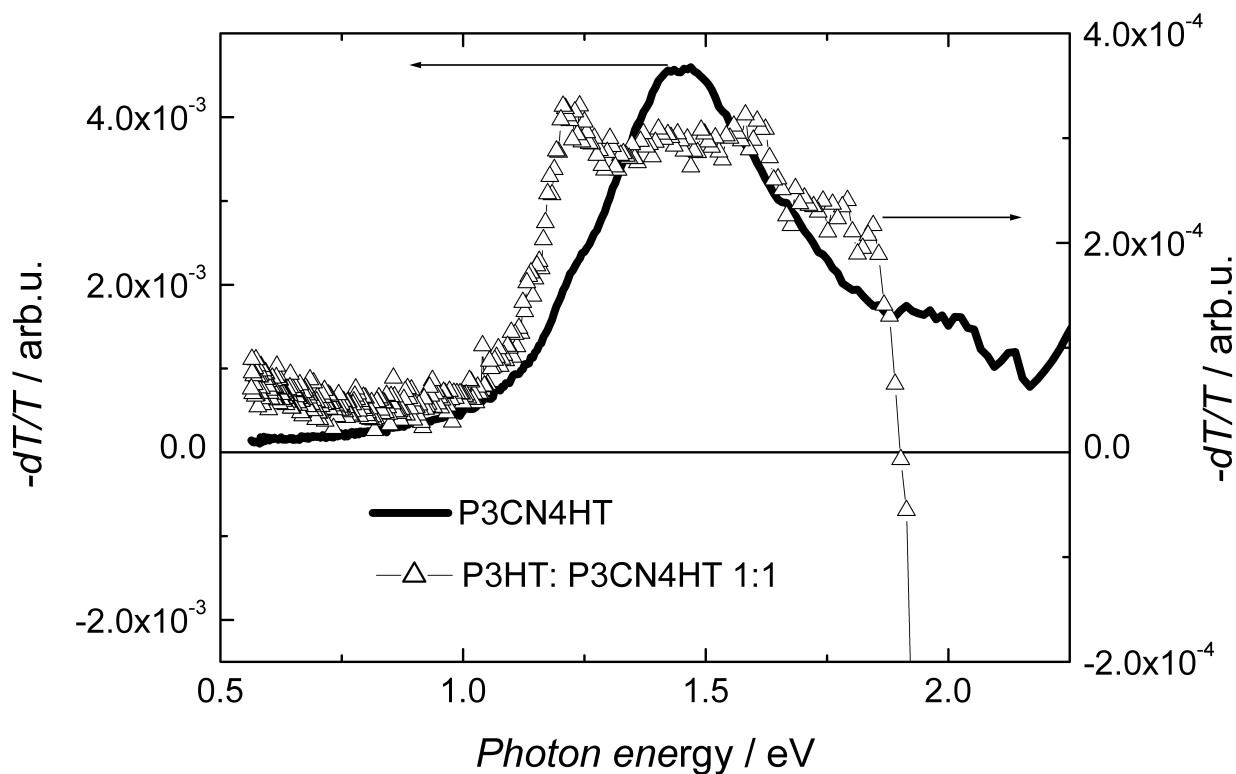
Figure 5. 15: PIA spectrum of P3CN4HT (full line) and P3HT: P3CN4HT 1:1 (open triangle) spin cast films on glass. Spectra are recorded at 80 K , excitation with 40 mW at 476 nm.
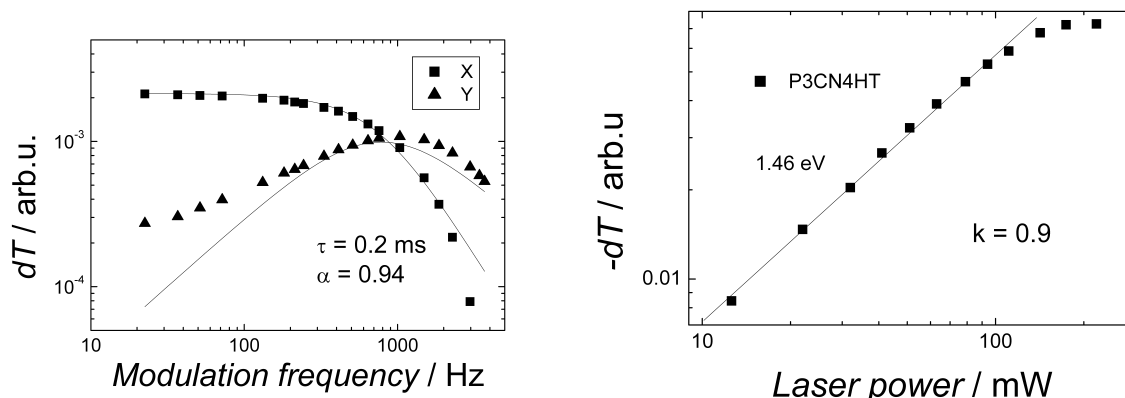

Figure 5. 16: Modulation frequency dependence (left) with 40 mW excitation power and excitation power dependence (right) with 37 Hz modulation frequency of the PIA signal at 1.44 eV of P3CN4HT. Measurements are done at 80 K.
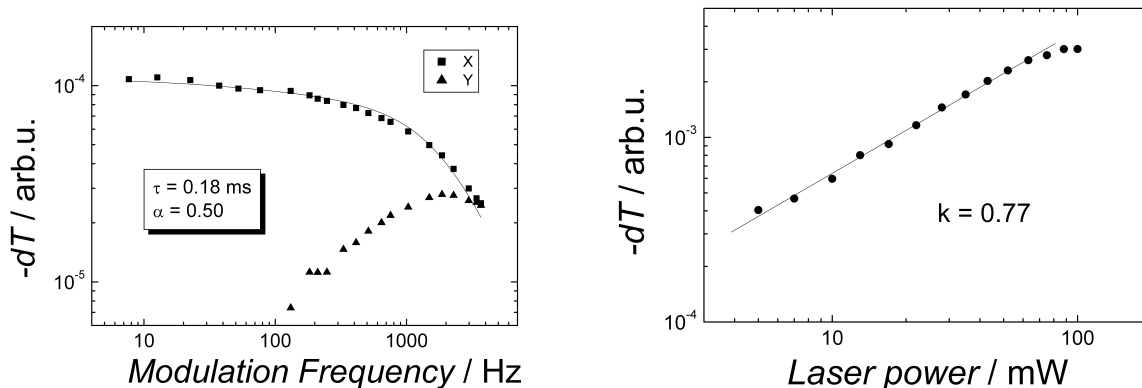
Figure 5. 17: Modulation frequency (left) with 40 mW excitation power and excitation power dependence (right) with 37 Hz modulation frequency of the PIA signal at 1.44 eV of P3HT: P3CN4HT. Measurements are done at 80 K. Fit for the modulation frequency dependence is only done with in phase data.

In summary, it can be concluded that photoinduced charge separation in P3HT: P3CN4HT blends is observed. The photoluminescence is quenched for both materials. Photoinduced charge transfer shows $T_1 \rightarrow T_n$ excitation in the pristine P3CN4HT and polaronic absorption in the blend with P3HT.

Devices from P3HT :P3CN4HT blend devices give a photocurrent of 50 μA cm^{-2} under solar illuminated light. The photovoltage is 170 mV.[25]

5.3 References

[1] E. Moons, *Journal of Physics: Condensed Matter* 2002, **14**, 12235

[2] G. Yu, A. J. Heeger, *Journal of Applied Physics* 1995, **78**, 4510

[3] M. Granström. K. Petritsch, A. C. Arias, A. Lux, M. R. Andersson, R. H. Friend, *Nature* 1998, **395**, 257

[4] J. J. M. Halls, A. C. Arias, J. D. MacKenzie, W. Wu, M. Inbasekaran, E. P. Woo, R. H. Friend, *Advanced Materials* 2000, **12**, 498

[5] C. M. Ramsdale, J. A. Barker, A. C. Arias, J. D. MacKenzie, R. H. Friend, N. C. Greenham, Jo*urnal of Applied Physics* 2002, **92**, 4266

[6] R. C. Pacios, D. Bradley, *Synthetic Metals* 2002, **127**, 261

[7] S. A. Jeneke, S. Yi, Applied Physics Letters 2000, 77, 2635

[8] A. G. Manoj, A. A. Alagiriswarny, K. S. Narayan, *Journal of Applied Physics* 2003, **94**, 4088

[9] X. Zhang, S. A. Jenekhe, *Macromolecules* 2000, **33**, 2069

[10] F. Naso, F. Babudri, G. M. Farinosa, *Pure and Applied Chemistry* 1999, **71**, 1485

[11] G. M. Farinola, T. Cassano, R. Tommasi, F. Babudri, A. Cardone and F. Naso, *Proc. SPIE* 2001, **4461**, 296.

[12] F. Babudri, A. Cardone, G. M. Farinola, F. Naso, T. Cassano, L. Chiavarone and R. Tommasi, *Macromol. Chem. Phys* .2003, **204**, 1621.

[13] T. Yohannes, H. Neugebauer, G. M. Farinola, C. Winder , F. Babudri, A. Cardone, F. Naso and N. S. Sariciftci to be submitted

[14] U. Salzner, *Journal of Physical Chemistry B* 2002, **106**, 9214

[15] G. Casalbore-Miceli, M. C. Gallazzi, S. Zeccin, N. Camioni, A. Geri, C. Bertarelli, *Advanced Functional Materials* 2003, **13**, 307

[16] F. Demanze, A. Yassar, F. Garnier, *Synthetic Metals* 1996, **76**, 269

[17] Y. Greenwald, J. Poplawski, E. Ehrenfreund, S. Speiser, *Synthetic Metals* 1997, **85**, 1353

[18] A. Yassar, F. Demanze, A. Jaafari, M. El Idrissi, C. Coupry, *Advanced Functional Materials* 2002, **12**, 699

[19] Y. Greenwald, X. Xu, M Fourmigué, G. Srdanov, C. Koss, F. Wudl, A. J. Heeger, *Journal of Polymer Science: Part A: Polymer Chemistry* 1998, **36**, 3115

[20] L. Smilowitz, N. S. Sariciftci, R. Wu, C. Gettinger, A. J. Heeger, F. Wudl, *Physical Review B* 1993, **47**, 13835

[21] Y. Greenwald, X. Wie, S. Jeglinski, J. Poplawski, E. Ehrenfreund, S. Speiser, Z. V. Vardeny, *Synthetic Metals* 1995, **69**, 321

[22] X. Jiang, R. Oesterbacka, O. Korovyanko, C. P. An, B. Horowitz, R. A. J. Jannsen, Z. V. Vardeny, *Advanced Functional Materials* 2002, **12**, 587

[23] Y. H. Kim, D. Spiegel, S. Hotta, A. J. Heeger, *Physical Review B* 1988, **38**, 5490

[24] X. M. Jiang, R. Österbacka, C. P. An, Z. V. Vardeny, *Synthetic Metals* 2003, **137**, 1465

[25] Markus Koppe, private communication

6. Donor-Acceptor Dyads

Dyad molecules[1,2,3,4], consisting of an electron acceptor moiety covalently linked to an electron donor, are possible candidates for photoactive systems[5]. Many of these molecules perform photoinduced charge separation, resulting in long living (up to few hundred μs in solution)[6] intra-molecular charge separated state.

6.1. π-extended tetrathiafulvalene-fullerene dyad exTTF-C_{60}

π-extended tetrathiafulvalene-bridge-fullerene dyad molecules are potential candidates for photoinduced charge transfer, leading to a long-living charge separated state.[7,8] The aim of this work is to study the charge transfer process in a particular π-extended tetrathiafulvalene-fullerene dyad, bridged by two phenylene vinylene units, ex-TTF-C_{60} and test it for its suitability for organic solar cells.[9] As reference compounds, the ex-TTF with the bridge and the fulleropyrrolidine are investigated. Further, the interaction with MDMO-PPV is investigated and the possibility to exploit such blends in photovoltaic cells.

6.1.1. Electrochemistry

Electrochemical measurements are performed in a dichlorobenzene: acetonitrile 4:1 solution with 0.1 M Bu_4NClO_4 as electrolyte. A glassy carbon electrode serves as working electrode, a SCE as reference electrode and a platinum wired as counter electrode. Scan rate is 200 mV/s. From the electrochemical measurements, an energy diagram for the dyad is drawn, shown in Figure 6.2.

The electrochemical band gap of ex-TTF is determined with 1.98 eV, which is slightly lower than the optical band gap of 2.1 eV.

The reduction peak of fulleropyrrolidine (C_{60}-P) at -700 mV vs. SCE is a comparable range with other [6,6] methanofullerenes.

The oxidation and reduction potential of the dyad are in the range of the ex-TTF (donor) oxidation and C_{60}-P (acceptor) reduction, respectively.
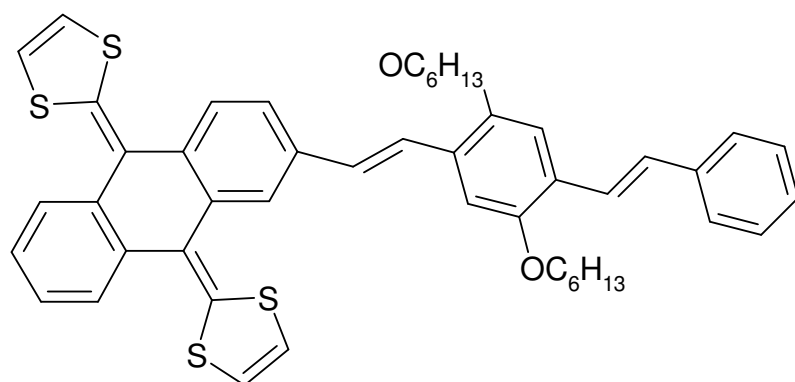
ex-TTF
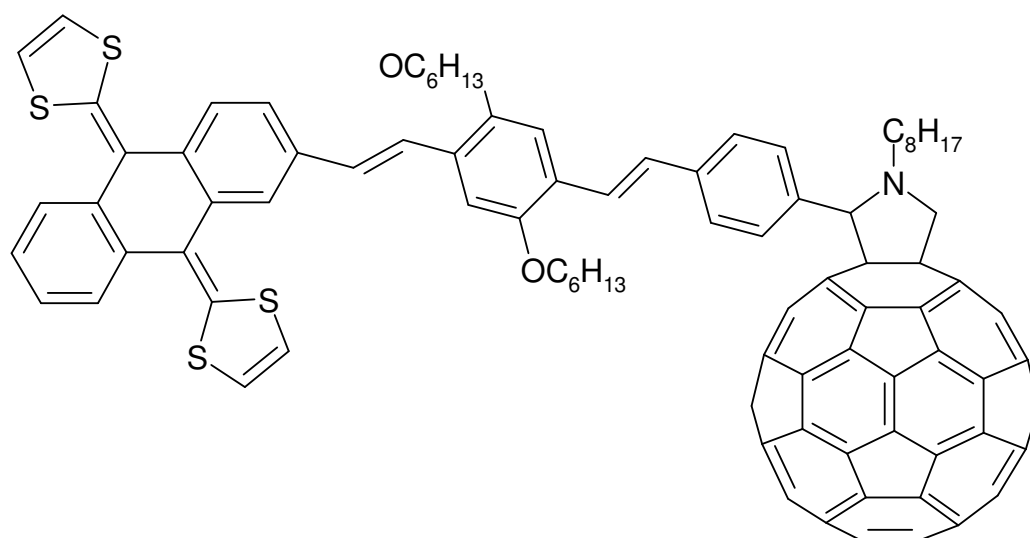
ex-TTF-C$_{60}$

Figure 6. 1: Chemical structure of the π-extended tetrathiafulvalene with a phenylene vinylene bridge (ex-TTF) and the π-extended tetrathiafulvalene-bridge-C$_{60}$ dyad (ex-TTF-C$_{60}$) is shown.

The energy diagram of the dyad system, see Figure 6.2, is derived from the electrochemical measurements, combined with optical absorption. The distinct offset of the LUMO and HOMO levels between the ex-TTF and C$_{60}$-P lets expect photoinduced charge separation.
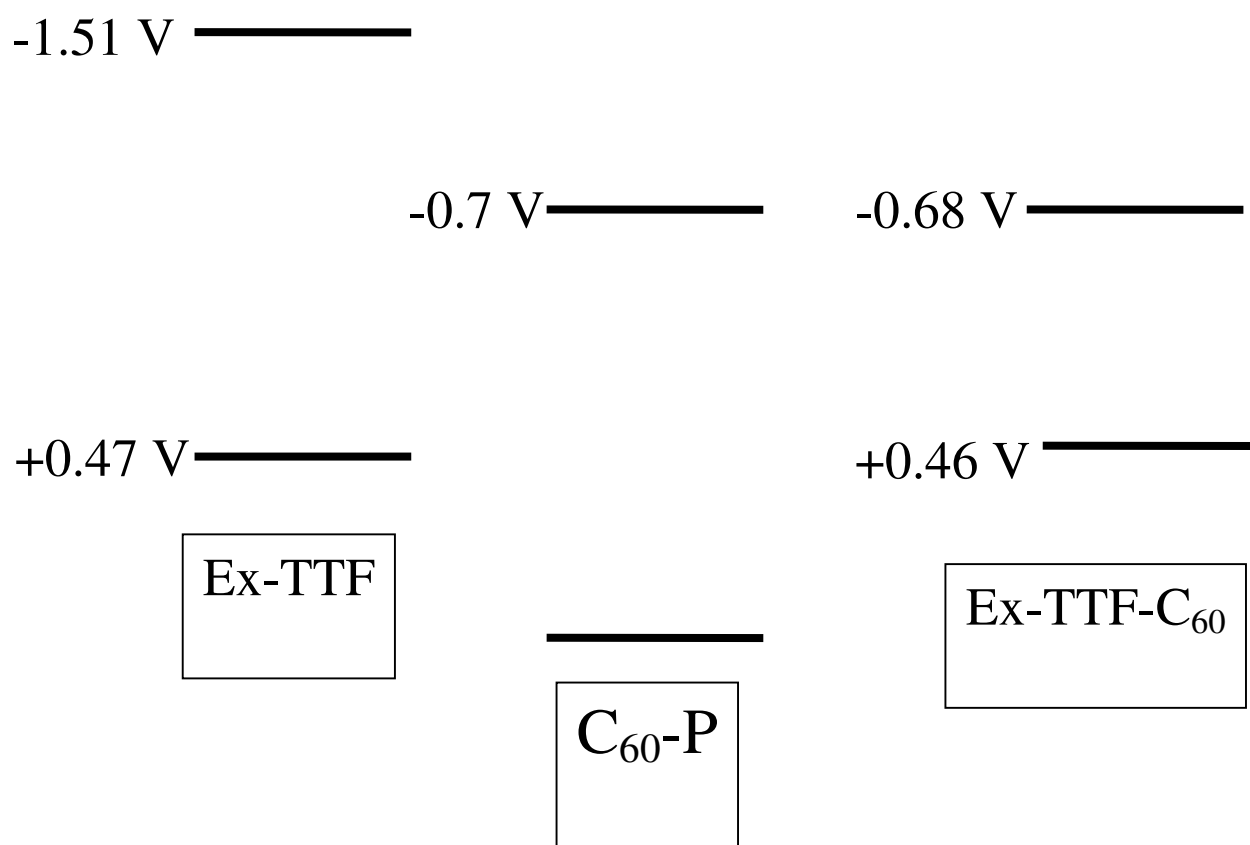
-1.51 V ━━━━

-0.7 V ━━━━   -0.68 V ━━━━

+0.47 V ━━━━   +0.46 V ━━━━

| Ex-TTF |

━━━━

| C_{60}-P |

| Ex-TTF-C_{60} |

Figure 6. 2: Energy diagram for ex-TTF, C_{60}-P and the dyad structure ex-TTF-C_{60}, energy values are taken from electrochemical measurements, the first reduction peak is assigned to the LUMO, the first oxidation peak to the HOMO, for C_{60}-P, no oxidation is observed. The band gap is assumed from the absorption with 1.8 eV.

6.1.2 Photophysical Properties

Figure 6.3 shows the absorption and emission of ex-TTF and the ex-TTF- C_{60} dyad. Ex-TTF-C_{60} shows the absorption around 450 nm of the ex-TTF and around 330 from C_{60}.

Ex-TTF films, excited at 476 nm, shows a luminescence with a maximum around 700 nm. The dyad shows no photoluminescence. The photoluminescence is measured with excitation at 476 nm, where the ex-TTF part is predominantly excited, and 664 nm, there the C_{60} is exclusively excited.
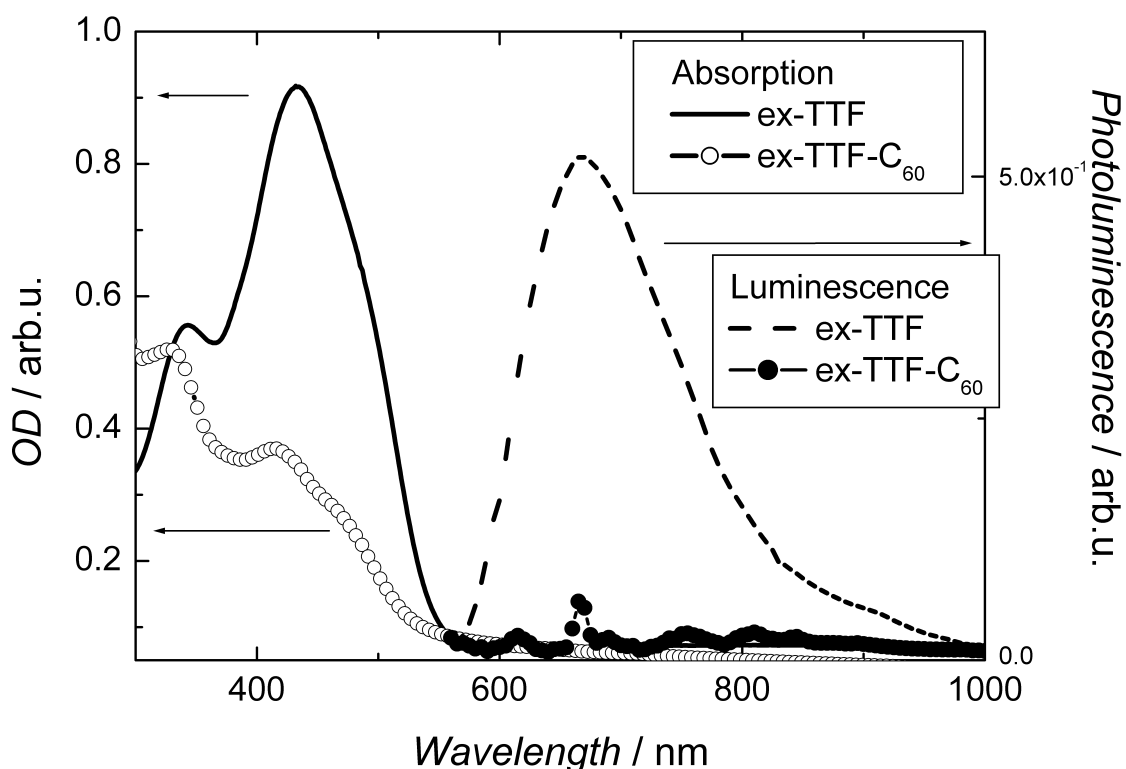
Figure 6.3: Absorption and luminescence of ex-TTF and ex-TTF-C_{60} spin cast film, thickness 50-70 nm, on glass substrates. Photoluminescence is measured at 80 K, excitation at 476 nm and 40 mW.

Figure 6.4 shows the PIA spectra of ex-TTF and ex-TTF-C_{60} in comparison. Ex-TTF shows a broad peak around 1.7 eV with a shoulder at 0.8 eV. The dependence on the modulation frequency at 1.57 eV and 0.83 eV is shown in Figure 6.5. Different behaviour is observed for the two features. For the maximum at 1.57 eV, a broad distribution of lifetimes around a mean lifetime $\tau = 0.17$ ms is observed. The signal at 0.83eV could not be fitted by the dispersive recombination model. The PIA around 1.57 eV might be assigned to a $T_1 \rightarrow T_n$ transition. The shoulder at low energies is from a different species, but its nature is not clear.

The PIA spectrum of the dyad molecule is different to the ex-TTF ones, see the comparison in Figure 6.4. A series of peaks in the range between 1.8 eV and 2.3 eV is observed. A second peak is observed around 1 eV with a side peak at 1.2 eV and a shoulder at 0.8 eV. All peaks show similar dependence on the chopper frequency with lifetimes around 0.8 ms, see Figure 6.6. The high energy feature of the ex-TTF-C_{60} PIA is comparable with the spectrum of the ex-TTF cation, taken from literature,[7,8] see the comparison in Figure 6.7. From this comparison, the formation of single oxidized ex-TTF after photoexcitation in the dyad can be assumed.

The absorption at 1.2 eV is well known for the C_{60}^-. The low energy peak at 1 eV is tentatively assigned to the ex-TTF cation as well.

The quenching of the peak at 1.6 eV in the ex-TTF, which is assigned to the triplet state, and the quenching of the ex-TTF photoluminescence are further indication for photoinduced charge separation in the dyad.
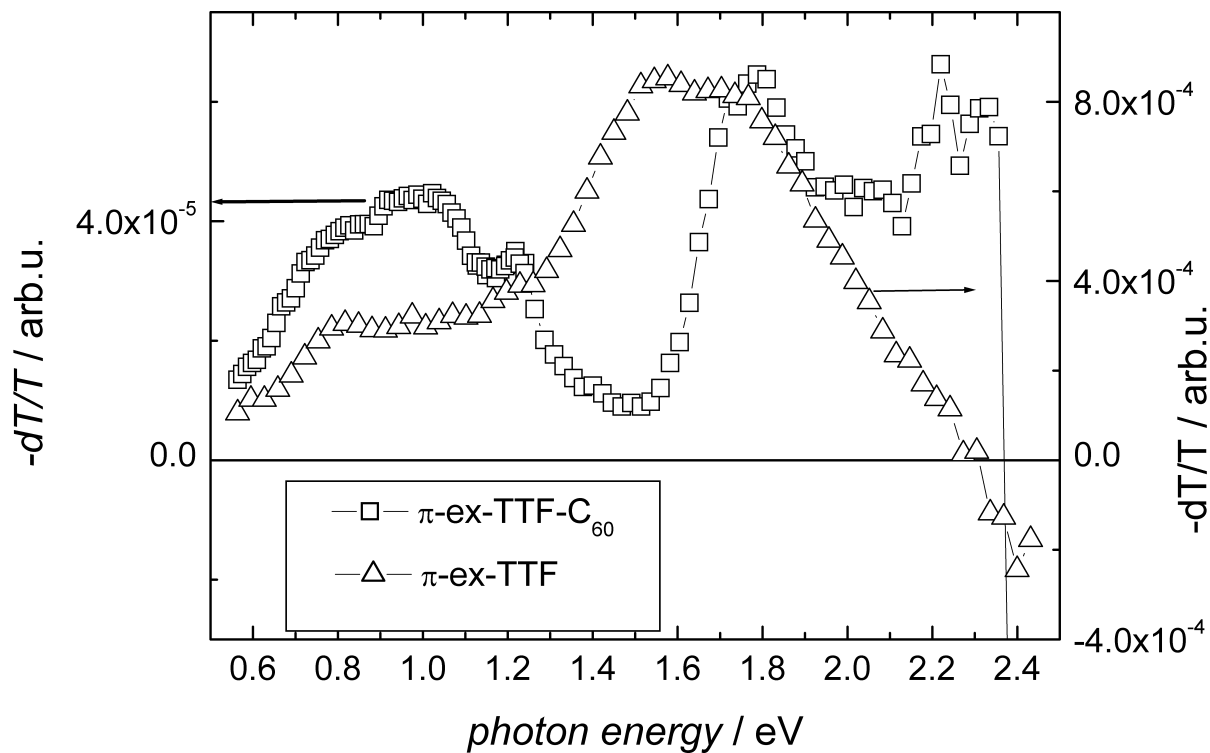

Figure 6. 4: PIA of ex-TTF and ex-TTF-C_{60} at 80 K, excitation at 476 nm (2.6 eV) with 40 mW, inset shows the low energy range between 0.5 and 1.6 eV.
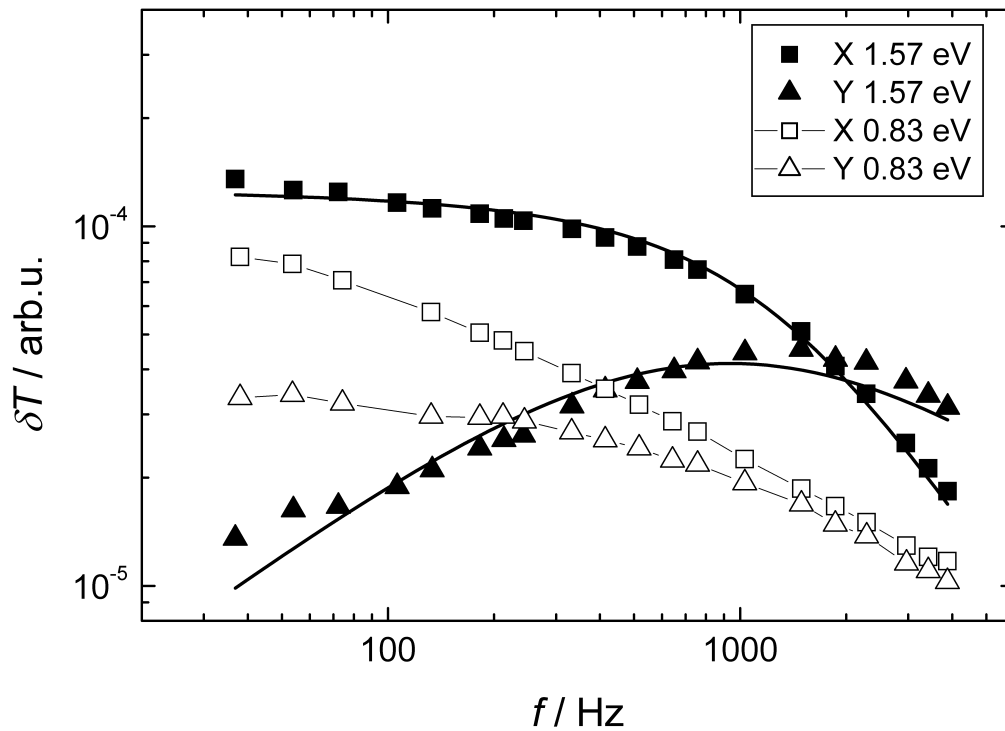
Figure 6. 5: Modulation frequency dependence of ex-TTF at 80 K, excitation with 40 mW at 476 nm (2.6 eV). The signal at 1.57 eV is fitted by the dispersive recombination model, $\tau = 0.57$ ms and $\alpha = 0.74$. The signal at 0.83 eV could not be fitted by this model, the lines are guide for the eye.

Figure 6. 6: Modulation frequency dependence of ex-TTF-C_{60} at 1.24 eV and 1.97 eV. Measurements are performed at 80 K, excitation with 40 mW at 476 nm (2.6 eV). Fits are done by the dispersive recombination model.

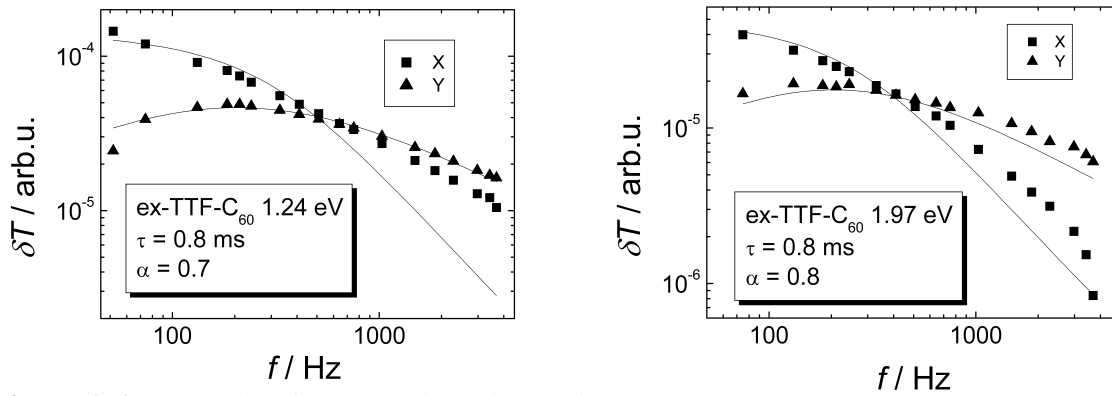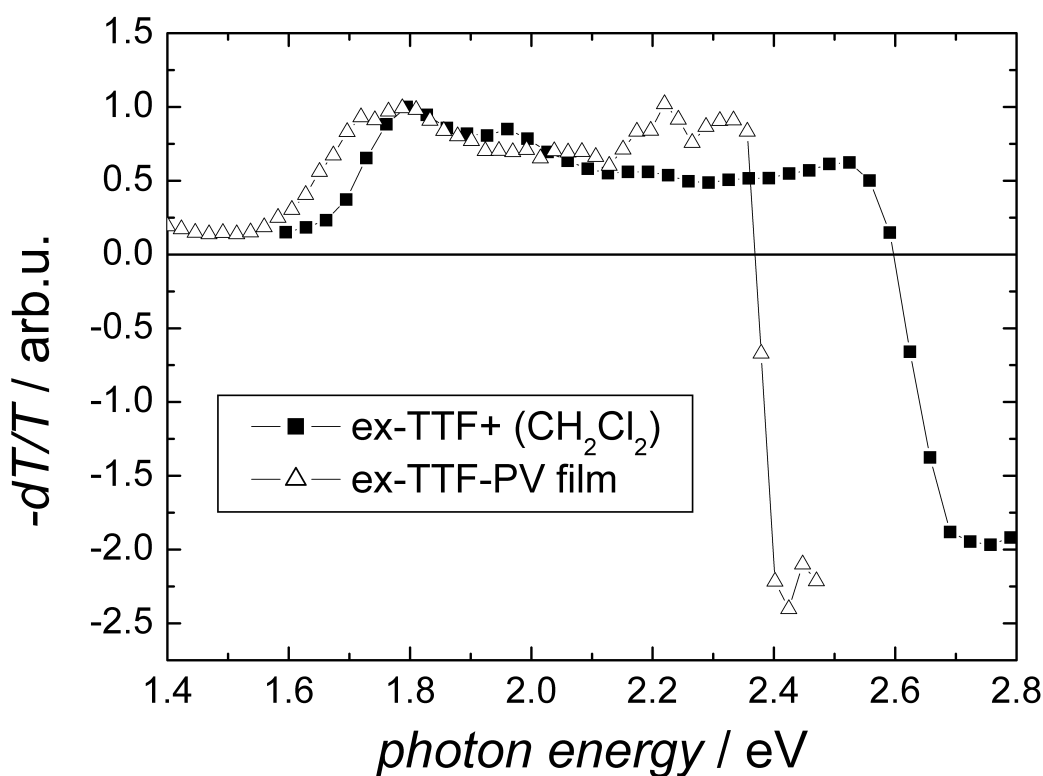**Figure 6. 7:** High energy part of the PIA spectrum of ex-TTF-C_{60} in comparison with the differential absorption spectrum of the ex-TTF cation, induced by pulse radiolysis, in CH_2Cl_2. Solution spectrum is taken from literature.[8]

6.1.3 Photovoltaic Devices

Photovoltaic devices are made with ex-TTF-C_{60}, spin cast from a chlorobenzene solution. The devices show a clear photovoltaic effect, see Figure 6.8. The power conversion efficiency is 0.02 % under solar simulated light with 80 mW cm^{-2}. The photocurrent spectrum is in good agreement with the absorption spectrum, The maximum is at 400 nm, which is slightly blue-shifted to the ex-TTF absorption maximum at 450 nm. The onset of the photocurrent matches with the absorption onset around 600.

Figure 6. 8: I-V characteristics (upper graph) of an ex-TTF-C_{60} dyad device in the dark and illumination from a solar simulator with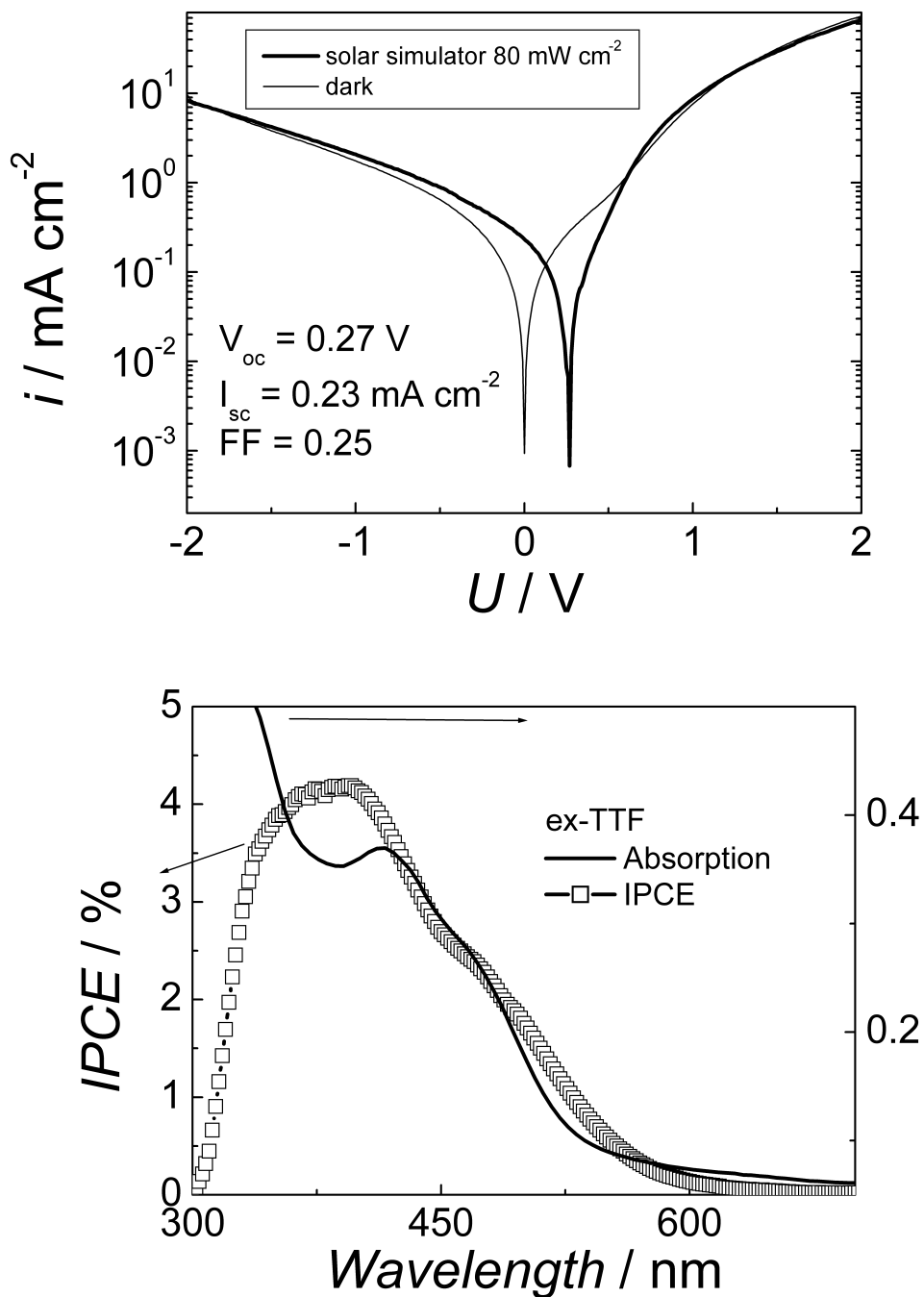 80 mW cm^{-2}, active layer thickness is around 50-70 nm. Photocurrent spectrum of the same device in comparison with the absorption spectrum of a thin film (lower graph).

6.1.4. Sensitizing MDMO-PPV

Blends of MDMO-PPV and ex-TTF-C_{60} are investigated for their photophysical and photovoltaic device properties. Blending with MDMO-PPV increases the light absorption between 500 and 600 nm, additional it should help forming better films.

An important question for such blends is the nature of the photophysical interaction between the two component. PIA is recorded at 80 K of a blend of MDMO-PPV : ex-TTF-C_{60} 1:2, see Figure 6.9. The PIA of MDMO-PPV: PCBM is shown for comparison. Both spectra shows the MDMO-PPV polaron absorption between 1.2 eV and 2 eV and < 0.8 eV. The maximum for the high energy peak is shifted for the ex-TTF-C_{60} blend from 1.35 to 1.2 eV. This absorption might originate from C_{60}^{-} anion, which is not observed in the case of PCBM.
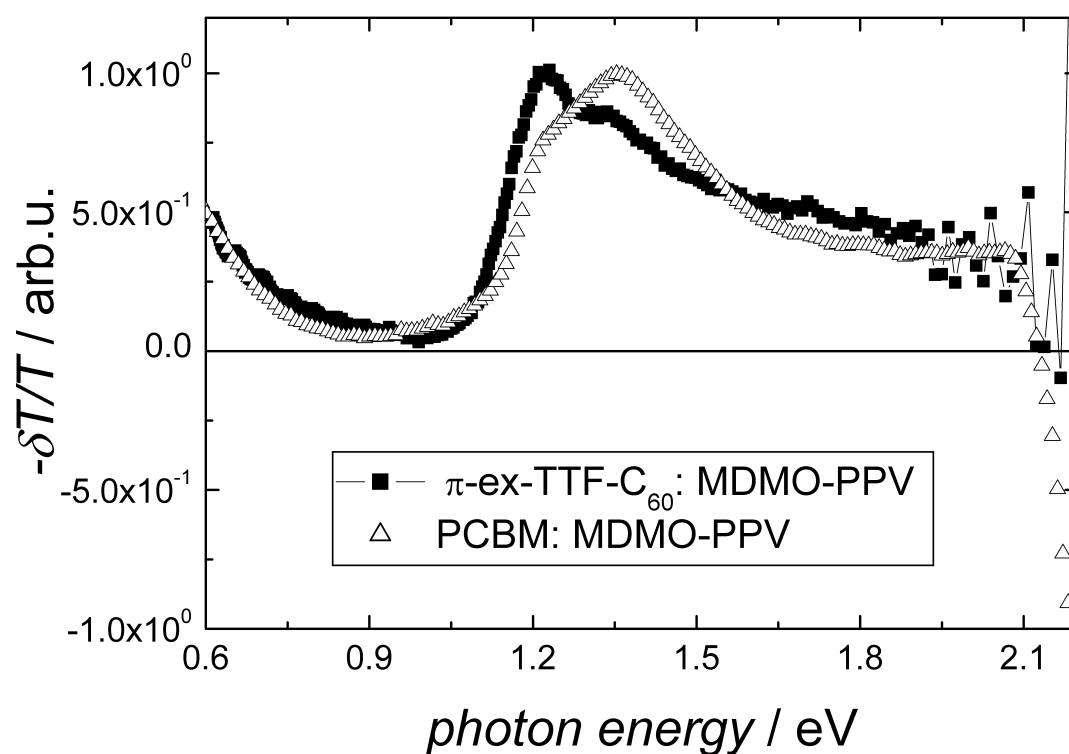
Figure 6. 9: PIA of MDMO-PPV: ex-TTF-C_{60} 1:2 blend in comparison with MDMO-PPV: PCBM 1:2 blend; both spectra are recorded at 80 K and excitation at 476 nm.

Photovoltaic devices from MDMO-PPV: ex-TTF-C_{60} blends. Figure 6.10 shows the I-V characteristics and the photocurrent spectra. An enhanced photovoltaic effect is observed in comparison with the dyad itself. The power conversion efficiency is mainly limited by the poor fill factor. The photocurrent spectra shows a broad feature between 350 and 550 nm with several peaks. The different contribution of C_{60}, ex-TTF and MDMO-PPV cannot be clearly distinghished.

Figure 6. 10: I-V characteristics under solar simulated light (80 mW cm^{-2} full line) and in the dark (dotted light) (to the right) and photocurrent spectra (to the left) of a MDMO-PPV: exTTF-C_{60} 1:2 device. Active layer thickness is approx. 100 nm.

6.2. Phthalocyanine-C_{60} dyad

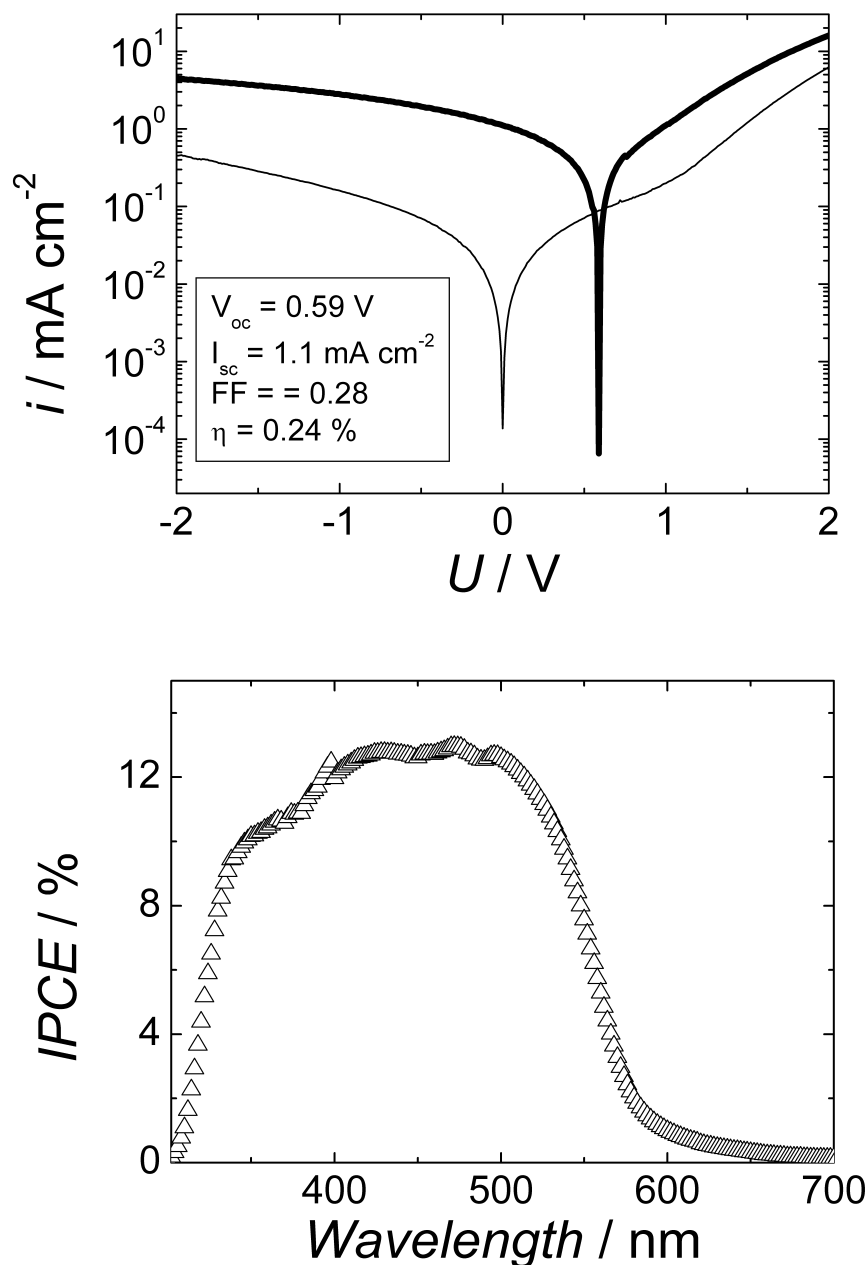Phthalocyanines are attractive and widely investigated materials for solar cell application due to their broad absorption between 600 and 800 nm, which is the range of the maximal solar photon flux.[10,11,12,13] Photovoltaic conversion efficiencies up to 3.5 (+/- 0.2) %[4] have been reported recently.[14]

Covalently linked phthalocyanine-fullerene dyads combine the attractive absorption profile of phthalocyanine with the electron accepting and transport properties of fullerenes. But, previous studies on phthalocyanine-fullerene dyads did not show photoinduced charge separated states.[15,16]

Recently, charge transfer states with lifetime of 3 ns in solution has been reported in a stronly coupled phthalocyanine-fullerene dyad compound for the first time.[17] For the structure of this compound, see Figure 6.11.

In this thesis, this specific compound is investigated for its photophysical properites in the solid state and its application in photovoltaic devices.[18] A short outline on published results on the photophysics will be given.[19,20] Application of the dyad molecule in photovoltaic systems is demonstrated. Further, photovoltaic devices of blends with MDMO-PPV and fullerene derivatives are discussed. In chapter 7, sensitization with MDMO-PPV and three component blends of Pc-C_{60}, MDMO-PPV and PCBM will be presented.
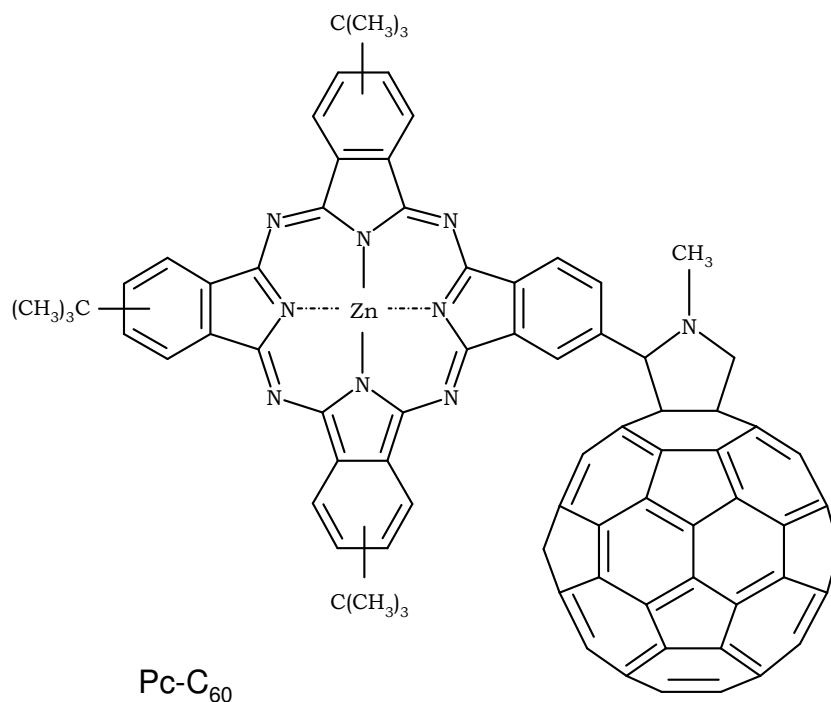

Figure 6. 11: Chemical structure of fulleropyrrolidine-Zn-phthalocyanine Pc-C_{60}.

---

[4] Uncorrected efficiency measured on a solar simulator at approx. 1 sun.

6.2.1 Photophysics of Pc-C$_{60}$

Figure 6.12 shows the absorption spectra of Pc-C$_{60}$ and the individual components of the dyad, the Zn-phthalocyanine (ZnTBPc) and the fulleropyrrolidine (C$_{60}$-P). The dyad absorption spectrum can be seen in first approximation as a superposition of the single component spectra. However, the photoluminescence of the phthalocyanine is quenched in the dyad molecule by a factor of ~ 50.
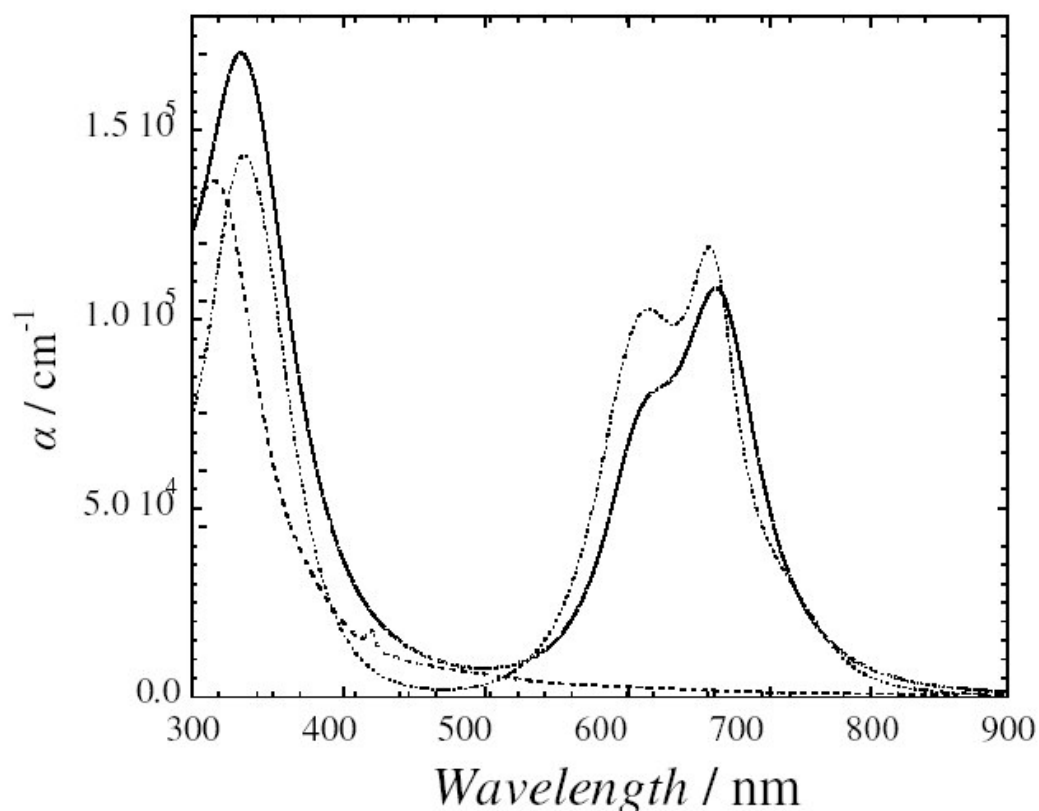
Figure 6. 12: Absorption coefficient of Pc-C$_{60}$ (full line) and the individual components, Zn-tetra-(*tert.*-butyl)-phthalocyanine ZnTBPc (dotted line) and fulleropyrrolidine C$_{60}$-P (dashed line).The absorption is fitted by a dielectric function model by the software SCOUT.

Figure 6.13 shows the PIA spectra of Pc-C$_{60}$ and the individual components, ZnTBPc and C$_{60}$-P. C$_{60}$-P, excited in the UV, shows a single peak around 1.75 eV, which is assigned to T$_1 \rightarrow$T$_n$ absorption. ZnTBPc shows a single peak around 1 eV, which is also assigned to a T$_1 \rightarrow$T$_n$ absorption as well. Further, bleaching of the ground state absorption for E >1.5 eV is observed. In the dyad molecule, both T$_1 \rightarrow$T$_n$ absorption of the phthalocyanine is quenched, instead two new absorption around 1.2 eV and <0.6 eV are observed. The 1.2 eV absorption is typical for the C$_{60}$ anion; the absorption at low probe energies might be assigned to the phthalocyanine cation. Further, bleaching is observed in the region of the phthalocyanine groundstate absorption. For

the photoexcitations in the dyad, typical lifetimes of 0.2 ms are determined for the solid state from the modulation frequency dependence.
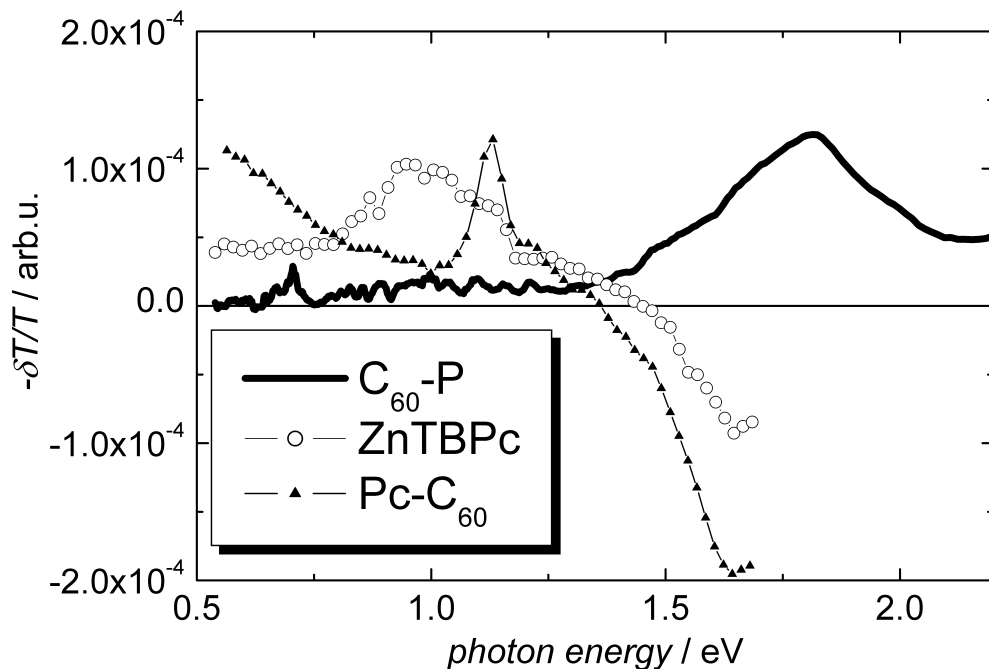
Figure 6. 13: PIA of Pc-C_{60} and the individual components ZnTBPc and C_{60}-P at 80 K. Pc-C_{60} and ZnTBPc are excited at 685 nm, C_{60}-P by a multiline UV laser.

6.2.2 Photovoltaic Devices from Pc-C_{60}

The I-V characteristics of a Pc-C_{60} device is shown in Figure 6.14. Diode behaviour with a rectification ratio of ~10 is observed in the dark. Under white light illumination with 80 mW cm^{-2}, an open circuit voltage V_{OC} = 0.46 V and a short circuit current I_{SC} = 0.51 mA cm^{-2} have been measured in the best case. The fill factor FF = 0.26 and a power conversion efficiency η_e = 0.08 % are determined. The V_{oc} (0.46 V) is in a similar range to the high efficient cells reported for evaported phthalocyanine:C_{60} mixture (V_{oc} = 0.53 V), but the I_{sc} is lower in the device containing the dyad molecule compared to the evaporated cells.

The spectrally resolved photocurrent of the Pc-C_{60} device, see Figure 6.14 as well, shows a maximum around 700 nm and 360 nm. The photocurrent spectra matches the absorption of the dyad. The maximal quantum efficiency is 3 %, showing the possibility for improvement of the device performance.

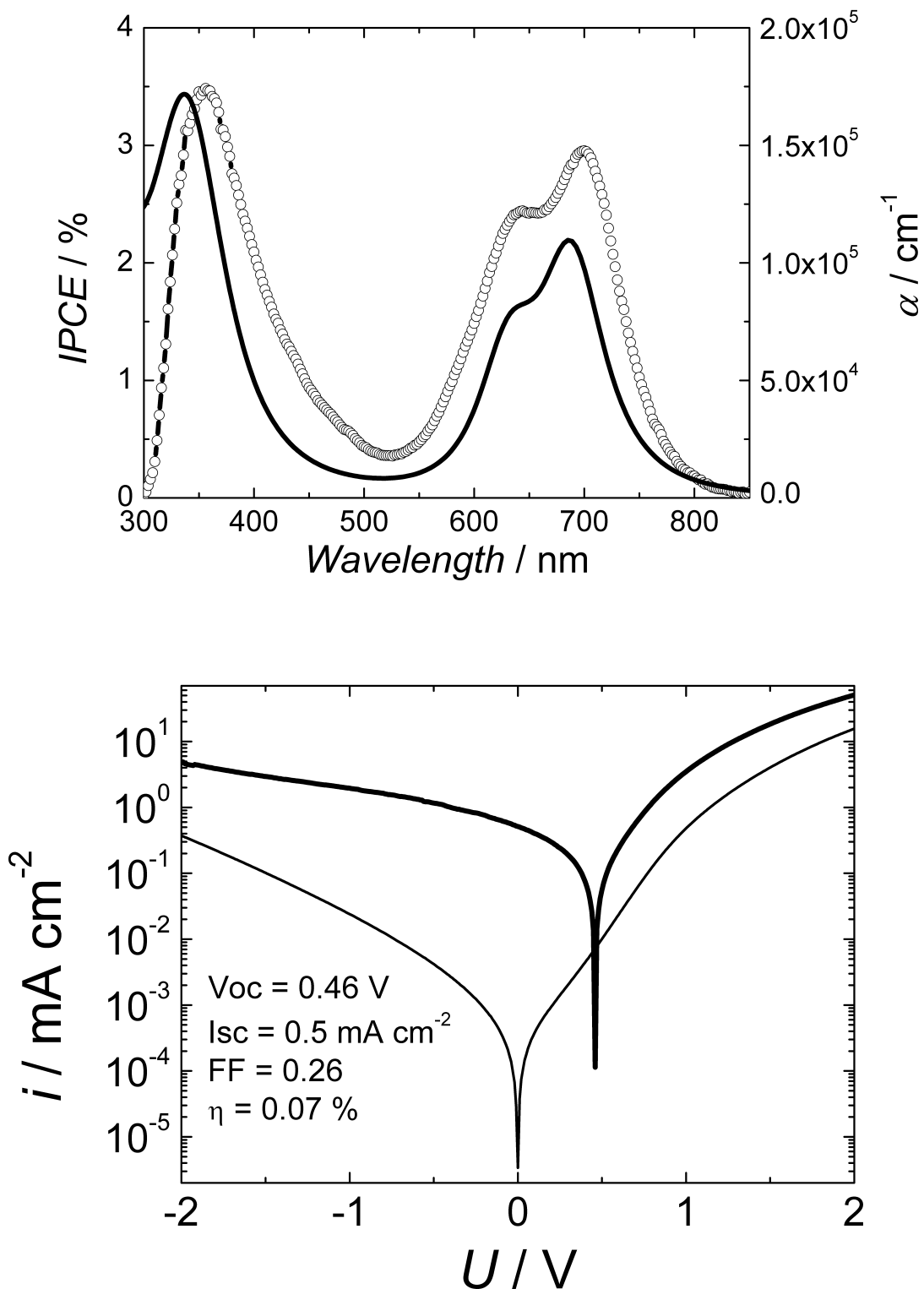**Figure 6. 14:** Photocurrent spectrum (open circles) of a Pc-C$_{60}$ device, thickness approx. 40 nm, spin cast from chlorobenzene, in comparison with the optical absorption (full line) (upper graph), current-voltage characteristics of the same device under illumination by a solar simulator, 80 mW cm^{-2} (thick line) and in the dark (thin line) (lower graph).

6.3 *Hexa*-thiophene-fluorene dyad 6TDTF

Poly-thiophenes with incorporated π-conjugated 1,3 Dithiole-2-ylidenefluorene have been reported as possible π-conjugated donor- acceptor structures.[21, 22, 23] The large variety of fluorene substitution chemistry opens the possibility to tune the electron affinity of the fluorene unit over a wide range. It was shown that the reduction potential, a measure for the electron affinity, can be described as a function of the substitution pattern by a Hammett type correlation.[22,24] Long lived photoinduced charge carriers were demonstrated for such polymers with trinitro-substituted fluorene acceptors.[22]

Since the solubility of this polymer systems is low, a novel hexa-thiophene oligomere structure with two 9-(thienodithiino[3,4-c:5,6-4]-1,3-dithiole-2-ylidene)-4,5-dinitro-2,7-(didodecyloxycarboxy)-fluorene units, 6TDTF, for the structure see Figure 6.15, was developed. The material was synthesized at the University of Manchester, group of Dr. Skabara. This material shows sufficient solubility in common organic solvents like chloroform or chlorobenzene.
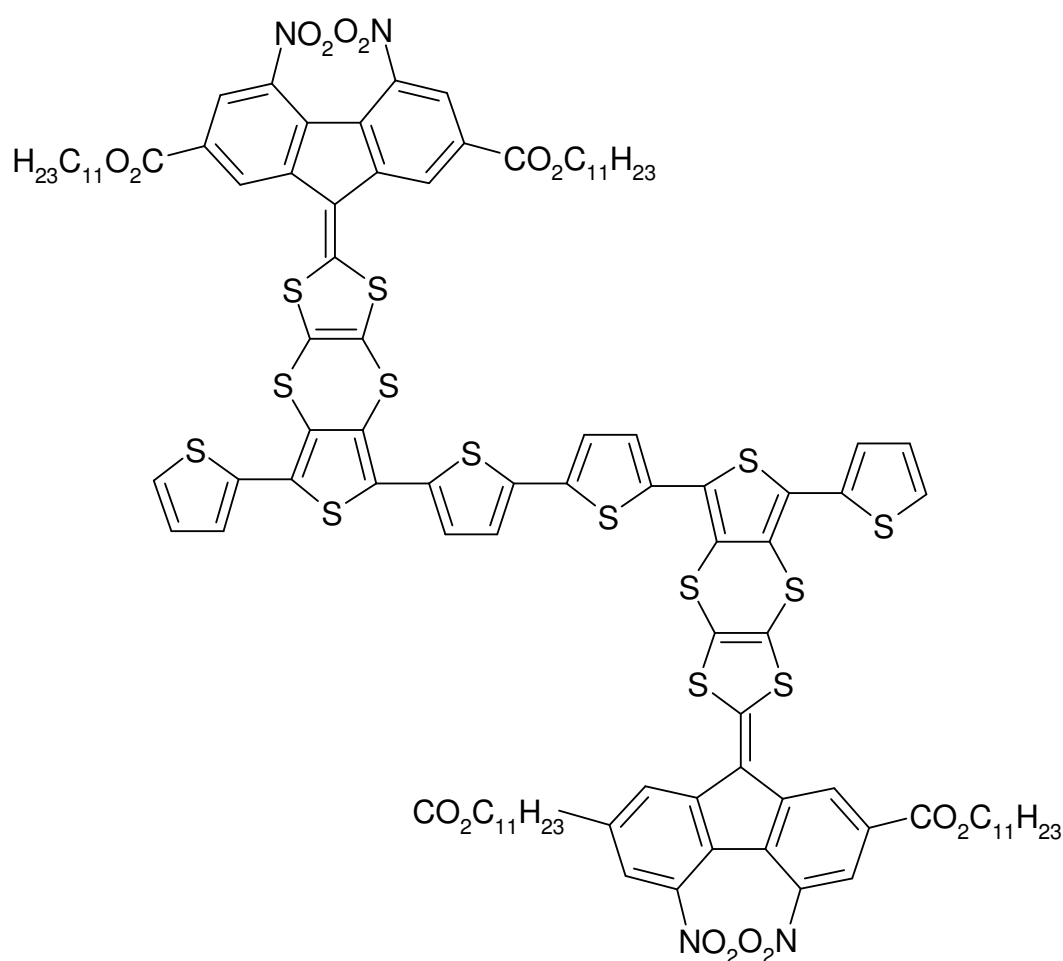
Figure 6. 15: Chemical structure of 6TDTF

6.3.1 Photophysical and Electrochemical Properties

The optical absorption of 6TDF, see Figure 6.16, shows an onset around 650 nm (Eg = 1.9 eV) in solution as well as in solid state. This is significant lower than the optical band gap of the bare *hexa*-thiophene 6T, λ_{max} = 540 nm (Eg = 2.3 eV).[24] The photoluminescence shows a single peak around 620 nm in a toluene solution and 700 nm in the solid state.

Cyclovoltammetry of 6TDTF shows oxidation and reduction at E_{OX} = 0.85 V and E_{RED} = -0.8 V vs Ag/AgCl, respectively. The electrochemical band gap is significantly lower than the optical, showing the dyad character of the molecule.
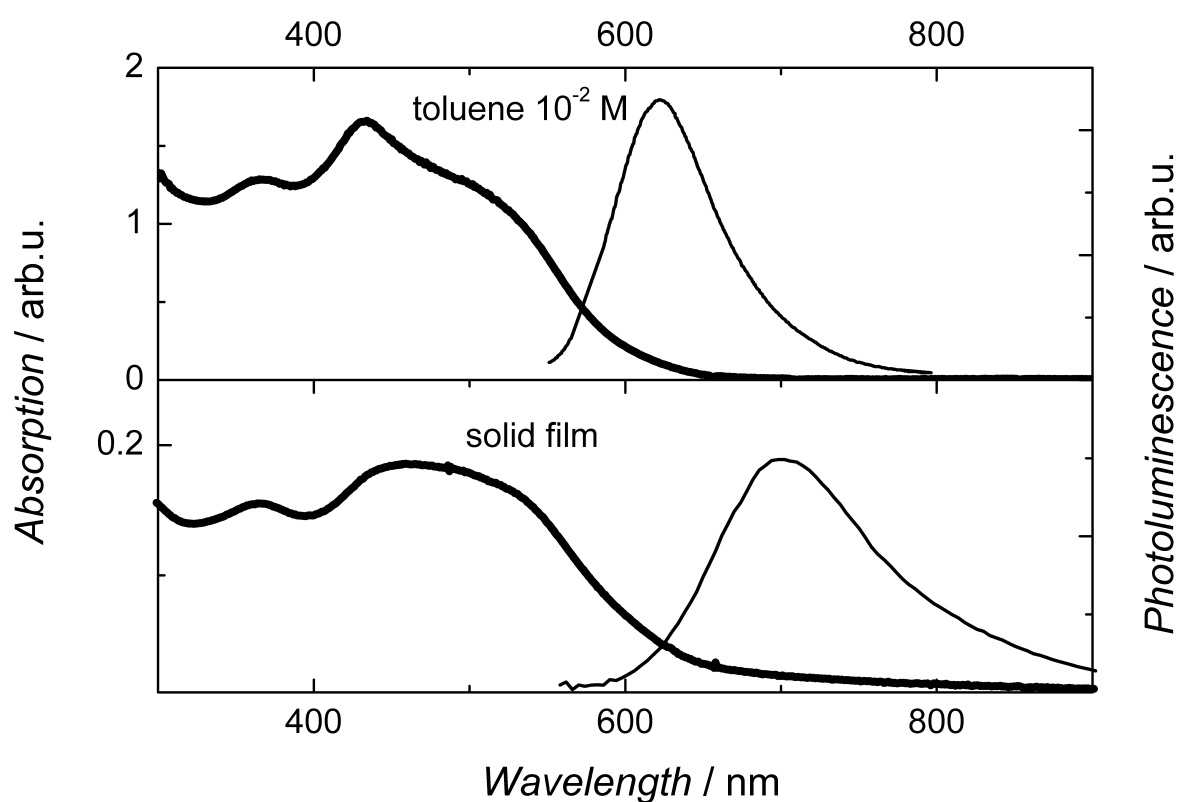
Figure 6. 16: Absorption (thick line) and photoluminescence spectrum (thin line) of 6TDTF in a 10^{-2} M toluene solution (upper part) and as solid film (lower part). Photoluminescence is excited at 500 nm for the solution and 476 nm for the thin film.

The PIA spectrum of 6TDTF, see Figure 6.17, shows a broad peak between 0.9 and 1.9 eV with a plateau between 1.2 and 1.5 eV and a shoulder at 1.0 eV. Additional, a raising PIA feature for small probe energies is observed. Figure 6.18 shows the expansion of the PIA for the NIR-MIR. A PIA peak around 0.4 eV and infrared active vibration (IRAV) bands in the MIR. The IRAV bands are clear indication for charged species. The PIA at 0.4 eV might be assigned to the cation absorption of 6TDTF.
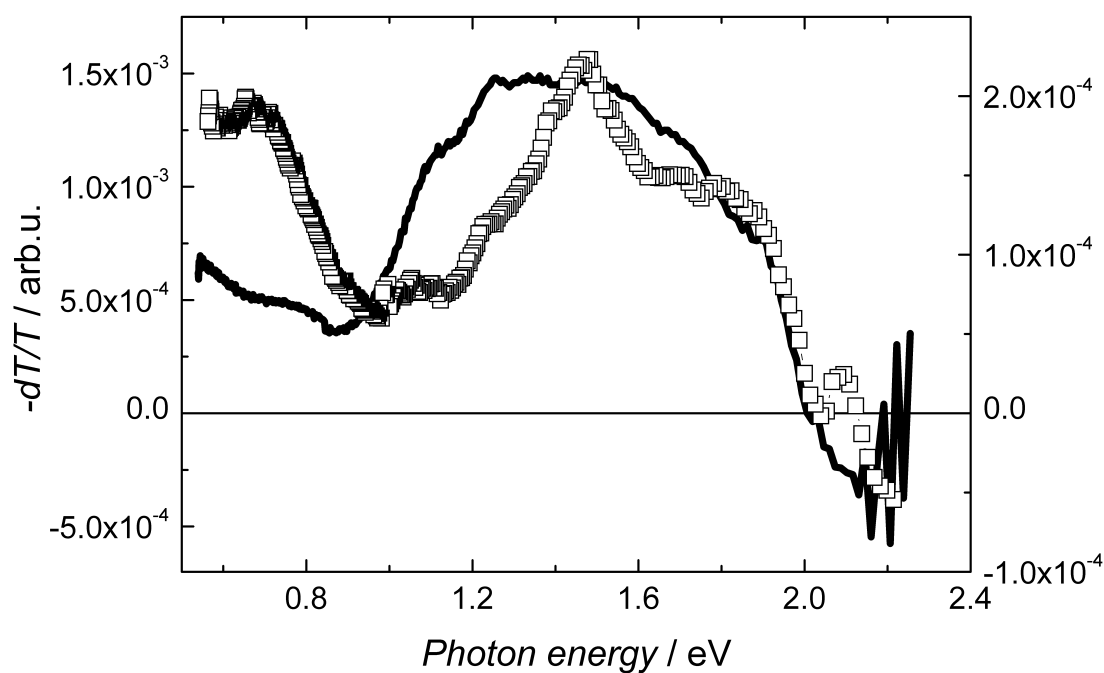
Figure 6. 17: PIA spectra of 6TDTF thin film (full line, left axis) and a 6TDTF: PCBM 1:1 blend film (open squares, right axis), spectra recorded at 80 K, excitation at 476 nm with 40 mW.
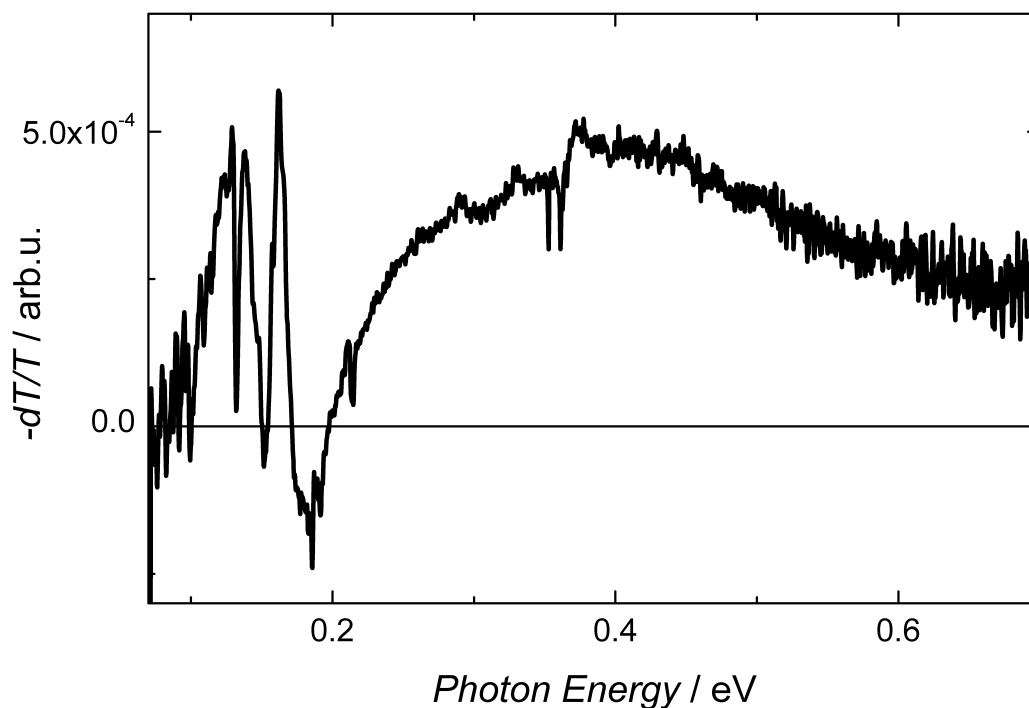
Figure 6. 18: PIA spectrum in the MIR-NIR infrared spectrum of a 6TDTF drop cast film on KBr. Spectra are recorded at 80 K, 30 mW illumination at 476nm. The PIA is obtained by subtracting the spectrum under illumination from the spectra in the dark.

The modulation frequency dependence of the PIA feature at 0.62 is shown in Figure 6.19. This feature can be correlated to the low energy absorption of the cation. The dependence is weak, this indicates long lifetimes. The curve could not be fitted by any applied model. The signal increases linear with the excitation power, see Figure 6.20. Such a dependence is assigned to monomolecular behaviour, which let conclude to intramolecular charge separated state.
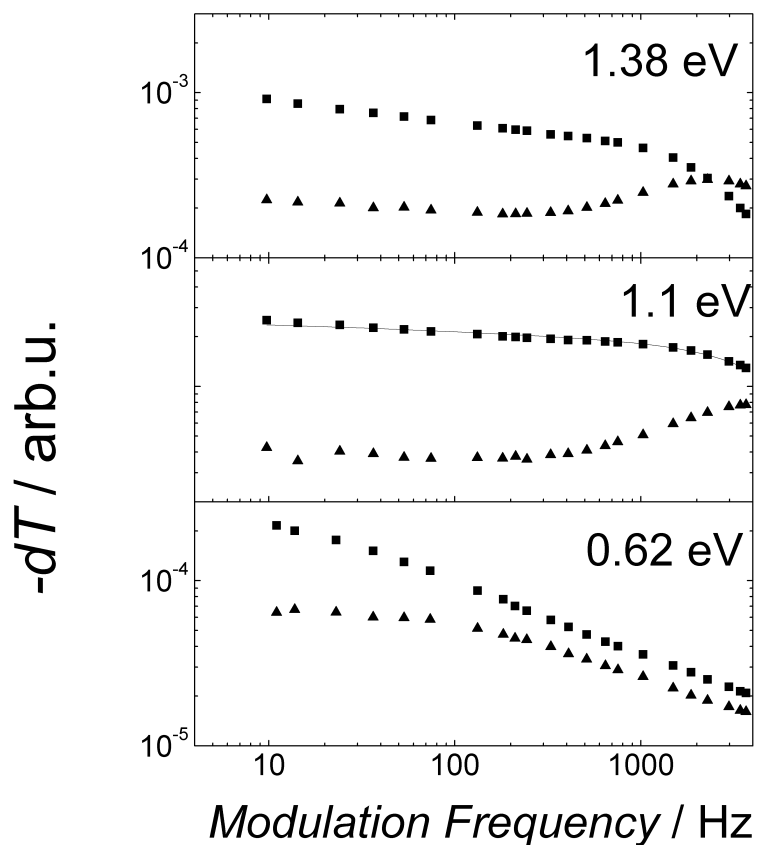
Figure 6. 19: Modulation frequency dependence of the PIA of 6TDTF at 1.38 eV, 1.1 eV and 0.62 eV. No satisfying fits could be obtained for these frequency dependencies. For the 1.1 eV PIA, the in phase component (squares) is fitted, giving a lifetime of 0.07 ms and a distribution factor of 0.4.

The PIA at 1.1 eV and 1.38 eV shows different modulation frequency dependencies, see Figure 6.19 as well. Therefore, it is concluded that the broad absorption in the VIS-NIR origin from more than one photoexciation. The shoulder at 1.1 eV shows a rather weak dependence on the modulation frequency, indicating short lifetimes. Fitting of the in phase component (X) results in a lifetime of $\tau = 0.07$ ms and a distribution factor of $\alpha = 0.40$. The measured range for the out-of-phase signal (Y) could not be fitted by any modulation frequency model.

The PIA at 1.38 eV shows a much stronger dependence, which indicates longer lifetimes.

At both probe energies, the PIA scales linear with the excitation power as well, see Figure 6.20.
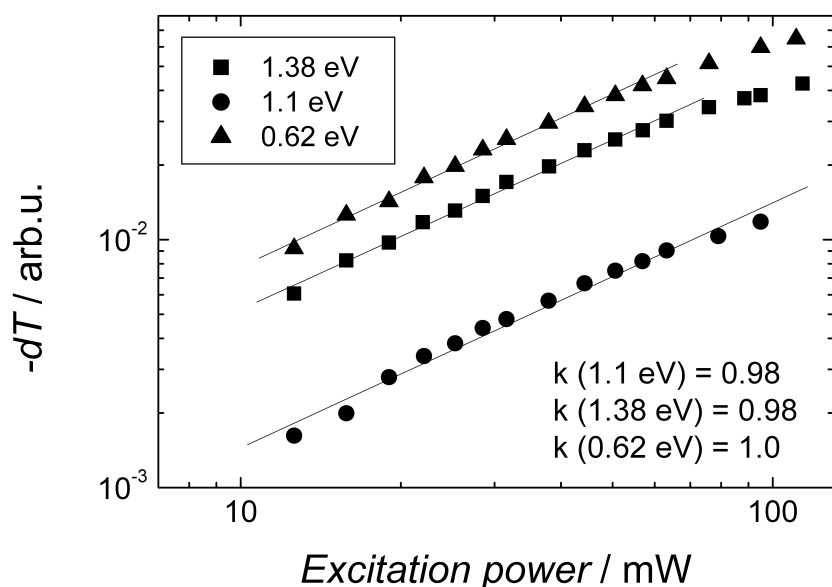
Figure 6. 20: Excitation power dependence of the PIA of 6TDTF at 1.38 eV, 1.1 eV and 0.62 eV. Fits (thin line) are done by a power law. For high excitation intensities, saturation is observed. These points are not included into the fitting procedure.

In order to find out more on the cation species of 6TDTF, a blend with PCBM as strong electron acceptor is investigated. PIA show peaks at 1.47 eV with a shoulder around 1.7 eV and at 0.7 eV. All peaks in the blend show quite similar dependence on the modulation frequency at all investiged probe energies, see Figure 6.21. None of them could be fitted by a modulation dependence model. The excitation power dependence, Figure 6.22, varies in a small range between k = 0.55 and k =0.65, fitted by a power law.

This indicate bimolecular recombination as dominant recombination mechanism. The recombination behaviour of the photoexcitations is quite different in the fullerene blend and the pristine 6TDTF. Different photophysical processes are involved.

For 6T cation, absorption at 1.55 and 0.8 eV are reported.[25,26,27,28] This energies are quite comparable with the PIA of the 6TDTF: PCBM blends. Although the two systems, 6T and 6TDTF, are not direct comparable, it might be concluded that the positive charge is primarily located on the *hexa*-thiophene backbone. Further, the PIA around 1.1 eV in 6TDTF is quenched in the blend with PCBM. The lifetime of this feature is found to be rather short and different to the positive charge. We assume therefore that this migth be correlated to a triplet state or to an charge transfer state.
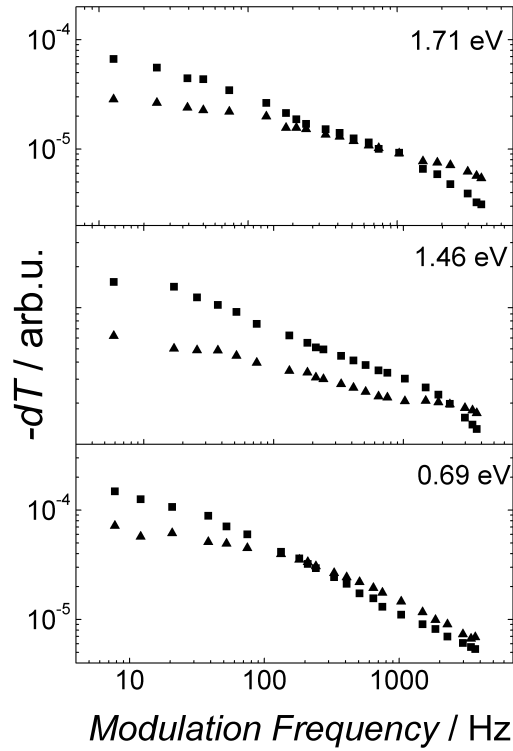
Figure 6. 21: Modulation frequency dependence of the PIA of 6TDTF: PCBM 1:1 blend at 1.71 eV, 1.46 eV and 0.69 eV.
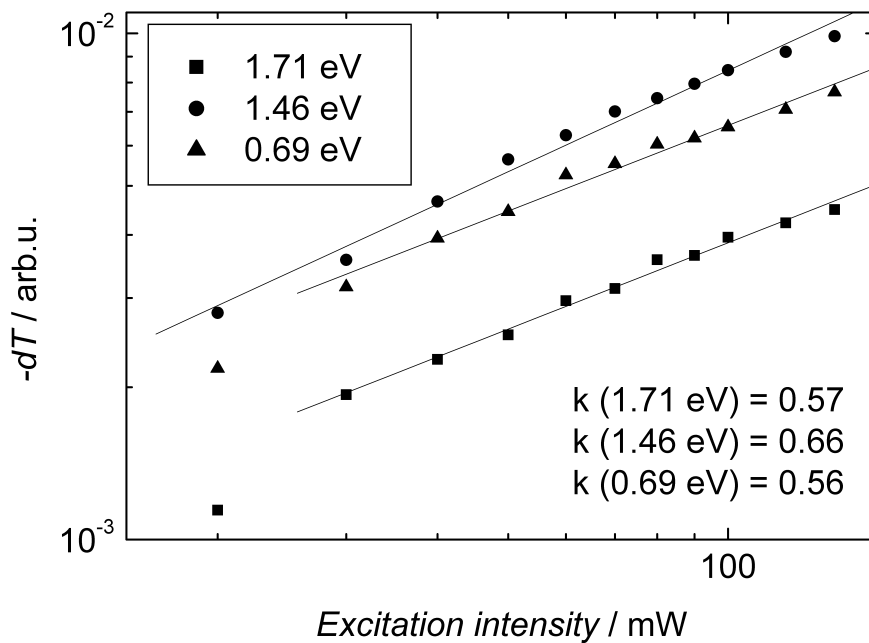
Figure 6. 22: Excitation power dependence of the PIA of 6TDTF:PCBM 1:1 at 1.71.eV, 1.46 eV and 0.69 eV. Measurements are done at 80 K with 37 Hz modulation. Fits are done by a power law (thin line).

6.3.2 Photovoltaic Devices

Photovoltaic devices are prepared for 6TDTF: PCBM blends. The I-V characteristics and photocurrent spectrum are shown in Figure 6.23. Devices show a photoeffect with a power conversion efficiency $\eta_e = 0.1$ %. The device performance is mainly limited by the low fill factor. The photocurrent spetrum matches the absorption spectrum in the well and show its onset around 650 nm, coinciding with 6TDTF.
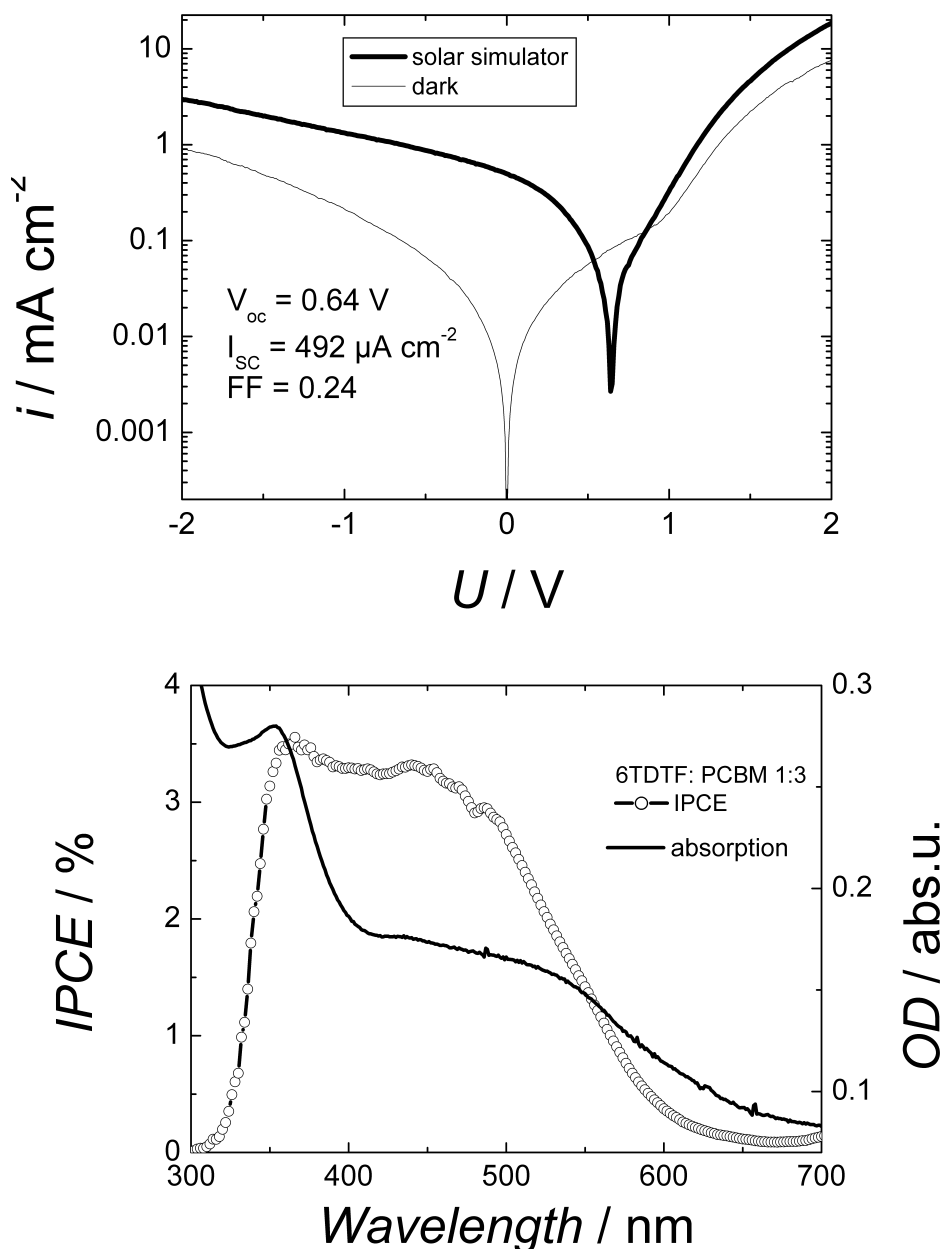
Figure 6. 23: I-V characteristics (left) under solar simulated light, 80 mW cm^{-2} and in the dark of a 6TDTF: PCBM 1:3 blend, spin cast from chlorobenzene. Photocurrent spectrum in comparison with the absorption spectrum (right).

6.4 References

[1] D. Gust, T. A. Moore and A. L. Moore, *Journal of Photochemistry and Photobiology B* 2000, **58**, 63

[2] D. Kuciauskas, S. Lin, G. R. Seely, A. L. Moore, T. A. Moore, D. Gust, T. Drovetskaya, C. A. Reed and P. D. W. Boyd, *Journal of Physical Chemistry* 1996, **100**, 15926

[3] T. Vemanen, N. V. Tkachenko, A. Y. Tauber, P. H. Hynninen and H. Lemmetyinen, *Chemical Physics Letters*. 2001, **345**, 213

[4] P. A. Liddell, D. Kuciauskas, J. P. Sumida, B. Nash, D. Nguyen, A. L. Moore, T. A. Moore and D. Gust, *Journal of the American Chemical Society* 1997, **119**, 1400

[5] E. Peeters, P. A. van Hal, J. Knol, C. J. Brabec, N. S. Sariciftci, J. C. Hummelen and R. A. J. Janssen, *Journal of Physical Chemistry B* 2000, **104**, 10174

[6] H. Imahori, D. M. Guldi, K. Tamaki, Y. Yoshida, C. Luo, Y. Sakata and S. Fukuzumi, *Journal of the American Chemical Society* 2001, **123**, 6617

[7] N. Martín, L. Sánchez, B. Illescas, S. González, M. A. Herranz, D. M. Guldi, *Carbon* 2000, **38**, 1577

[8] L. Sánchez, I. Pérez, N. Martín, D. M. Guldi, *Chemical European Journal* 2003, **9**, 2457

[9] C. Winder, H. Neugebauer, N. S. Sariciftci, F. Giacalone, J. L. Segura, N. Martin, submitted to *The Proceedings of the Electrochemical Society, San Antonio 2003*

[10] C. W. Tang, *Applied Physics Letters* 1986, **48**, 183

[11] M. Westphalen, U. Kreibig, J. Rostalski, H. Lüth and D. Meissner, *Solar Energy Materials and Solar Cells*, 2000, **61**, 97

[12] P. Peumans, S. R. Forrest, *Applied Physics Letters*, 2001, **79**, 126; Erratum: *Applied Physics Letters* 2002, **80**, 338

[13] D. Gebeyehu , B. Maennig, J. Drechsel, K. Leo, M. Pfeiffer, *Solar Energy Materials and Solar Cells* 2003, **79**, 81

[14] S. Uchida, J. Xue, B. P. Rand. S. R. Forrest, *Applied Physics Letters* 2004, **84**, 4218

[15] T. G. Linssen, K. Dürr, M. Hanack and A. Hirsch, *Journal of the Chemical Society, Chemical Communication* , 1995, **103**

[16] A. Sastre, A. Gouloumis, P. Vázquez, T. Torres, V. Doan, B. J. Schwartz, F. Wudl, L. Echegoyen and J. Rivera, *Organic Letter*, 1999, **1**, 1807.

[17] D. Guldi, A. Gouloumis, P. Vázquez and T. Torres, *Chemical Communication* 2002, 2056

[18] A. Gouloumis, S.-G. Liu, A. Sastre, P. Vàzquez, L. Echegoyen and T. Torres, *Chem. Eur. J.* 2000, **6**, 3600

[19] M. A. Loi, P. Denk, H. Hoppe, H. Neugebauer, C. Winder, D. Meissner, C. Brabec, N. S. Sariciftci, A. Gouloumis, P. Vázquez, T. Torres, *Journal of Materials Chemistry* **13**, 700-704 (2003)

[20] H. Neugebauer, M. A. Loi, C. Winder, N. S. Sariciftci, G. Cerullo, A. Gouloumis, P. Vázquez, T. Torres, *Solar Energy Materials and Solar Cells* 2004, **83**, 201

[21] P. J. Skabara, I. M. Serebryakov, I. F. Perepichka, N. S. Sariciftci, H. Neugebauer, A. Cravino, *Macromolecules* 2001, **34**, 2232

[22] P. J. Skabara, I. M. Serebryakov, I. F. Perepichka, *Journal of the Chemical Society, Perkin Transaction* **2** 1999, 505

[23] D. F. Perepichka, M. R. Bryce, A. S. Batsanov, E. J. L. McInnes, J. P. Zhao, R. D. Farley, *Chemistry, A European Journal* 2002, **8**, 4656

[24] P. A. Lane, X. Wei, Z. V. Vardeny, J. Poplawski, E. Ehrenfreund, M. Ibrahim, A. J. Frank, *Chemical Physics* 1996, **210**, 229

[25] R. A. J. Janssen, D. Moses, N. S. Sariciftci, *Journal of Chemical Physics* 1994, **101**, 9519

[26] P. A. Lane, M. Liess, X. Wei, J. Partee, J. Shinar, A. J. Frank, Z. V. Vardeny, *Chemical Physics* 1998, **227**, 57

[27] N. Yokounuma, Y. Furukawa, M. Tasumi, M. Kuroda, J. Nakayama, *Chemical Physics Letters* 1996, **255**, 431

[28] J. A. E. H. van Haare, E. E. Havinga, J. L. J. van Dongen, R. A. J. Janssen, J. Cornil, J. L. Bredas, *Chemistry, A European Journal* 1998, **4**, 1509

7. Photon Harvesting by Multi-Component Blend

7.1 Sensitization Mechanism

By shifting the polymer absorption to the red part of the VIS spectrum or even to the near infrared, the absorption in the blue-green region of the spectrum is lowered concurrently. An additional component can be added to the blend, absorbing in this spectral range. [1,2,3] Such components are for example organic dye molecules or wide band gap conjugated polymers. Alternatively, the two photoactive absorber can be linked by a σ-bond. Such dyad systems were introduced to avoid problems of three component mixtures.[4,5]

The excited state of the wide band gap absorber ought to make an energy transfer to the lower band gap polymer. Then, the low band gap material makes subsequently the charge transfer. Alternatively, the mechanism of an individual electron transfer by the dye molecule to the fullerene and hole transfer to the polymer is possible. The two mechanism are shown schematically in Figure 7.1.
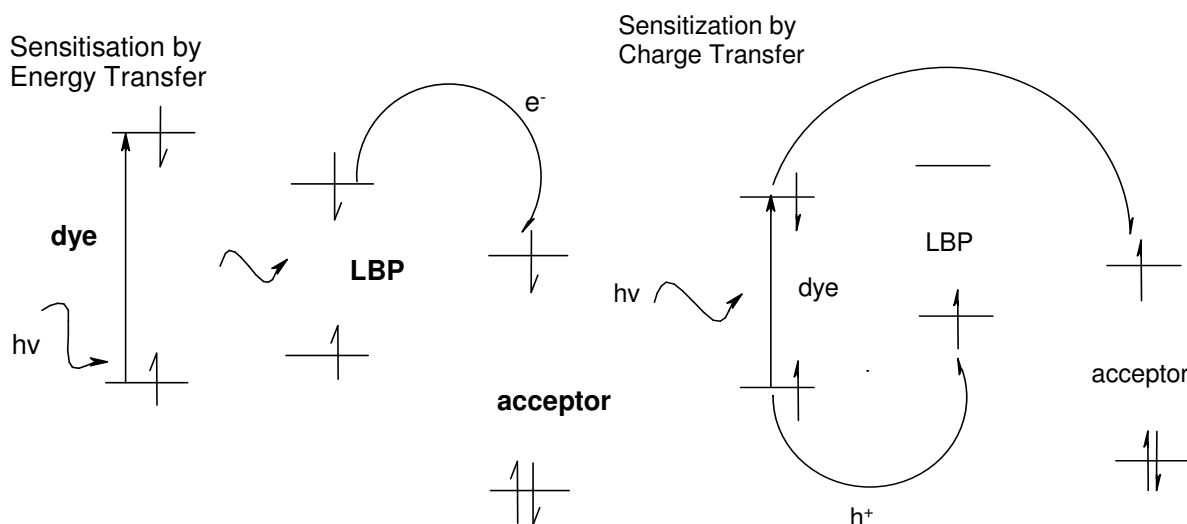
Figure 7. 1: Sensitizing mechanism for bulk heterojunction solar cells by a wide band gap absorber. Sensitization by energy transfer from the dye to the low band gap polymer (left); sensitization by separate electron and hole transfer from the dye on the acceptor and polymer, respectively.

7.2 Sensitized Organic Solar Cells

Different photon harvesting systems containing more than two organic absorbers have been proposed in the literature.

Roman et al showed blends containing two polythiophenes and C_{60}.[6]

This route was followed later, sensitizing PTPTB: PCBM (see Chapter 4) photovoltaic cells with MDMO-PPV.[7] Significant contribution from both polymer to the photocurrent was found, also the overall efficiency was smaller as compared to the parent systems. Alternatively, the sensitization with the highly absorbing dye molecule 9-(Diethylamino)-5-*H*-benzoe[a]phenoxazin-5-one (nile red), chemical structures see Figure 7.2, was investigated. The photocurrent spectra of this system show contribution from the dye absorption as well as the absorption of the polymer. The overall power conversion efficiency of this system is $\eta = 0.5$ %. For all this systems, energy transfer is assumed as dominant sensitization mechanism.
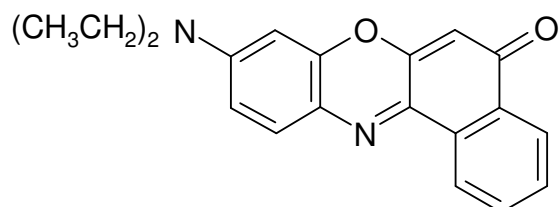
Nile Red

Figure 7. 2: Chemical structure of 9-(Diethylamino)-5*H*-benzo[a]phenoxazin-5-one (nile red).

Chen reported polymer blend/ C60 bilayer devices.[1] Different polymer blends were used, typically containing a wide band gap PPV derivative and a low band gap PT derivative. Energy transfer was demonstrated as sensitization mechanism by photoluminescence experiments. Photocurrent measurements show a broad coverage of the spectrum and contribution from both polymers. Maximal conversion efficiency of IPCE = 38 % at 430 nm and enhanced conversion efficiency is reported.

Takahashi reported sensitization of PT: perylene bilayer devices.[8] Porphyrine was used to sensitize the perylene acceptor layer. All three materials are shown to contribute to the photocurrent. Sensitization by charge transfer is assumed to be the sensitizing mechanism.

7.3. MDMO-PPV: Pc-C_{60} blends

7.3.1 Photophysics of Pc-C_{60} : MDMO-PPV blends

The combination of Pc-C_{60} and MDMO-PPV shows absorption over the whole visible range. In this blend, three photophysical and electronically active components, C_{60}, MDMO-PPV and ZnTBPc are present and can interact with each other. C_{60} is known to be electron acceptor towards both the other two components.

Unknown is the excited state interaction between the two donors ZnTBPc and MDMO-PPV. A 5% ZnTBPc doped MDMO-PPV film, excited at 476 nm, shows only ZnTBPc photoluminescence. At the excitation wavelength, MDMO-PPV primarily absorbs. This indicates energy transfer from MDMO-PPV to ZnTBPc.

In time resolved photoinduced absorption measurements, the bleaching of the MDMO-PPV as well as of the ZnTBPc groundstate absorption can be observed. The bleaching of the MDMO-PPV absorption is quenched in a timescale of about 10 ps. This band is taken as indication for the MDMO-PPV excited state, which is primarily excited. In a similar timescale, the ground state bleaching of the ZnTBPc raises.

Further, the blend of MDMO-PPV and Pc-C_{60} is investigated. No steady state photoluminescence could be observed. Steady state photoinduced absorption, excited at 476 nm, shows absorption peaks at 1.1 eV, which is unambiguously assigned to C_{60}^-, and around 0.7 eV. Further bleaching is observed around 1.8 eV, indicating a long lived excited state of ZnTBPc. Time resolved measurements are performed on a MDMO-PPV film with 10 % Pc-C_{60} (the phthalocyanine concentration is equivalent to the 5 % ZnTBPc in MDMO-PPV). The groundstate bleaching of MDMO-PPV vanishes in a timescale of 10 ps, the groundstate bleaching of the phthalocyanine arise is the same timescale.

The decay time for the MDMO-PPV excited state and the raising time for the phthalocyanine excited state are in a similar timescale for blends with ZnTBPc and Pc-C_{60} . It is therefore concluded, that in the photoexcited state of MDMO-PPV makes primarily an energy transfer to ZnTBPc, followed from an electron transfer to the C_{60}.

7.3.2 Photovoltaic devices from MDMO-PPV: Pc-C$_{60}$ blends

Photovoltaic devices from the Pc-C$_{60}$ dyad were discussed in Chapter 6.2. The photophysical interaction of MDMO-PPV and Pc-C$_{60}$ shows energy transfer from MDMO-PPV to phthalocyanine, with subsequent charge transfer. This sensitization mechanism should be exploited for solar cell devices.

A series of photovoltaic devices are prepared, containing different ratios of MDMO-PPV and Pc-C$_{60}$. Long living, positive charge carriers on the phthalocyanine molecule are demonstrated for such combination. Therefore, the positive charges are expected to be primarily transported by the phthalocyanine.

Figure 7.3 shows the I-V characteristics for the MDMO-PPV: Pc-C$_{60}$ blend devices under illumination and in the dark. For this representation, the best device is chosen out of a series of 6 devices. In Table 7.1, the average values of a this series are shown.

The addition of MDMO-PPV leads to a significant decrease of the photocurrent. Also the current injection at positive bias is decreased, the 1:1 blend device shows a nearly symmetric behaviour without reaching the injection regime up to a forward bias of +2 V.

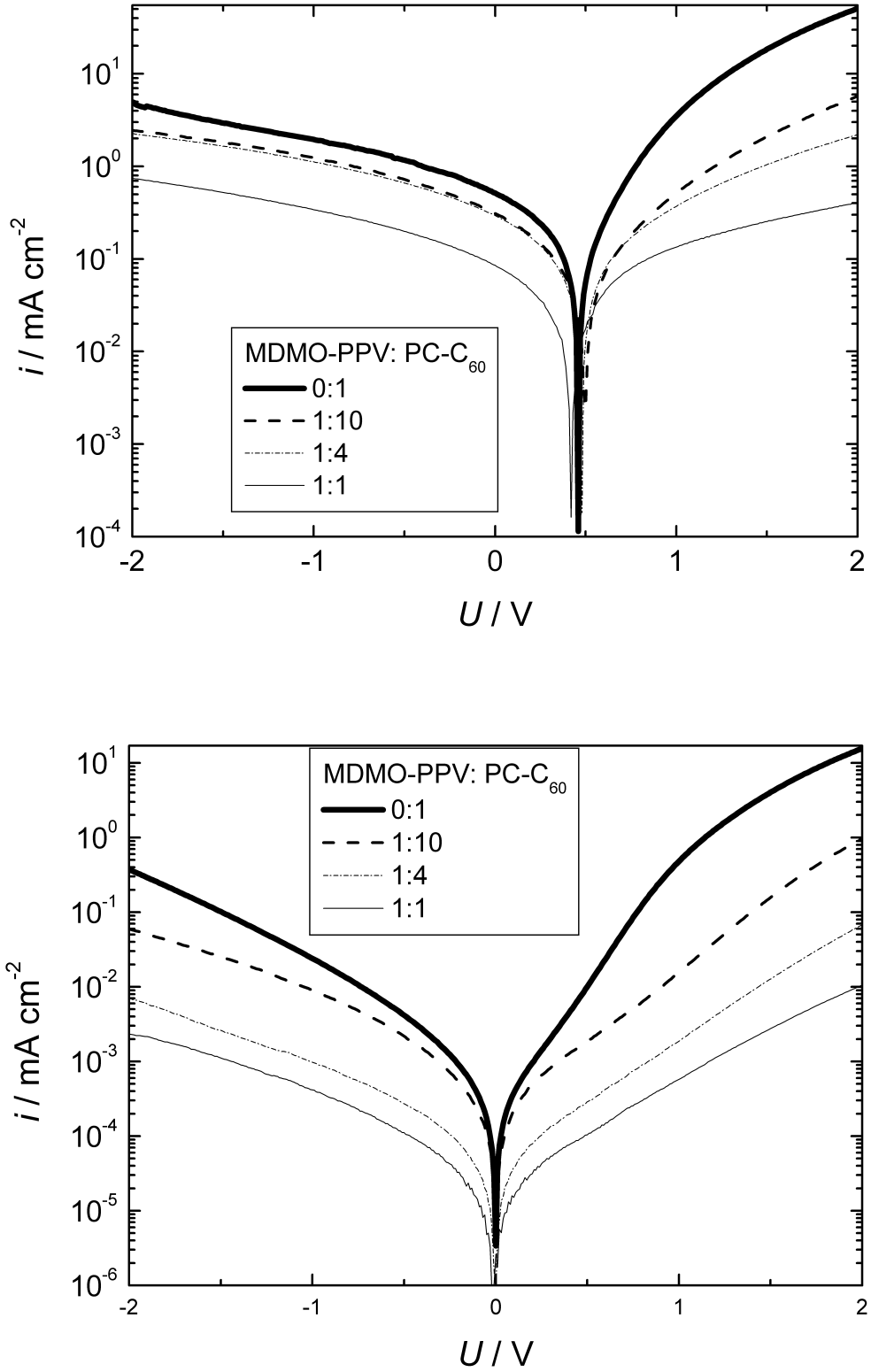**Figure 7. 3:** Current voltage curves for MDMO-PPV: Pc-C_{60} devices with different ratios, under illumination from a solar simulator 80 mW cm^{-2} (upper graph), best device from a series of six, in the dark for the same device (lower graph).

The maximal observed V_{oc} is not significantly affected by the addition of MDMO-PPV. The distribution of the V_{OC} is smaller in the blends with MDMO-PPV. which might originate from a better film quality. This indicates a lower possibility for shunts for the MDMO-PPV containing devices. These shunts are decreasing the V_{oc}. The addition of MDMO-PPV increases the film forming property.

Table 7. 1: Photovoltaic parameters of photovoltaic devices of MDMO-PPV: Pc-C_{60} with different ratios. V_{oc}, I_{sc} and FF are the average values of a series of six devices, η is the efficiency calculated from these values. The quantum efficiencies IPCE are for one representative device.

MDMO-PPV: Pc-C_{60}	V_{oc} [V]	I_{sc} [mA cm^{-2}]	FF	η [%]	IPCE % (350 nm)	IPCE % (480 nm)	IPCE % (700 nm)
0:1	0.320	0.46	0.26	0.048	3.4	0.6	3
1:10	0.400	0.33	0.26	0.043	2.5	1.6	2.2
1:4	0.420	0.28	0.24	0.035	1.7	1.5	1.4
1:1	0.370	0.07	0.25	0.008	1.3	1.2	0.8

The photocurrent spectra, see Figure 7.4, show for the MDMO-PPV: Pc-C_{60} blend devices three peaks at 350 nm, 500 and 700 nm, which can be assigned to the absorption of C_{60}, MDMO-PPV and ZnTBPc, respectively. The IPCE efficiencies of C_{60} and ZnTBPc are decreased in the blends more, as would be expected by the dilution with MDMO-PPV. For the latter, maximal conversion efficiency is observed at the smallest addition of 10%.
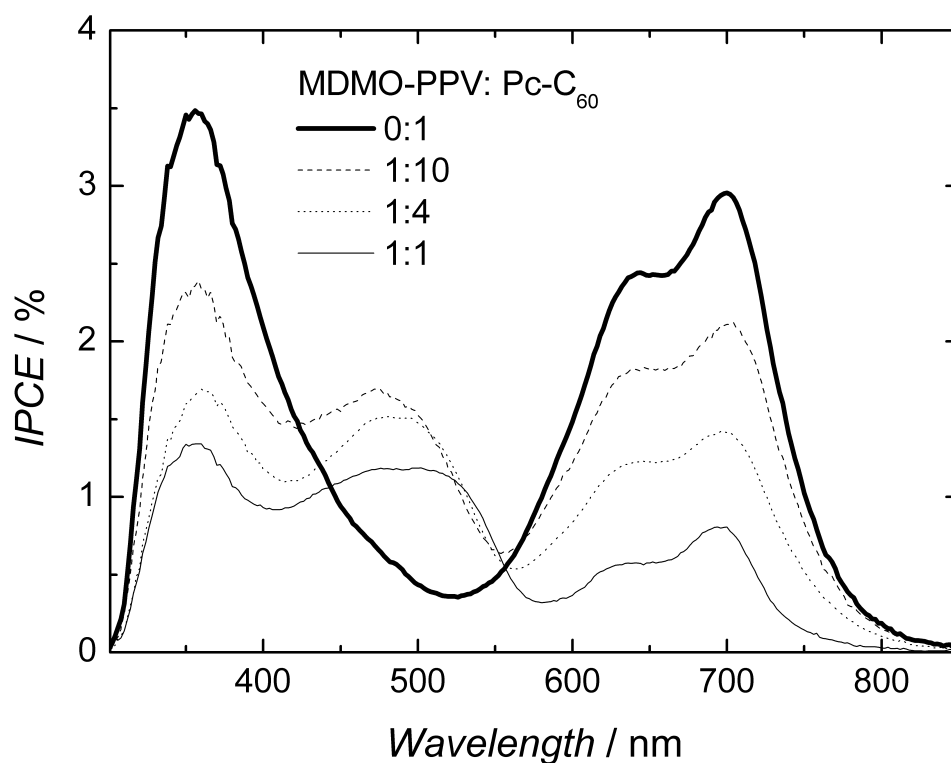
Figure 7. 4: Photocurrent spectra of MDMO-PV: Pc-C_{60} blend devices with different ratios. The photocurrent spectrum of Pc-C_{60} is shown in comparison.

In summary, it was shown that MDMO-PPV: Pc-C60 blend devices can cover the whole visible range. Contribution of all three components to the photocurrent is shown. No improvement of the power conversion efficiency of Pc-C_{60} devices is found by blending with MDMO-PPV. From the I-V characteristics, significant decrease of the charge injection and transport is observed for the blends. It is concluded that the charge transport is hindered in the blends due to unfavourable morphology and dilution of charge transport pathways. Blending with MDMO-PPV lead to better film forming properties by spin cast techniques. As a consequence, shunt are less probable and a better reproducibility of the device fabrication could be achieved.

7.3.3 MDMO-PPV:Pc-C$_{60}$: PCBM blends

The photophysics of para-phenylene vinylene, phthalocyanine and fullerene mixtures was
discussed in chapter 7.3.1. Energy transfer from MDMO-PPV to phthalocyanine with subsequent
charge transfer to fullerene was demonstrated. This mechanism can be applied in photovoltaic
devices, as was demonstrated in chapter 7.3.2. But addition of MDMO-PPV led to a decrease of
the overall photovoltaic performance. This was assigned to reduced hole mobility.
In this chapter, Pc-C$_{60}$ in blends with MDMO-PPV and PCBM is investigated for bulk
heterojunction devices.
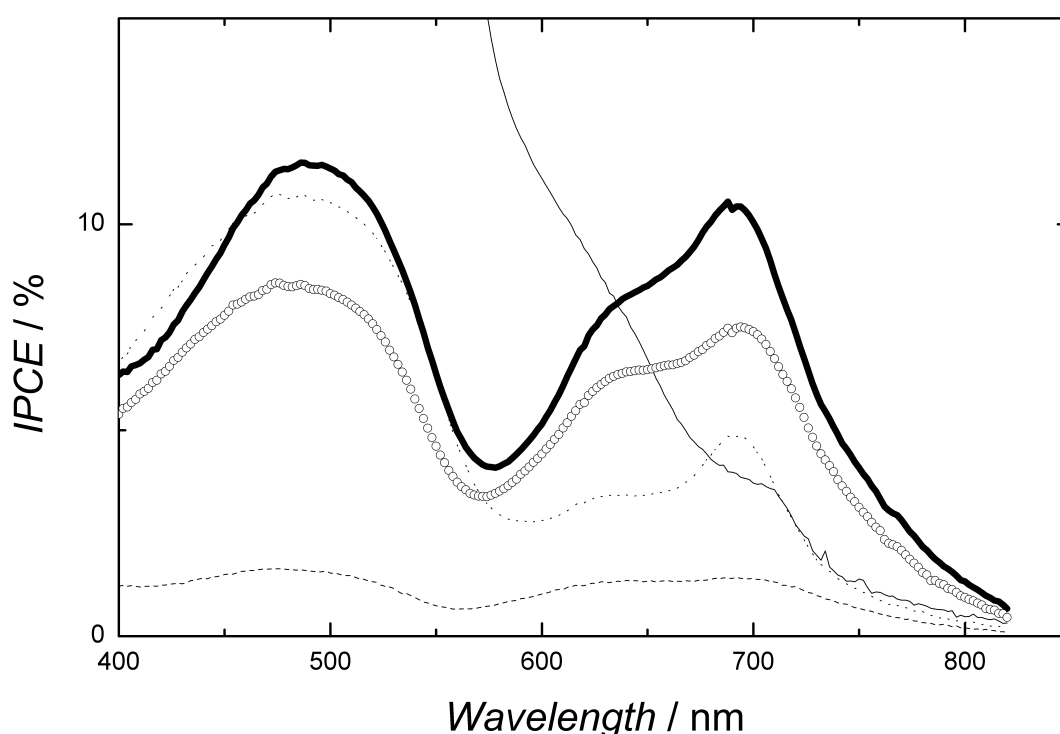
Figure 7. 5: IPCE spectra from MDMO-PPV: fullerene 1:4 devices, for the fullerene, different ratios of
PCBM and Pc-C$_{60}$ are used, 0 % Pc-C$_{60}$ (thin line), 10 % (dotted line), 30 % (thick line), 60 % (open
circles) and 100 % (slashed line).

The photocurrent spectra for several three component blends with a constant MDMO-PPV :
acceptor ratio of 1:4 (w/w) is shown in Figure 7.5. The overall fullerene concentration is varying
only slightly in these experiments. The devices containing Pc-C$_{60}$ show two peaks at 500 and
700 nm in the photocurrent. These two peaks are assigned to MDMO-PPV and phthalocyanine.
The IPCE efficiencies are increasing with increasing PCBM addition.
Figure 7.6 and Table 7.2 show the I-V characteristics and photovoltaic parameters for the three
component blends, respectively. The V$_{OC}$ is decreased by addition of Pc-C$_{60}$ from ~800 mV for

the MDMO-PPV: PCBM to V_{OC} ~ 500 mV for the three component devices. Similar values for the V_{OC} have been reported in Chapter 7.3.2 for different phthalocyanine fullerene blends. The V_{OC} seems to be limited to this value for the phthalocyanine: fullerene combination.
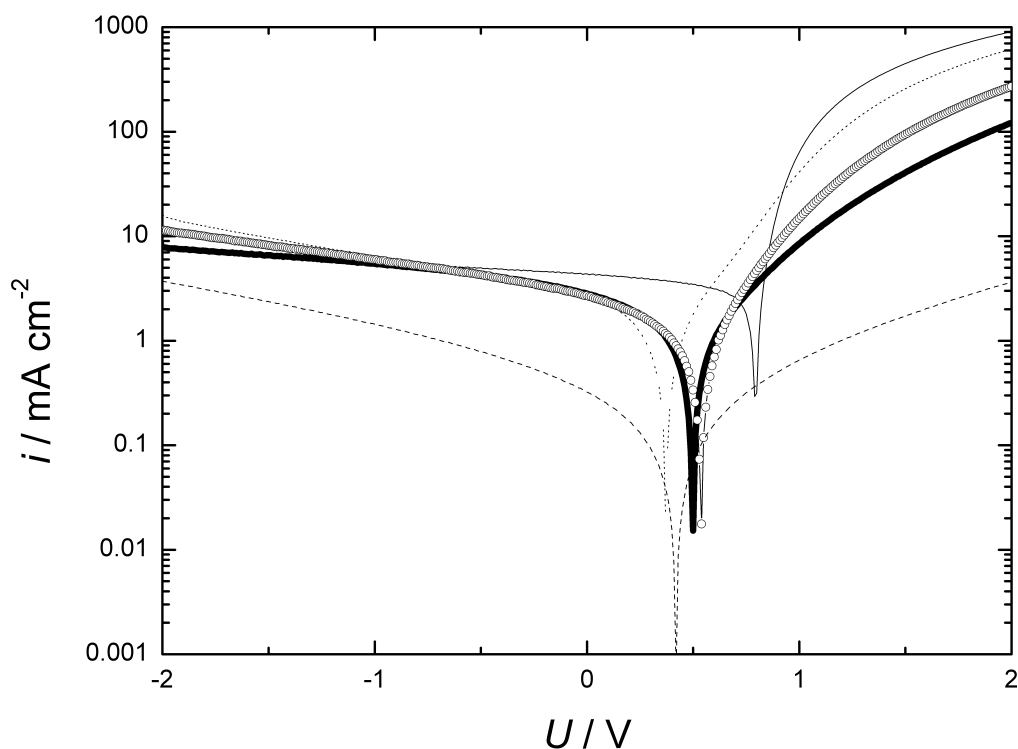
Figure 7. 6: I-V characteristics of MDMO-PPV: fullerene 1:4 devices, for the fullerene, different ratios from PCBM and Pc-C_{60} are used, 0 % Pc-C_{60} (thin line), 10 % (dotted line), 30 % (thick line), 60 % (open circles) and 100 % (slashed line).

Interestingly, the forward bias current at +2V is increasing with increasing PCBM concentration and varies over more than two orders of magnitude. All devices are of comparable thickness around 100 nm. Therefore, this increase can be attributed to the current transport and electrode injection property of Pc-C_{60} and PCBM by the different substitution.

Likewise, the I_{SC} is higher for the PCBM containing devices, even the absorption is less. The different electrical behaviour of PCBM and Pc-C_{60} can only be rationalized by the different substitution pattern of the two molecules.

Table 7. 2: Photovoltaic parameter of MDMO-PPV: Pc-C_{60}: PCBM devices under illumination from a solar simulator 80 mW cm^{-2}

Pc-C_{60} / %	V_{oc} / V	I_{sc} / mA cm^{-2}	FF	Eff. / %
0	0.79	4.3	0.56	2.4
10	0.37	2.8	0.32	0.41
30	0.51	3.1	0.32	0.63
60	0.54	2.7	0.31	0.56
100	0.45	0.34	0.25	0.05

7.4 References

[1] L. Chen, L. S. Roman, D. M. Johansson, M. Svensson, M. R. Andersson, R. A..J. Janssen, O. Inganaes, *Advanced Materials* 2000, **12**, 1100

[2] C. Winder, H. Matt, J. C. Hummelen, R. A. J. Janssen, N. S. Sariciftci, C. J. Brabec, *Thin Solid Films* 2002, **403-404**, 373

[3] J. Cabanillas-Gonzales, S. Yeates, D. D. C. Bradley, *Synthetic Metals* 2003, **139**, 637

[4] D. M. Russel, A. C. Arias, R. H. Friend, C. Silva, C. Ego, A. C. Grimsdale, K. Muellen, *Applied Physics Letters* 2002, **80**, 2204

[5] H. Neugebauer, M.A. Loi, C. Winder, N. S. Sariciftci, G. Cerullo, A. Gouloumis, P. Vazquez, T. Torres, *Solar Energy Materials and Solar Cells* 2004, **83**, 201

[6] L.S. Roman, M. R. Andersson, T. Yohannes, O. Inganäs *Advanced Materials* 1997, **9**, 1164

[7] C. Winder, Diplomarbeit, Universität Linz 2001

[8] K. Takahashi, I. Nakajima, K. Imoto, T. Yamaguchi, T. Komura, K. Murata, *Solar Energy Materials and Solar Cells* 2003, **76**, 115

8. Conclusion, Summary and Outlook

The efficiency of polymer based bulk heterojunction devices could be steadily increased over the last decade. Several strategies are used for photon harvesting in organic solar cells. In this thesis, several novel materials have been investigated by spectroscopic means and have been tested for implementation into devices:

- *Low band gap polymer:* Due to increased theoretical understanding and much synthetic effort, the absorption of CP´s could be shifted to the red part of the VIS and even into the NIR.

- *Acceptor polymers* are a cheap alternative for C_{60} based structures. Further, they show a much stronger absorption bands compared to fullerenes.

- *Dyad molecules*, combination of donor and acceptor molecules, are implemented into photovoltaic devices. They show inherently negligible phase separation and can combine the absorption profile of tetrathiafulvalene or phthalocyanine with the electron accepting and transport properties of fullerenes.

- *Multicomponent blends* to carpet a wider range of the solar spectrum.

.

Several other approaches have been proposed in the literature for increased photon harvesting:

- Multiple layer solar cells with materials of different band gaps, similar to the tandem cells for inorganic materials. Serial connection of organic solar cells could be demonstrated by implementing a thin metal layer as tunnelling layer between individual cells[1,2].

- The use of light scattering nano or micro particles embedded in the optically active layer to enhance the optical pathways in the film due to scattering.

- The use of light trapping mechanisms by structuring the interface of the photovoltaic devices as presented by Niggemann et.al.[3,4] and Roman[5]

- Hybrid solar cells[6,7] are a combination of conjugated polymer donors and inorganic nanoparticles acceptors. Power conversion efficiency of P3HT: CdSe blend devices with 1.7 % have been demonstrated for such devices. This approach combines the easy processability of polymer materials with the advantageous absorption profile of inorganic materials. Additional, the inorganic materials show good transport, which can be optimised by tuning their shape.

- Dye sensitised solar cells, which are using organic dyes with an absorption onsets around 800 nm on a nanoporous electrode, typically TiO_2. This approach is widely used in

photoelectrochemical cells with an electrolyte as hole conductor. For such cells, power conversion efficiency of 10 % were demonstrated.[8] Recently, an all-solid-state dye sensitized cell, replacing the liquid electrolyte by an organic hole transport layer, with efficiencies of 3.2 % was shown[9].

8.2 References

[1] H. Hiramoto, M. Suezaki, M. Yokoyama, *Chemical Letters* 1990, **3**, 327

[2] A. Yakimov, S. Forrest, *Applied Physics Letters* 2002, **80**, 1667

[3] M. Niggemann, B. Bläsi, A. Gombert, A. Hinsch, H. Hoppe, P. Lalanne, D. Meissner, V. Wittwer, Proceedings of 17th European Photovoltaic Solar Energy Conference, 2001

[4] M. Niggemann, M. Glatthaar, A. Gombert, A. Hinsch, V. Wittwer, *Thin Solid Films* 2004, **451**, 619

[5] L.S Roman, O. Inganaes, T. Granlund, T. Nyberg, M. Svensson, M. R. Andersson, J. C. Hummelen, *Advanced Materials* 2000, **12**, 189

[6] N. C. Greenham, X. Peng, A. P. Alivisatos, *Physical Review B* 1996, **54**, 17628

[7] W. U. Huynh, J. J. Dittmer, A. P. Alivisatos, *Science* 2002, **295**, 2425

[8] D. O Reagan, M. Graetzel, *Nature* 1991, **353**, 737

[9] J. Krueger, R. Plass, M. Graetzel, H. J. Matthieu, *Applied Physics Letters* 2002, **81**, 367

Lebenslauf

Dipl. Ing. Christoph Winder

geboren. 27.12 1975 in Bregenz

Familienstand: verheiratet

Ausbildung

- November 2001 bis November 2004:

  Doktoratsstudium an der Johannes Kepler Universität Linz, Linzer Institute für Organische Solarzellen, Prof. N. Serdar Sariciftci

- Oktober 1994-Oktober 2001:

  Studium der Technischen Chemie an der Johannes Kepler Universität Linz, Diplomarbeit: „ Sensitization of Low Band Gap Polymer Bulk Heterojunction Solar Cells", Abschluss mit Auszeichnung

- September 1986- Juni 1994:

  Neusprachliches Gymnasium Bregenz Blumenstrasse 4, 6900 Bregenz, Abschluss mit gutem Erfolg

- September 1982-Juni 1986

  Volksschule Hörbranz

Arbeitgeber und Praxis

- November 2001 bis Dezember 2004:

  Christian Doppler Laboratorium für Plastiksolarzellen an der Universität Linz, Altenbergerstrasse 69, 4040 Linz, Österreich,

  Forschungsassistent,

- Oktober 2000- Jänner 2003:

  Tutor für Physikalische Chemie an der *Johannes Kepler Universität Linz,*

- August- September 2000:

  Omicron Surface Science Ltd., East Grinstead, Großbritannien, Praktikant

- Juli- September 1998:

  Fluka Chemie AG, Industriestrasse 25, 9470 Buchs SG, Schweiz, Praktikant

List of Publications

<u>Year 2004</u>

- "Electric field induced enhancement of the photoinduced absorption in conjugated polymer/fullerene bulk heterojunction solar cells" Christoph winder, Christoph Lungenschmied, N. Serdar Sariciftci, Christian Arndt, Uladizimir Zhokhavets und Gerhard Gobsch, submitted to *Organic Electronics*
- „Stabilization of the nanomorphology of polymer/fullerene "bulk heterojunction" blends using a novel polymerizable fullerene derivative" Martin Drees, Harald Hoppe, Christoph Winder, Niyazi S. Sariciftci, Wolfgang Schwinger, Friedrich Schaeffler, Christoph Topf, Markus C. Scharber, Zhengguo Zhu, Russ Gaudiana, submitted to Advanced Functional Materials
- „Photophysics and photovoltaic device properties of phthalocyanine-fullerene dyad: conjugated polymer mixtures" Helmut Neugebauer, Maria Antonietta Loi, Christoph Winder, N. Serdar Sariciftci, Giulio Cerullo, Andreas Gouloumis, Purificación Vázquez, Tomás Torres, *Solar Energy Materials and Solar Cells* **93**, 201-209 (2004)
- "Nanoscale morphology of conjugated polymer/fullerene based bulk heterojunction solar cells" Harald Hoppe, M. Niggeman, Christoph Winder, Andreas Hirsch, Juergen Kraut, Renate Hiesgen, Dieter Meissner, N. Serdar Sariciftci, accepted by *Advanced Functional Materials*
- "Photoinduced absorption studies on conjugated polymer/fullerene mixtures at low temperature and high frequencies" Markus Scharber, Christoph Winder and N. Serdar Sariciftci, *Synthetic Metals* **141**, 109-112 (2004)
- "Low Band Gap Polymers for Photon Harvesting in Bulk Heterojunction Solar Cells" Christoph Winder and N. Serdar Sariciftci, *Journal of Material Chemistry* 2004, **14**, 1077-1086, invited feature article

<u>Year 2003</u>

- " A soluble PEDOT-derivative for Polymeric Solar Cells: Photophysics and Devices" C. Winder, M.A. Loi, A. Cravino, C.J. Brabec, M. C. Scharber, H. Neugebauer, N. S. Sariciftci, I. F. Perepichka, J. Roncali; , submitted to *Synthetic Metals*
- „ Charge Recombination in conjugated polymer/fullerene solar cells studied by transient absorption spectroscopy" Ana F. Nogueira, Ivan Montanari, Jenny Nelson, James R. Durrant, Christoph Winder, N. Serdar Sariciftci, Christoph J. Brabec, *Journal of Physical Chemistry B* **107,** 1567 (2003)
- "Long living photoinduced charge separation for solar cell applications in fulleropyrrolidine-phthalocyanine dyad thin films" M. Antonietta Loi, Patrick Denk, Harald Hoppe, Helmut Neugebauer, Christoph Winder, Dieter Meissner, Christoph Brabec, N. Serdar Sariciftci, Andreàs Gouloumis, Purificatión Vázquez and Tomàs Torres, *Journal of Materials Chemistry* **13**, 700-704 (2003)

<u>Year 2002</u>

- „A Soluble Low-Band Gap Polymer for Near-IR Optoelectronic Devices" C.J. Brabec, Christoph Winder, N. Serdar Sariciftici, Jan.C. Hummelen, Anantharaman Dhanabalan, Paul A.van Hal, René A. J. Janssen, Advanc*ed Functional Materials* **10,** 709 (2002)
- "Transient optical studies of charge recombination dynamic in a polymer/fullerene composite at room temperature" Ivan Montanari, Ana F. Nogueira, Jenny Nelson, James R. Durrant, Christoph Winder, M. Antonietta Loi, N. Serdar Sariciftci, Christoph J. Brabec, *Applied Physics Letters* **81,** 3001 (2002)

- "The Effect of LiF/Metal Electrodes on the Performance of Plastic Solar Cells" Christoph J. Brabec, Sean E. Shaheen, Christoph Winder, N. Serdar Sariciftci, *Applied Physics Letters* **80**, Nr. 7, 1288

<u>Year 2001</u>
- "Influence of Disorder on the Photoinduced Excitations in Phenyl Substituted Polythiophenes" Christoph Brabec, Christoph Winder, Markus Scharber, N. Serdar Sariciftci, J.Kees Hummelen, Mathias Svensson and Mats R.Andersson; *Journal of Chemical Physics* **115**, No. 15, p.7235 (2001)
- Diploma thesis " Sensitization of Low Band gap Polymer Bulk Heterojunction Solar Cells" Universität Linz, September 2001

Conference Proceedings

<u>Year 2004</u>
- "Photophysics and Photovoltaic Devices of a π-Extended Tetrathiafulvalene-Fullerene Dyad" Christoph Winder, Helmut Neugebauer, N. Serdar Sariciftci, Francesco Giacalone, José L. Segura, Nazario Martin, submitted to the proceedings of the ECS annual meeting, San Antonio 2004
- "Electroabsorption Studies on Organic Diodes" Christoph Lungenschmied, Christoph Winder, Markus Scharber, Attila Mozer, Gebhard Matt, Helmut Neugebauer, Niyazi Serdar Sariciftci, submitted to *Molecular Crystals and Liquid Crystals*
- "Blue emitting self-assembled nano-fibers of para-sexiphenyl grown by Hot Wall Epitaxy"A. Andreev, F. Quochi , A. Kadashchuk , H. Sitter, C. Winder , H. Hoppe , S. Sariciftci , A. Mura , G. Bongiovanni , *Physica status solidi a,* 201, 2288, (2004)
- " Investigation of Excited States in Polymer/Fullerene Solar Cells by means of Photoinduced Reflection/- Absorption Spectroscopy" Christian Arndt, Uladimir Zhokavets, Gerhard Gobsch, Christoph Winder, Christoph Lungenschmied, N. Serdar Sariciftci, *Thin Solid Films*, 451-452, 60-63 (2004) proceedings of the EMRS 03, Strassburg

<u>Year 2003</u>
- "Organic Solar Cells based on polymer/ fullerene interpenetrating networks" Christoph Winder, N. Serdar Sariciftci, summary for Minatec conference, Grenoble 2003, for presentation see http://www.minatec.com/minatec2003/us/index.htm
- "Towards Increasing the Photon Harvesting in Bulk Heterojunction Polymer Solar Cells" Christoph Winder, M. Antonietta Loi, N. Serdar Sariciftci, Patrick Denk, Franz Padinger, Jan. C. Hummelen, René A. J. Janssen, Andreas Gouloumis, Purification Vazquez, Tomàs Torres; *Proceedings of the SPIE,* **4801**, p. 22 (2003)
- "Optoelectronic Devices based on para-sexiphenyl Films grown by Hot Wall Epitaxy" Christoph Winder, Andrei Andreev, Helmut Sitter, Gebi Matt, N. Serdar Sariciftci, Dieter Meissner, *Synthetic Metals* **139**, 573 (2003) proceedings Optical Probes 03
- "Excited State Spectroscopy in Conjugated Polymer/ Fullerene Photovoltaic Devices under Working Conditions" Christoph Winder, Christoph Lungenschmied, N. Serdar Sariciftici, Ana. F Nogueira, Ivan Montanari, James R. Durrant, Christian Arndt, Uladimir Zhokhavets, Gerhard Gobsch, *Synthetic Metals* **139**, 577 (2003)
- "Fulleropyrrolidine-phthalocyanine dyad for photovoltaic application" M. Antonietta Loi, Patrick Denk, Harald Hoppe, Helmut Neugebauer, Dieter Meissner, Christoph

Winder, Christoph Brabec, N. Serdar Sariciftci, Andreas Gouloumis, Purification Vázquez, Tomàs Torres, , *Synthetic Metals* **137**, 1491 (2003)

- "Spectroscopic properties of PEDOTEHIITN, a novel soluble low band-gap conjugated polymer" Antonio Cravino, M. Antonietta Loi, Markus C. Scharber, Christoph Winder, Helmut Neugebauer, Patrick Denk, H. Meng, Y. Chen, Fred Wudl, N. S. Sariciftci, *Synthetic Metals* **137**, 1435 (2003)
- „ Charge Recombination in conjugated polymer/fullerene solar cells studied by transient absorption spectroscopy" Ana F. Nogueira, Ivan Montanari, Jenny Nelson, James R. Durrant, Christoph Winder, N. Serdar Sariciftci, Christoph J. Brabec, *Synthetic Metals* **137**, 1505 (2003)

Year 2002

- "Polymer Solar Cells and Infrared Light Emitting Diodes: A Dual Function Low Band Gap Polymer" C. Winder, S. Sariciftci, C. Brabec, R. A. J. Janssen, J. C. Hummelen; *Molecular Crystals and Liquid Crystals* **385**, 93-100 (2002)
- "Low Band Gap Polymer Bulk Heterojunction Solar Cells and their Sensitization" Christoph Winder, Christoph J. Brabec, Gebi Matt, N. Serdar Sariciftci, J. Keeps Hummelen, René A. J. Janssen, *Thin Solid Films* **403-404**, p. 373-379 (2002)

Year 2000

- "The Influence of Ordering on the Photoinduced Charge Transfer in Composites of Phenyl-type substituted Polythiophenes with Methanofullerenes" Christoph .J. Brabec, Christoph Winder, Markus Scharber, N. Serdar Sariciftci, Mats R.Andersson, Olle Inganäs, J. Kees Hummelen, *Mat. Res. Symp. Proc.* Vol. 598, B 3.24.1-6 (2000)

Contribution to Conferences (presenting author)

Year 2004

- "Spectroscopic Studies on conjugated polymer-fullerene bulk heterojunction devices" Christoph Winder, Christoph Lungenschmied, N. Serdar Sariciftci, Christian Arndt, Uladzimir Zhokavets, Gerhard Gobsch, ICEPOM-5, Kiev, Ukraine
- "Novel Fullerene Compounds for Organic Solar Cells" Christoph Winder, Helmut Neugebauer, N. Serdar Sariciftci, Tomas Torres, Nazario Martin, talk ECS 03, San Antonio

Year 2003

- "Polymer- Fullerene bulk heterojunction devices- a route to the Plastic Solar Cell" Christoph Winder, N. Serdar Sariciftci, invited talk annual meeting of the Optical Society of America OSA 4th- 8th of October 2003, Tucson, Arizona
- " Organic solar cells based on polymer fullerene interpenetrating network" Christoph Winder, N. Serdar Sariciftci, invited talk MINATEC conference, 22.-26 September 2003, Grenoble
- "Organic solar cells based on polymer/ fullerene solar cells" Christoph Winder, N. Serdar Sariciftci, talk at "Discussion Meeting on Functional Mechanisms in Organic and Dye Sensitized Solar Cells" 9th -10th of July 2003, Imperial College London
- "Excited State Spectroscopy in Conjugated Polymer/ Fullerene Photovoltaic Devices under Working Conditions" Christoph Winder, Christoph Lungenschmied, N. Serdar

Sariciftici, Ana. F Nogueira, Ivan Montanari, James R. Durrant, Christian Arndt, Uladimir Zhokhavets, Gerhard Gobsch, poster presentation, *Optical Probes 03* Venice
- "Optoelectronic Devices based on para-sexiphenyl Films grown by Hot Wall Epitaxy" Christoph Winder, Andrei Andreev, Helmut Sitter, Gebi Matt, N. Serdar Sariciftci, Dieter Meissner, poster presentation *Optical Probes 03*, Venice

Year 2002
- "Plastic Solar Cells" Christoph Winder, N. Serdar Sariciftci, Patrick Denk, Roman Rittberger, Franz Padinger, talk polyscene workshop 28. 10 2002, München
- "Novel fullerene acceptors for bulk heterojunction solar cells" Christoph Winder, Maria A. Loi, David Muehlbacher, Helmut Neugebauer, N. Serdar Sariciftci, Elisabeth Wirtl, Patrick Denk, José Segura, N. Martin, Francesco Giacalone, Andreas Gouloumis, Purificacion Vazquez, Tomàs Torres EUROMAP annual meeting Madrid
- "Plastic Solar Cells" Christoph Winder, Antonio Cravino, exhibition at the PV in Europe conference, Rome 7-11 october 2002
- "New materials for Photon Harvesting in Polymer Based Solar Cells" Christoph Winder, M.Antonietta Loi, N. Serdar Sariciftci, René A. J. Janssen, Jan. C. Hummelen, Tomàs Torres, Talk 81st Bunsenkolloquium on Charge Transfer at Conducting Polymers: Fundamentals and Applications
- "Functional Materials for Photon Harvesting in Organic Polymeric Solar Cells" Christoph Winder, Maria Antonietta Loi, N. Serdar Sariciftci, Jean Roncali, Igor Perepichka, Fred Wudl, René A. J. Janssen, Andreas Gouloumis, Purificacion Vazquez, Tomàs Torres, Talk at COST D-14 mid term evaluation workshop Puidoux-Chexbres, 7-10 September 2002
- "Photon Harvesting in Bulk Heterojunction Polymer Solar Cells" Christoph Winder, M. Antonietta Loi, N. Serdar Sariciftci, Patrick Denk, Franz Padinger, Jan. C. Hummelen, R.A.J. Janssen, Andreas Gouloumis, Pucificacion Vazquez, Tomas Torres, talk at the SPIE 2002 Seattle
- „PEDOT-DERIVATIVES AS PHOTOACTIVE MATERIALS FOR POLYMER SOLAR CELLS" Christoph Winder, Maria A. Loi, Antonio Cravino, Christoph J. Brabec, Helmut Neugebauer, N. Serdar Sariciftci, Igor F. Perepichka, Jean Roncali, Poster ICSM 2002, Shanghai, China
- "A Dual Function Low Band gap Polymer: Infrared LED and Photovoltaics" Christoph Winder , Christoph Brabec, N. Serdar Sariciftci, Rene A. J. Janssen, J. Kees Hummelen, talk at the "International Conference on Electronic Processes in Organic Materials" (ICEPOM-4)", June 3-8, 2002, L'viv, Ukraine

Year 2001
- "Low Band gap Polymer Bulk Heterojunction Solar Cells and their Sensitization" Christoph Winder, Christoph J. Brabec, Gebi Matt, N. Serdar Sariciftci, J. Kees Hummelen, René. A. J. Janssen, EMRS 2001 spring meeting Strassbourg (Poster)